

AD-A035 379

TETRA TECH INC PASADENA CALIF

DEVELOPMENT OF AN OFF-DESIGN PREDICTIVE METHOD FOR SUPERCAVITAT--ETC(U)

DEC 76 O FURUYA

N00600-76-C-0790

F/G 13/10

NL

UNCLASSIFIED

TETRAT-TC-676

1 OF 2
AD-A
035 379



U.S. DEPARTMENT OF COMMERCE
National Technical Information Service

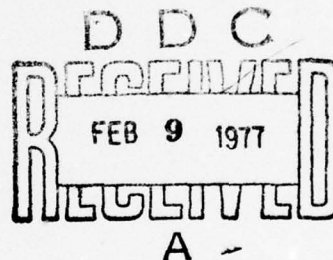
AD-A035 379

DEVELOPMENT OF AN OFF-DESIGN PREDICTIVE
METHOD FOR SUPERCAVITATING PROPELLER PERFORMANCE

TETRA TECH, INCORPORATED, PASADENA, CALIFORNIA

DECEMBER 1976

ADA 035379



This Document has been Approved for
Public Release and Sale; Its Distribution
is Unlimited.

FINAL REPORT

DEVELOPMENT OF AN OFF-DESIGN PREDICTIVE
METHOD FOR SUPERCAVITATING PROPELLER
PERFORMANCE

Tetra Tech Contract TC-676
Contract No. N00600-76-C-0790

December 1976

REPRODUCED BY
NATIONAL TECHNICAL
INFORMATION SERVICE
U. S. DEPARTMENT OF COMMERCE
SPRINGFIELD, VA. 22161

TETRA TECH

FINAL REPORT

DEVELOPMENT OF AN OFF-DESIGN PREDICTIVE METHOD FOR
SUPERCAVITATING PROPELLER PERFORMANCE

Prepared for:

David W. Taylor Naval Ship Research and
Development Center
Bethesda, Maryland

Prepared by:

Okitsugu Furuya, Ph. D.

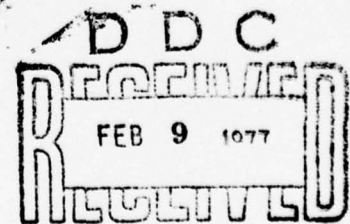
Tetra Tech Contract TC-676
Contract No. N00600-76-C-0790

DISTRIBUTION STATEMENT A

Approved for public release;
Distribution Unlimited

December 1976

Tetra Tech, Inc.
630 North Rosemead Boulevard
Pasadena, California 91107
(213) 449-6400



A

ABSTRACT

This is the Final Report, describing all the tasks accomplished in Phases A and B of Contract No. N00600-76-C-0790, including a listing of the computer program developed under the present contract and manual describing input and output data.

In order to incorporate the three-dimensional effect and cascade effect into the performance prediction of the supercavitating propellers, a two-dimensional supercavitating (2-D s/c) cascade theory and a lifting line theory were combined. The force coefficients obtained from the 2-D s/c cascade theory will account for the cascade effect whereas the three-dimensionality is incorporated in terms of effective flow incidence angles at each selected spanwise location of the blade for the 2-D program.

An inherent difficulty in applying the 2-D s/c cascade theory to three-dimensional flows arises due to the existence of the choking condition but was overcome by correcting the effective upstream velocities depending on the cavity thickness. Mathematical formulation combining the 2-D s/c cascade theory and a lifting line theory is described. The method proposed for the cavity thickness correction is explained, followed by numerical procedures to solve the problem.

Numerical results made with the 2-D s/c cascade program for a s/c NSRDC Model 3770 propeller geometry have shown a most significant cavitating cascade effect. These results seem to explain very well the

with Section	<input checked="" type="checkbox"/>
with Section	<input type="checkbox"/>

REPRODUCTION AVAILABILITY CODES		
Dist.	AVAIL.	and/or SPECIM.
A		

discrepancy existing between previous experimental data and design data. The propeller characteristics such as thrust, torque coefficients and efficiency have been calculated and compared with experimental data, having provided a good correlation over a supercavitating range of speed coefficient, J .

However, for J 's beyond the above range, the present results quickly deviate from the experimental data because a part of the propeller near the hub is at partially cavitating condition to which the present theory is not applicable.

TABLE OF CONTENTS

ABSTRACT.....	i
LIST OF FIGURES.....	iv
LIST OF TABLES.....	vii
NOMENCLATURE.....	viii
1. INTRODUCTION.....	1
2. MATHEMATICAL FORMULATIONS.....	9
3. NUMERICAL PROCEDURES.....	17
3.1 Substitutional Iterative Method.....	17
3.2 Newton's Iterative Method.....	19
4. CALCULATIONS OF THRUST, TORQUE COEFFICIENTS AND EFFICIENCY.....	23
5. NUMERICAL RESULTS OF THE TWO-DIMENSIONAL SUPERCAVITATING CASCADE.....	27
6. CALCULATIONS OF PROPELLER PERFORMANCE FOR NSRDC MODEL 3770 SUPERCAVITATING PROPELLER.....	35
7. CONCLUSIONS AND RECOMMENDATIONS.....	41
REFERENCES.....	86
APPENDIX A - Two Dimensional Nonlinear Supercavitating Cascade Theory (Reference [4]).....	A-1
APPENDIX B - Calculations of Induced Velocities w_a and w_t by a Lifting Line Theory.....	B-1
APPENDIX C - Geometric and Hydrodynamic Configurations of Supercavitating Propeller Model TMB(NSRDC)3770....	C-1
APPENDIX D - Computer Program Listing and Input and Output Data Setup.....	D-1

LIST OF FIGURES

Figure 1	Flow Configuration in Cascade Geometry of Propeller at a Constant Radius r with Velocity Diagram.....	45
Figure 2	Change of Circulations Γ in Cascade Flow.....	46
Figure 3	Representation of Cavity Thickness by Distribution of Source Singularities in a Cascade Row.....	47
Figure 4	Geometric Mean Angle α_m , Force Normal to Geometric Mean Velocity U_m in Cascade Flow and Thrust and Torque Components.....	48
Figure 5	Flow Chart of Substitution Procedures Iterative.....	49
Figure 6	Flow Chart of Newton's Iterative Procedures.....	50
Figure 7(a)	Lift Coefficient C_L Normal to the Upstream Velocity vs. Cavitation Number σ for Incidence Angles $\alpha_e = 2^\circ$, 3° , 4° and 6° at the Blade Spanwise Location of $x = 0.9$ where the Solidity is 0.244 and geometric stagger angle γ is 74.03° .	
	are C_L Values of $\alpha_e = 2^\circ$, 4° , 6° Respectively Calculated from a Linearized Theory for a Single Foil (Equation 47).....	51
Figure 7(b)	The Same as Figure 7(a) Except That $x = 0.8$ where the Solidity is 0.365 and γ is 72.40°	52
Figure 7(c)	The Same as Figure 7(a) Except That $x = 0.7$ where the Solidity is 0.479 and γ is 70.33°	53
Figure 7(d)	The Same as Figure 7(a) Except That $x = 0.6$ where the Solidity is 0.594 and γ is 67.61°	54
Figure 7(e)	The Same as Figure 7(a) Except That $x = 0.5$ where the Solidity is 0.728 and γ is 63.94°	55
Figure 7(f)	The Same as Figure 7(a) Except That $x = 0.4$ where the Solidity is 0.912 and γ is 58.77°	56

LIST OF FIGURES CONTINUED

Figure 8(a)	Drag Coefficient C_D Corresponding to Figure 7(a) ($x = 0.9$).....	57
Figure 8(b)	Drag Coefficient C_D Corresponding to Figure 7(b) ($x = 0.8$).....	58
Figure 8(c)	Drag Coefficient C_D Corresponding to Figure 7(c) ($x = 0.7$).....	59
Figure 8(d)	Drag Coefficient C_D Corresponding to Figure 7(d) ($x = 0.6$).....	60
Figure 8(e)	Drag Coefficient C_D Corresponding to Figure 7(e) ($x = 0.5$).....	61
Figure 8(f)	Drag Coefficient C_D Corresponding to Figure 7(f) ($x = 0.4$).....	62
Figure 9(a)	Normalized Circulation Γ/dV_e vs. σ_e Corresponding to Figure 7(a) ($x = 0.9$).....	63
Figure 9(b)	Γ/dV_e vs. σ_e Corresponding to Figure 7(b) ($x = 0.8$).....	64
Figure 9(c)	Γ/dV_e vs. σ_e Corresponding to Figure 7(c) ($x = 0.7$).....	65
Figure 9(d)	Γ/dV_e vs. σ_e Corresponding to Figure 7(d) ($x = 0.6$).....	66
Figure 9(e)	Γ/dV_e vs. σ_e Corresponding to Figure 7(e) ($x = 0.5$).....	67
Figure 9(f)	Γ/dV_e vs. σ_e Corresponding to Figure 7(f) ($x = 0.4$).....	68
Figure 10(a)	Length of Cavity vs. σ_e for Incidence Angles $\alpha_e = 2^\circ, 4^\circ,$ and 6° at $x = 0.9$	69
Figure 10(b)	The Same as Figure 10(a) Except That $x = 0.8$	70
Figure 10(c)	The Same as Figure 10(a) Except That $x = 0.7$	71
Figure 10(d)	The Same as Figure 10(a) Except That $x = 0.6$	72
Figure 10(e)	The Same as Figure 10(a) Except That $x = 0.5$	73
Figure 10(f)	The Same as Figure 10(a) Except That $x = 0.4$	74

LIST OF FIGURES CONTINUED

Figure 11(a)	Lift-to-Drag Ratio L/D vs. C_L for Incidence Angles $\alpha_e = 2^\circ, 4^\circ$ and 6° at $x = 0.9$	75
Figure 11(b)	The Same as Figure 11(a) Except That $x = 0.8$	76
Figure 11(c)	The Same as Figure 11(a) Except That $x = 0.7$	77
Figure 11(d)	The Same as Figure 11(a) Except That $x = 0.6$	78
Figure 11(e)	The Same as Figure 11(a) Except That $x = 0.5$	79
Figure 11(f)	The Same as Figure 11(a) Except That $x = 0.4$	80
Figure 12	Performance Prediction for 3770 at Design $\sigma_{Va} = .617$	81
Figure 13	Comparison of 3770 Performance between the Present Theory and Experimental Data [5] at $\sigma_{Va} = .500$	82

LIST OF TABLES

Table 1	Design Characteristics of NSRDC Model 3770 Supercavitating Propeller (from Reference [5]).....	83
Table 2	Comparison of K_T , K_Q and η between the Present Result, Design Data and Experimental Data for 3770 Supercavitating Propeller at Design Point, $\sigma_{Va} = .617$ and $J = .440$	84
Table 3	Comparison of the Detailed Flow Characteristics of 3770 between the Design Method [5] and Present Method at Design Point, $\sigma_{Va} = .617$ and $J = .440$	85

APPENDIX C

Table C-1	Geometric and Hydrodynamic Configurations of Supercavitating Propeller Model TMB(NSRDC) 3770.....	C-3
Table C-2	Geometric Flow Angles β and Geometric Flow Incidence Angles α_g at Various Radial Locations of the Propeller 3770 for Various J's.....	C-4
Table C-3	Local Cavitation Numbers σ Based on $V(= \left\{ (wr)^2 + V_a^2 \right\}^{\frac{1}{2}})$ for Various J's for $\sigma_{Va} = 0.617$ based on V_a	C-4

NOMENCLATURE

a, b, c	=	ξ -coordinates in two-dimensional cascade problem
\tilde{A}	=	scale factor of cascade mapping function
c	=	chord length of blade
C_p	=	power coefficient ($= P / \frac{1}{2} \rho V_a^3 \pi R^2$)
C_T	=	thrust coefficient ($= T / \frac{1}{2} \rho V_a^2 \pi R^2$)
d	=	spacing between two blades
D	=	propeller diameter ($= 2R$)
g	=	number of blades
G	=	normalized circulation ($= \Gamma / 2\pi R V_a$)
i_a, i_t	=	induction factors for the axial and tangential induced velocities w_a and w_t
J	=	speed coefficient ($V_a \pi / \omega R = \pi \lambda$)
n	=	propeller rotational speed
P_1, P_c	=	static pressures at upstream uniform flow and inside the cavity
P	=	power
Q	=	torque
r	=	radial position from the propeller axis
r_h	=	propeller hub radius
R	=	propeller radius
s	=	arc length on the blade measured from the cavity separation point
	=	solidity ($= c/d$)
S	=	total wetted arc length of the blade
T	=	thrust

U_1	=	velocity at upstream infinity with downwash correction (but not including cavity correction) ($= V_e + V_c$)
U_2	=	velocity at downstream infinity
U_∞	=	geometric mean velocity
V	=	relative velocity to the blade ($= ((\omega r)^2 + V_a^2)^{\frac{1}{2}}$)
V_a	=	advance speed (axial flow speed)
V_c	=	induced velocity due to the cavity thickness effect
V_e	=	effective velocity including induced velocities ($= \left\{ (\omega r - w_t)^2 + (w_a + V_a)^2 \right\}^{\frac{1}{2}} - V_c$)
w_a, w_t	=	induced velocities in the axial and tangential directions, respectively
x	=	normalized radial position ($= r/R$)
α_2	=	deflected flow angle referred to the nose-tail line
α_1	=	induced flow angle
α_e	=	effective incidence angle
α_g	=	geometric incidence angle
α_∞	=	geometric mean flow angle
β	=	pitch angle ($= \tan^{-1} V_a / \omega r = \tan^{-1} J / \pi x$)
β_i	=	pitch angle including downwash effect ($= \tan^{-1} (w_a + V_a) / (\omega r - w_t)$)
$\bar{\beta}$	=	local slope of blade
γ	=	geometric stagger angle
Γ	=	circulation
δ	=	stagger angle in potential plane ($= \alpha_e + \gamma$)
ζ	=	transform potential plane
η	=	propeller efficiency ($= C_T / C_p$)

- λ = advance coefficient ($= V_a / \omega R$)
 ξ = real axis of the ζ -plane
 ρ = density of fluid
 σ_e = local cavitation number ($= (p_1 - p_c) / \frac{1}{2} \rho V_e^2$)
 ω = angular velocity of propeller

1. INTRODUCTION

The development of a prediction method for supercavitating propeller performance at off-design conditions is a difficult task due to an additional complexity of the cavity flow to that of three-dimensional propeller configurations.

Unlike the conventional propellers used at relatively low ship speeds, supercavitating propellers are expected to have strong cascade effects. The existence of blade cavities causes blocking or choking effects on the flow passages as the extent of cavity becomes large both in length and thickness. Some propeller designers already pointed out the importance of the cascade effect in s/c propeller design in their earlier papers such as [1] *.

A similar effect was also found important even for subcavitating propellers: the paper by Kerwin and Leopold [2] showed that large incidence angle corrections are necessary due to blade thickness effect even if the thickness is small. The correction becomes particularly significant as the thickness ratio to the blade spacing becomes high, i. e., near the hub. This is considered to be exactly the same blocking effect as that for the cavity flow. It is now evident that the cascade effect of blocking effect must be correctly incorporated into the performance prediction of s/c propellers.

* Number in brackets designates Reference at end of paper

Although linearized s/c cascade theories in [3] have long existed, such theories are unable to accurately predict hydrodynamic characteristics of these highly nonlinear s/c cascade flows. It was not until just recently that a fully nonlinear 2-D s/c cascade theory [4] was developed, greatly facilitating the calculation of these cascade effects and providing a powerful engineering tool.

The method of solving the present problem is a combination of the 2-D s/c cascade theory with a lifting line theory. The procedure to be used is stated as follows. Specifying all physical and geometric conditions of the s/c propeller, 2-D solutions at several radial or spanwise locations of blades will be obtained. A difficult question however arises as to what effective flow incidence angles, α_e , must be used for the 2-D analysis. The downwash effect in propeller flows are usually so strong that the geometric flow incidence angles, α_g (see Figure 1 for definition and also Table C2 for actual values of α_g for the 3770 supercavitating propeller), are completely different from the effective incidence angles, α_e .

The present propeller problem is very much similar to that of a single airfoil of finite span for which an integral equation of a lifting line theory must be solved. The result determines Γ , the distribution of circulation, or equivalently lift over the blade span so as to provide a right amount of downwash effect everywhere for generating the above circulation, Γ . The evaluation of the downwash angle, α_i , in this case is most simply made by a propeller lifting line theory but in a somewhat complicated form. The effective angle of flow incidence, α_e , is then obtained by

subtracting α_i from α_g . Applying this α_e to the lift curves calculated by the 2-D s/c theory, we can determine the circulation distribution, eventually ending up with an integral equation for α_e with the span location as a variable.

A different type of difficulty arises when applying a two-dimensional flow approach to a three-dimensional flow, although this type of approach has been well adopted for subcavitating propeller design. Contrary to the supercavitating propeller problem, the same method for subcavitating propellers creates no serious problems in determining the forces at any blade location for any given effective incidence angle, α_e , since the lift and drag forces used for subcavitating propellers are continuous function of α_e . However, in the present problem, due to the choking condition the force curves obtained by the 2-D s/c cascade theory are discontinued right at that point (see Figures 7(a) to (f) for choking conditions on the lift curves). The physical meaning of this is explained as follows. The cavity length and thickness increase as the incidence angle increases, and finally the cavity extends to downstream infinity with a maximum cavity thickness. This blocks or chokes the flow path of cascade. It therefore becomes impossible to increase the total mass flow going through a cascade beyond that point at the choking condition.

This type of 2-D choking condition never occurs in the three-dimensional (3-D) flow configuration even if the flow cavitates and locally chokes. Consider a cascade of blades having finite span length. The 3-D cascade

can have a similar choking condition locally, but the amount of flow we can push from the upstream infinity with any incidence angle is unlimited since any mass flow in excess of that going through the cascade can go around the corners of cascade in the direction of span. Thus, the 'effective' flow velocity going through the propeller remains almost constant at each blade radial position. The terminal values depend on the cavity thickness but not depend on the upstream velocity. As long as the cascade span is finite this phenomenon holds true. However, once the span extends to infinity, going back to a totally two-dimensional configuration, the inherent problem mentioned above arises.

As a first step for resolving the present difficult situation, we use a simple, intuitive method with the above physical picture of 3-D cavity flow in mind. The upstream velocity is corrected at each spanwise location by distributing line sources in cascade configuration whose strengths are determined based on the cavity thickness. The effective velocity obtained with this method is always smaller than that of the original flow so that the cavitation number to be used for the 2-D analysis becomes larger thus being able to avoid the choking condition. It must be pointed out that the correction here is not on the incidence angle as downwash correction but on the upstream velocity or equivalently the cavitation number.

In this report, we present a mathematical formulation which combines the 2-D s/c cascade theory with a lifting line theory and a method for correcting the cavity choking effect, followed by numerical procedures

to solve the problem. Computed 2-D s/c cascade results for a chosen NSRDC Model 3770 propeller geometry are then presented, showing a remarkable cascade effect. With these 2-D s/c force coefficients used, the propeller performance was calculated and compared with the experimental data [5].

The results correlate well in the supercavitating regions but quickly deviate as the speed coefficient, J , becomes larger due to the appearance of partial cavitation near the hub. This discrepancy is naturally expected since the present theory is only applicable to the fully supercavitating propellers.

Originally, the present work had been planned to incorporate the results of the above computations into a lifting surface theory (see Reference [6] for the detailed procedure of this method). However, it has been found that the present method combining the 2-D s/c cascade theory, lifting line theory and cavity thickness correction provides accurate results correlating well with existing experimental data. We describe several theoretical backgrounds why the method accounts for all supercavitating propeller characteristics as follows;

- i) By having used the results of 2-D s/c cascade theory, we have accounted for a most important effect of supercavitating propeller flows, i. e. the existence of the cavity in cascade

geometry. The forces on the s/c cascade used as the basis for propeller calculations corrected by a lifting line theory are found to be much smaller than those of a single foil due to the influence of the low pressure region of the cavity on the pressure side of an adjacent blade. In addition, the blocking effect due to the cavity has also been incorporated in terms of a cavitation number correction.

- ii) The finite aspect ratio correction to s/c propeller blades is usually smaller than that on fully wetted propeller blades (see [8]) and also limited by the choking condition. Therefore the lifting line theory used above is considered fairly accurate as this has been proven by a good correlation with experimental data.
- iii) Although a lifting surface theory will give all boundary value corrections including both the wetted portion of the blade and cavity streamlines as mentioned in [6] , no information about the correction for upstream flow velocity is obtained by the present method, it has been proven that a correction for cavitation number

is a most important feature in applying a 2-D s/c cascade theory to calculations of the propeller performance.

- iv) For those cases in which the cavitation number, σ , is close to that of the choking condition, the 2-D s/c cascade theory itself fails to converge in the numerical iterative procedure as will be explained later. For such σ 's, the 2-D theory may not provide a convergent solution for new boundary values set by a lifting surface theory. In the present approach, however, this difficulty is overcome by an interpolation scheme as will be seen later.

Consequently, we believe that the present approach accurately accounts for all the hydrodynamic effects of supercavitating propellers which a lifting surface theory will provide and furthermore that the former is superior to the latter from the viewpoints of simplicity in concept and economy in computation.

2. MATHEMATICAL FORMULATIONS

A two-dimensional supercavitating cascade hydrodynamic problem has recently been solved by using the hodograph variables to satisfy the exact boundary conditions. In this method the blade and cascade geometry, the upstream flow conditions and the cavitation number are specified. A system of five nonlinear functional equations involving five unknown solution parameters was formulated and solved numerically using a functional iterative method combined with Newton's method. The details of the theory and numerical method are described in [4].

In order to incorporate the two-dimensional (2-D) cascade theory into the analysis of supercavitating (s/c) propellers, the effective angle of incidence, α_e (see Figure 1), must be determined. The geometric flow incidence α_g , which is determined by the propeller blade pitch, rotational speed ω , and axial flow speed V_a , is typically much larger than α_e due to the strong downwash effects generated by the propeller helical vortex sheets. For example, in some cases of s/c propellers, the downwash angle $\alpha_i = \alpha_g - \alpha_e$ can be as high as ten degrees although the effective angle of incidence is only four degrees. It has become clear that neglecting the downwash in two-dimensional cascade calculations can result in a solution far from the actual propeller flow situation. One of the ideas in capturing the three-dimensional effect is to incorporate vortex singularities into a lifting line theory.

Preceding page blank

With the geometry of cascade and propeller blades, w^* and V_a specified, the 2-D cascade problem can be solved if α_e and effective upstream velocity, V_e , are assumed known at each radial station r since α_e , β_i and σ are obtained:

$$\alpha_i = \alpha_g - \alpha_e \quad (1)$$

$$\beta_i = \beta + \alpha_i \quad (2)$$

$$\sigma = \frac{p_1 - p_c}{\frac{1}{2}\rho V_e^2} \quad (3)$$

Five equations in the 2-D problem are now rewritten :

$$f_1 \equiv \operatorname{Re} \{w(\zeta_1)\} - \alpha_e = 0 \quad (\text{Upstream flow angle condition}) \quad (4)$$

$$f_2 \equiv \operatorname{Im} \{w(\zeta_1)\} + \ln U_2 = 0 \quad (\text{Upstream flow velocity condition}) \quad (5)$$

$$f_3 \equiv g_3 - \alpha_2 = 0 \quad (\text{Downstream flow angle condition}) \quad (6)$$

$$f_4 \equiv s(1) - S = 0 \quad (\text{Scaling between the physical and transform planes}) \quad (7)$$

$$f_5 \equiv g_5 - d \left\{ \sin(\alpha_e + \gamma) - U_2 \sin(\alpha_2 + \gamma) \right\} = 0 \quad (\text{Continuity equation}) \quad (8)$$

* See Nomenclature and also the Blade Definition Figure 1 for the definition of each symbols.

where explicit expressions for $\text{Re } w(\zeta_1)$, $\text{Im } w(\zeta_1)$, g_3 , $s(-1)$ and g_5 are given in Appendix A (and also see 4). It is noted that in equations (4) thru (8) α_e 's simply replace α_1 in equations (7), (8), (9), (15) and (16) in 4. It must be mentioned that the upstream velocity, V_e , used for these 2-D calculations is different from the velocity simply composed of the axial flow, V_a , and the rotational velocity, w_r , as is shown in Figure 1. Due to the three-dimensional downwash effect and the cavity blocking effect, V_e is given by a following equation:

$$V_e = U_1 - V_c \quad (9)$$

where

$$U_1 = [(w_r - w_t)^2 + (V_a + w_a)^2]^{\frac{1}{2}}$$

w_a, w_t = propeller induced flow velocities in the axial and tangential directions

V_c = retarding flow velocity due to the cavity blocking effect.

Before describing the methods of determining w_a , w_t and V_c , first look at how to obtain the circulation, Γ , from the above two-dimensional calculations, which will be used in a lifting-line theory. Taking the control volume designated by ABCD shown in Figure 2, the differences in potential between the points A and D, and B and C are calculated respectively by

$$\Delta\phi_{DA} = V_e d \sin(\gamma + \alpha_e)$$

$$\Delta\phi_{CB} = U_2 d \sin(\gamma + \alpha_2),$$

thus the net change of the potential in this control volume, that is, $\Gamma(x)$, is given by

$$\begin{aligned}\Gamma(x) &= \Delta\phi_{DA} - \Delta\phi_{CB} \\ &= V_e d \sin(\gamma + \alpha_e) - U_2 d \sin(\gamma + \alpha_2)\end{aligned}\quad (10)$$

where $x \equiv r/R$.

This formula holds both for the finite and infinite cavity cascade flows, but for the former case a simpler form is obtained by using a continuity equation between the upstream and downstream flows, i. e.

$$V_e d \cos(\gamma + \alpha_e) = U_2 d \cos(\gamma + \alpha_2);$$

$$\Gamma(x) = V_e d \frac{\sin(\alpha_e - \alpha_2)}{\cos(\gamma + \alpha_2)}, \quad \text{for finite cavity flows.} \quad (11)$$

$\Gamma(x)$ calculated in Equation (10) or (11) connects the 2-D results with a three-dimensional lifting-line theory to find the propeller induced velocities.

The induced velocities in the axial and tangential directions w_a and w_t , for the case where the blades extend from the hub at $r = r_h$ to the tip $r = R$, are obtained (see [7] for detailed derivations) from:

$$\frac{w_a}{V_a} = \frac{1}{2} \int_{x_h}^1 \frac{dG(x')}{dx'} \frac{1}{x-x'} i_a(\beta_1) dx' \quad (12)$$

$$\frac{w_t}{V_a} = \frac{1}{2} \int_{x_h}^1 \frac{dG(x')}{dx'} \frac{1}{x-x'} i_t(\beta_i) dx' \quad (13)$$

where $G(x)$ is a normalized circulation:

$$G(x) = \frac{\Gamma(x)}{2\pi R V_a} \quad (14)$$

and

$$x_h = r_h / R. \quad (15)$$

i_a and i_t are the induction factors obtained by Lerb [7] and detailed expressions are found in Appendix B. It must be mentioned that for s/c propellers the propeller loading is expected to be moderate to heavy, thus the downwash effects (12) and (13) must be evaluated by taking into account the deflection of the vortex sheet location behind the bound vortices. Lerb [7] showed from a discussion of energy balance between the propeller disk and the ultimate wake that the location of vortex sheets should be on a helical surface having an angle β_i (instead of β), which is a function of r . In the present calculations of w_a and w_t we use β_i to evaluate i_a and i_t . The downwash angle α_i is then obtained from the following equation to an accuracy of first order in β_i :

$$\beta_i = \tan^{-1} \frac{1 + w_a/V_a}{\pi x/J - w_t/V_a} \quad (16)$$

$$\alpha_i = \beta_i - \beta.$$

It has now come to a point of how we incorporate the choking or cavity thickness effect into the problem, which relates to determining V_c in Figure 1. The physical picture of the choking phenomena in the 2-D and 3-D flows has already been discussed in the Introduction of this report. A rigorous treatment of this type of problem will require an enormous effort involving complicated mathematics, although it must be done some time in the near future. Meanwhile, we use a somewhat more intuitive method as a first step to avoid an inherent difficulty in applying the results of 2-D s/c cascade flow to the propeller problem.

In order to represent the cavity thickness, a row of source singularities of strength m are placed with a distance d in a uniform flow, the velocity of which is U_1 with a stagger angle, $\gamma + \alpha_e$, as depicted in Figure 3. The velocity potential of the flow is given by

$$W = U_1 Z e^{-i(\gamma + \alpha_e)} + m \ln \left\{ \sinh \left(\frac{\pi Z}{d} \right) \right\}, \quad (17)$$

thus the velocity potential is obtained:

$$\frac{dW}{dz} = U_1 e^{-i(\gamma + \alpha_e)} + \frac{m\pi}{d} / \tanh(\pi z/d). \quad (18)$$

As $x \rightarrow \pm\infty$, the x - component of the velocity changes by $\pm m\pi/d$, respectively. If we know the thickness of the cavity, $d \cdot e$, the strength of source, m , is calculated by using the continuity equation

$$\left\{ U_1 \cos(\gamma + \alpha_e) - \frac{m\pi}{d} \right\} d = \left\{ U_2 \cos(\gamma + \alpha_2) + \frac{m\pi}{d} \right\} (d - de)$$

or

$$\frac{m\pi}{d} = \frac{U_1 \cos(\gamma + \alpha_e) - U_2 \cos(\gamma + \alpha_2)(1 - e)}{2 - e} \quad (19)$$

It means that although the mass flow, $U_1 \cos(\gamma + \alpha_e) \cdot d$ per blade from the upstream infinity, comes into the cascade, the amount of $m\pi$ is rejected to go through the blade passage due to the existence of cavity. The rejected mass flow, $m\pi$, should go normal to the paper plane, in reality, in the radial direction of the propeller. Therefore V_c is calculated from (19) by taking the component in the U_1 direction;

$$V_c = \frac{m\pi}{d} \frac{1}{\cos(\gamma + \alpha_e)} \quad (20)$$

The effective upstream flow velocity to be used in the 2-D analysis is now obtained

$$\begin{aligned} V_e &= U_1 - V_c \\ &= \left\{ U_1 + U_2 \frac{\cos(\gamma + \alpha_2)}{\cos(\gamma + \alpha_e)} \right\} \cdot \frac{1 - e}{2 - e} \end{aligned} \quad (21)$$

where e is a function of σ and α_e , obtained from the results of the 2-D computations. Strictly speaking, the present method is only valid for the infinite cavity flow cases in which the cavity is fully developed. However, even for the finite cavity cases it is considered that the same cavity blockage evaluation holds true by taking the cavity thickness at the end

points of cavity as e in Equations (19) and (21).

It must be noted here that the correction of the upstream velocity by (21) changes the cavitation number, σ , for which e is obtained at α_e . It needs an iterative scheme to satisfy the relationship in Equation (21) by starting with e for $\sigma(U_1)$ and α_e as an initial step and then finding a new e for a new $\sigma(V_e)$ where V_e is just obtained from (21). It has been found in the actual computations that the convergence of the iteration is rather fast.

The problem to be solved is now fully defined. With the propeller geometry, V_a and ω specified, one can determine a circulation distribution, $\Gamma(x)$, in such a way that the free vortex sheets associated with the Γ distribution generate a correct amount of downwash velocity to have a sectional blade lift equal to $\rho U_\infty \Gamma$ where U_∞ is the geometric mean velocity of the upstream and downstream velocities (see Figure 4).

It is immediately seen that the problem is completely nonlinear including integral equations and thus cannot be solved explicitly. Two numerical iterative methods are proposed to solve this type of situation and both procedures used here will be explained in the following section.

3. NUMERICAL PROCEDURES

Two numerical methods for solving the above nonlinear integral equations are proposed and have been tested in actual computations for their convergence. The first method is what is called a substitutional iterative method and the second one is Newton's iterative method similar to that used in the problem of three-dimensional supercavitating hydrofoils [8].

3.1 Substitutional Iterative Method

This method exactly follows the steps of the mathematical formulation, the flow chart being shown in Figure 5.

Assuming the effective incidence angles $\alpha_e^{(n)}(x)$, $n=0$, at each spanwise location one can find downwash angles $\alpha_i^{(n)}(x)$ and a cavitation number $\sigma(x)$ from equations (1) and (3). The solutions of the two-dimensional s/c cascade problem provide α_2 , the deflected flow angle at downstream infinity. In actual computations it is convenient to establish a functional relationship of α_2 as a function of α_e and σ at each blade section. Since α_2 is a smooth function of α_e and σ , the 2-D calculations for several values of α_e and σ 's will be sufficient to represent α_2 by functionally establishing the results at discrete points. By doing this one can save a considerable amount of computer time since the 2-D computations are the most time consuming part of the calculation. If this relation is not established at the beginning of the computation procedure, the 2-D program must be run for each iterative loop. This can

be seen in the flow chart, Figure 5, where the returned loop will now go back to the 2-D calculation box instead of the α_2 -box. In some cases in which the stagger angle and blade solidity are large, the 2-D s/c cascade program becomes numerically unstable as was reported in [4]. This problem, however, is overcome if the 2-D features are completely calculated at the initial stage of the numerical procedure.

The induced velocity, V_c , due to the existence of cavity and thus the effective flow velocity, V_e , are obtained by a small iterative procedure in Equation (21). The sectional circulation distribution $\Gamma(x)$ is then obtained by Equation (10) or (11), thereby enabling us to calculate w_a , w_t and $\alpha_i^{(n+1)}(x)$. The values of $\alpha_i^{(0)}(x)$ first assumed are now checked to determine that they are corrected. If not, with a new $\alpha_i^{(n+1)}(x)$ and $\sigma_i^{(n+1)}$, we proceed to the next iteration until a convergent solution is obtained. In each iteration, $\beta_i^{(n)}$, starting with an assumed value $\left(\beta_i^{(0)} = \beta + \alpha_i^{(0)} \right)$, must be calculated and a new value of $\beta_i^{(n)}$ must be used in calculations of w_a and w_t . It must also be noted that the cavitation number σ based on V is used for the first iteration but σ_e based on V_e is used from the second iteration on.

If the test for the convergence of solution parameters, for example, α_i , is passed, we proceed to calculate the propeller characteristics such as thrust, power coefficients and efficiency.

When the method was applied to the present problem, we found that converged solutions were obtained only if assumed starting values of $\alpha_e^{(0)}$

were close to the actual solutions. It is for this reason that a second method using Newton's technique is proposed for seeking a better convergence.

3.2 Newton's Iterative Method

We incorporate Newton's method into the nonlinear integral equations for improving the convergence of iteration. This requires a new arrangement of the problem in order to identify the solution parameters.

From Equations (16), (B-16) and (B-17),

$$\begin{aligned} \underline{f} \equiv \tan \left(\beta_g(x) - \alpha_e(x) \right) & \left(\frac{\pi x}{J} - \frac{1}{1-x_h} \sum_{m=1}^k m G_m h_m^a (\varphi(x)) \right) \\ & - \left\{ 1 + \frac{1}{1-x_h} \sum_{m=1}^k m G_m h_m^t (\varphi(x)) \right\} = 0 \end{aligned} \quad (22)$$

and from Equations (14) and (B-11),

$$\underline{g} \equiv \sum_{m=1}^k G_m \sin m \varphi(x) - \frac{\Gamma(x, \alpha_e(x), \sigma_e)}{2\pi R V_a} = 0 \quad (23)$$

Choosing discrete control points in the radial direction of the blade for which the computations will be made, say $x = 0.4$ to 0.9 by 0.1 increment, we have six independent equations in (22) so that the same number of G_k 's are chosen for the solution parameters, in this case $k = 6$. Since all other quantities in equations (22) and (23) are known except for $\alpha_e(x)$'s, they are naturally chosen as another six solution parameters,

called α_{ek} . We now have $2k$ solution parameters for a system of nonlinear integral equations having an order of $2k$.

Rewriting these equations and parameters symbolically by

$$\underline{F} = (\underline{f}, \underline{g})$$

$$\underline{x} = (G_k, \alpha_{ek}),$$

we can describe the above set of equations as follows:

$$\underline{F}(\underline{x}) = 0$$

thus Newton's iterative loop is established by

$$\underline{J}(\underline{x}^{(n)}) \cdot (\underline{x}^{(n+1)} - \underline{x}^{(n)}) = -\underline{F}(\underline{x}^{(n)}) \quad (24)$$

where \underline{J} is a Jacobian matrix whose component is given by

$$\underline{J} = \partial F_i / \partial x_j. \quad (25)$$

In the present case each component of \underline{J} is either analytically or numerically calculated;

$$\frac{\partial F_i}{\partial x_j} = \begin{cases} \frac{\partial f_i}{\partial G_j} = \tan(\beta_g(x_i) - \alpha_{ei}) \left\{ -j h_j^a(\varphi(x_i)) \right\} / (1 - x_k) \\ -j h_j^t(\varphi(x_i)) / (1 - x_h); i = 1 \sim 6, j = 1 \sim 6 \end{cases} \quad (26)$$

$$\left\{ \begin{array}{l} \frac{\partial f_i}{\partial \alpha_{ek}} = - A(x_i) \delta_{ik} / \cos^2(\beta_g(x_i) - \alpha_{ek}) ; i = 1 \sim 6, \\ j = 7 \sim 12, k = j - 6 \end{array} \right. \quad (27)$$

$$\frac{\partial F_i}{\partial x_j} = \left\{ \begin{array}{l} \frac{\partial g_k}{\partial G_j} = \sin\{j\varphi(x_k)\} ; i = 7 \sim 12, j = 1 \sim 6, k = i - 6 \end{array} \right. \quad (28)$$

$$\left\{ \begin{array}{l} \frac{\partial g_k}{\partial \alpha_{el}} = - \frac{\delta_{kl}}{2\pi R V_a} \cdot \frac{\partial}{\partial \alpha_{el}} \Gamma(x_k, \alpha_{ek}, \sigma_e) ; i = 7 \sim 12, \\ j = 7 \sim 12, k = i - 6, l = j - 6 \end{array} \right. \quad (29)$$

where all partial derivatives are analytically calculated except for Γ for which a finite difference method is used.

Iterative numerical procedures for this case shown in Figure 6 are very similar to those of the first method shown in Figure 5. Our experience in using this Newton's method for the present problem indicated rather slow but steady convergences for almost all cases. It has also been found that the method is much less sensitive to the initial starting values of solution parameters.

4. CALCULATIONS OF THRUST, TORQUE COEFFICIENTS AND EFFICIENCY

In the cascade flow the lift force acting on the blades is known to be normal to a geometric mean angle α_∞ (see References [4] and [9]) which is depicted in Figure 4:

$$\alpha_\infty = \cos^{-1} \left\{ \frac{1}{2U_\infty} (V_e \cos \alpha_e + U_2 \cos \alpha_2) \right\} \quad (30)$$

where

$$U_\infty = \frac{1}{2} \left\{ V_e^2 + U_2^2 + 2V_e U_2 \cos(\alpha_e - \alpha_2) \right\}^{\frac{1}{2}}$$

or

$$\frac{U_\infty}{V_a} = \frac{1}{2} \left(\frac{V_e}{V_a} \right) \left\{ 1 + \left(\frac{U_2}{V_e} \right)^2 + 2 \frac{U_2}{V_e} \cos(\alpha_e - \alpha_2) \right\}^{\frac{1}{2}}, \quad (31)$$

V_e is taken to be unity in the 2-D calculations and from Figure 1

V_e/V_a is calculated from

$$\frac{U_1}{V_a} = \frac{V_e + V_c}{V_a} = \left(\cot \beta - \frac{w_t}{V_a} \right) \frac{1}{\cos \beta_i} . \quad (32)$$

Thus, a sectional thrust is obtained:

$$dT = g \left\{ \rho U_\infty \Gamma \cos(\beta_i + \alpha_e - \alpha_\infty) - (D_\infty + D_f) \sin(\beta_i + \alpha_e - \alpha_\infty) \right\} dr$$

where D_∞ and D_f are pressure drag on the cavitating blade parallel to the direction of U_∞ and friction drag on the propeller blade;

$$D_\infty = C_{D_\infty} \cdot c \frac{1}{2} \rho U_\infty^2$$

$$D_f = C_f \cdot c \frac{1}{2} \rho U_\infty^2$$

Preceding page blank

$$\begin{aligned}
T &= g \int_{r_h}^R \left\{ \rho U_\infty \Gamma \cos(\beta_i + \alpha_e - \alpha_\infty) - (D_\infty + D_f) \sin(\beta_i + \alpha_e - \alpha_\infty) \right\} dr' \\
&= g 2\pi R^2 \rho V_a^2 \int_{x_h}^1 \left\{ \frac{U_\infty}{V_a}(x') G(x') \cos(\beta_i + \alpha_e - \alpha_\infty) \right. \\
&\quad \left. - \frac{1}{4\pi} \frac{c(x')}{R} \left(\frac{U_\infty}{V_a} \right)^2 (C_{D_\infty} + C_f) \sin(\beta_i + \alpha_e - \alpha_\infty) \right\} dx'.
\end{aligned} \tag{33}$$

The thrust coefficient C_T is obtained by normalization:

$$\begin{aligned}
C_T &= \frac{T}{\frac{1}{2}\rho V_a^2 \pi R^2} = 4g \int_{x_h}^1 \left\{ \frac{U_\infty(x')}{V_a} G(x') \cos(\beta_i + \alpha_e - \alpha_\infty) \right. \\
&\quad \left. - \frac{1}{4\pi} \frac{c(x')}{R} \left(\frac{U_\infty(x')}{V_a} \right)^2 (C_{D_\infty} + C_f) \sin(\beta_i + \alpha_e - \alpha_\infty) \right\} dx'.
\end{aligned} \tag{34}$$

Similarly the power coefficient C_p is calculated as:

$$dP = r\omega dF dr$$

$$= r\omega g \left\{ \rho U_\infty \Gamma \sin(\beta_i + \alpha_e - \alpha_\infty) + (D_\infty + D_f) \cos(\beta_i + \alpha_e - \alpha_\infty) \right\} dr$$

or

$$\begin{aligned}
P &= g 2\pi\omega R^3 \rho V_a^2 \int_{x_h}^1 x' \left\{ \frac{U_\infty(x')}{V_a} G(x') \sin(\beta_i + \alpha_e - \alpha_\infty) \right. \\
&\quad \left. + \frac{1}{4\pi} \frac{c(x')}{R} \left(\frac{U_\infty(x')}{V_a} \right)^2 (C_{D_\infty} + C_f) \cos(\beta_i + \alpha_e - \alpha_\infty) \right\} dx'
\end{aligned} \tag{35}$$

and

$$\begin{aligned}
C_p &= \frac{P}{\frac{1}{2}\rho V_a^3 \pi R^2} = \frac{4g}{\lambda} \int_{x_h}^1 x' \left\{ \frac{U_\infty(x')}{V_a} G(x') \sin(\beta_i + \alpha_e - \alpha_\infty) \right. \\
&\quad \left. + \frac{1}{4\pi} \frac{c(x')}{R} \left(\frac{U_\infty}{V_a} \right)^2 (C_{D_\infty} + C_f) \cos(\beta_i + \alpha_e - \alpha_\infty) \right\} dx'
\end{aligned} \tag{36}$$

where

$$\lambda = \frac{V_a}{\omega R} .$$

It must be emphasized that U_∞ is calculated as a nondimensional number in the 2-D cascade theory problem, referring it to V_e . However, U_∞ in Equations (33) to (36), need to be absolute values. They must be multiplied by V_e in these calculations. Similarly, Γ calculated in the 2-D problem by equation (10) must use 'd' which has a dimension since again in 2-D calculations d is normalized by the chord length c. The propeller efficiency η is finally calculated as:

$$\eta = \frac{C_T}{C_P} . \quad (37)$$

Another definition of thrust and torque coefficients, using symbols K_T and K_Q , is given by

$$K_T = T / \rho n^2 D^4 \quad (38)$$

$$K_Q = Q / \rho n^2 D^5 , \quad (39)$$

thus the relations between these numbers and C_T and C_P are obtained

$$K_T = \frac{\pi J^2}{8} C_T \quad (40)$$

$$K_Q = \frac{J^3}{16} C_P \quad (41)$$

and

$$\eta = \frac{K_T}{K_Q} \frac{J}{2\pi} . \quad (42)$$

An alternative way to obtain these coefficients is that instead of using Γ and D_{∞} , we can directly use C_L and C_D which are normal and parallel to the direction of the upstream velocity, V_e . C_T and C_p are now expressed by the following formulae:

$$C_T = 2 \int_{x_h}^1 \text{sol}(x') \left(\frac{V_e(x')}{V_a} \right)^2 x' \left\{ C_L \cos \beta_i - C_D \sin \beta_i - C_f \sin \beta_g \right\} dx' \quad (43)$$

$$C_p = \frac{2}{\lambda} \int_{x_h}^1 \text{sol}(x') \left(\frac{V_e(x')}{V_a} \right)^2 x'^2 \left\{ C_L \sin \beta_i + C_D \cos \beta_i + C_f \cos \beta_g \right\} dx' \quad (44)$$

where $\text{sol}(x')$ is a solidity of the blade at x .

5. NUMERICAL RESULTS OF THE TWO-DIMENSIONAL SUPER-CAVITATING CASCADE

As shown in the flow charts of Figures 4 and 5 the first step in the numerical procedure of the present method is the calculation of the two-dimensional hydrodynamic characteristics of supercavitating cascade.

It is intended that results of trial computation will be compared with existing experimental data [5] and those being currently obtained at David Taylor Naval Ship Research and Development Center (DWTNSRDC). The geometry of a supercavitating propeller Model 3770 designed on the basis of the method developed by DWTNSRDC [1] has therefore been chosen. The profiles of the blades were designed based on a Tulin-Burkart two-term camber with an additional camber to account for a lifting surface correction [10]. Appendix C describes the equations of the two-term camber with some representative coordinates and K, correction factors, including other hydrodynamic design and geometric parameters.

In order to cover a complete matrix of possible effective incidence angles α_e and local cavitation numbers σ_e with J in the 2-D computations, the following procedure is used.

The design cavitation number of Model 3770, based on the ship speed V_a , is chosen to be 0.617. First of all, the local cavitation number σ_v based on $V(= \left\{ (\omega r)^2 + V_a^2 \right\}^{\frac{1}{2}})$ can be calculated at each radial location:

$$\begin{aligned}\sigma_V &= \frac{P_1 - P_c}{\frac{1}{2}\rho V^2} \\ &= \sigma_{Va} \left\{ 1 + (\pi x/J)^2 \right\}^{-1}.\end{aligned}\tag{45}$$

σ_V 's calculated this way are listed in Table C2 of Appendix C.

Strictly speaking, however, the cavitation number to be used for 2-D calculations must be based on the effective upstream flow velocity V_e so that

$$\begin{aligned}\sigma_e &= \frac{P - P_c}{\frac{1}{2}\rho V_e^2} = \frac{P - P_c}{\frac{1}{2}\rho V_a^2} \left(\frac{V_a}{U_1} \right)^2 \left(\frac{U_1}{V_e} \right)^2 \\ &= \sigma_{Va} \left(\frac{V_a}{U_1} \right)^2 \left(1 + \frac{V_c}{V_e} \right)^2\end{aligned}$$

where V_a/U_1 and V_c/V_e are calculated from Equations (32) and (21), respectively. As a matter of fact, these σ_e 's have been used in the present propeller computations.

From the flow angles β , blade setting angles β_g and speed coefficient J , the geometric incidences angles α_g can be calculated to estimate the initial values for α_e . Since β_g is shown in the Table C1 of Appendix C and β is calculated from:

$$\beta = \tan^{-1}(J/\pi x),\tag{46}$$

α_g is easily obtained and is tabulated in Table C3.

It is seen from Table C3 that the maximum and minimum values of α_g are 21.11 degrees and 2.06 degrees at $x=0.3, J=0.3$ and $x=0.9, J=0.7$, respectively. The range of cavitation number based on V in Table C2 is found to be 0.0069 to 0.2194. Based on these values it was decided to calculate the 2-D s/c cascade characteristics at four different incidence angles, 2, 3, 4 and 6 degrees with a cavitation number ranging from the choking condition to about 0.08. For any other combination of an incidence angle and σ which will arise in the iterative procedure, the 2-D flow characteristics will be extrapolated or interpolated analytically. It is noted that the maximum value of α_e , i. e. 6 degrees does not seem to cover a value of α_g of 21.11 degrees. However, the downwash effect near the hub is so large that the effective angle of attack will be near or within 6 degrees. It is also obvious that no supercavitation occurs at $\sigma = .2194$.

Figures 7(a) thru 7(f) show the calculated lifts C_L normal to the upstream flow as functions of cavitation number σ_e at normalized radius locations, $x=0.4, 0.5, 0.6, 0.7, 0.8$ and 0.9 . The 2-D calculations were left out for the point at $x=0.3$ because the cavitation number is too large and the solidity is too high to obtain convergent solutions in the 2-D computations. In addition, the propeller performance can be accurately calculated without the information at that point by an interpolation scheme as will be seen later.

Two different computer programs (see [4]) were used, one for the choking condition at which the cavity extends downstream to infinity and the

other for the finite cavity case. In these figures we see that a significant cascade effect occurs in cavity flows. In Figure 7(a), for example, where the solidity is small, 0.244, near the tip (at $x = 0.9$) with a stagger angle of 74 degrees, it is seen that the lift coefficient C_L increases as the incidence angle increases. This phenomenon is quite similar to that observed in single lifting foil cases. It means that the solidity of 0.244 at this location with $\gamma = 74^\circ$ is yet too small to see much of a cascade effect and thus the flow is similar to that of a single foil except that the choking phenomenon appears. However, at $x = 0.8$ where the solidity becomes slightly larger, 0.365, with a stagger angle of 72.4 degrees, the lift coefficient C_L at $\alpha_e = 6^\circ$ loses its value as σ becomes small (see Figure 7(b)), until finally its value becomes even smaller than that obtained at $\alpha_e = 4^\circ, 3^\circ$ and 2° . The reason why this occurs at smaller σ 's is obvious: the smaller the cavitation number, the longer and thicker is the cavity (see Figures 10(a) thru 10(f)), so that the cavity boundary with a low cavity pressure is close to the pressure side of the neighboring blade, causing a loss in lift. It is also seen that the cavitation number σ_e at which this change in C_L occurs in Figures 7(a)-(f) checks quite well with the value of σ_e at which the length of cavity starts extending to infinity (choking conditions) as shown in Figures 10. One can also observe a similar behavior in C_L for $\alpha_e = 4^\circ$, occurring here at a smaller σ_e than for the $\alpha_e = 6^\circ$ case. This trend becomes even stronger (see Figures 7(c) thru 7(f)) since the solidity becomes larger increasing from 0.479 to 0.912. In Figure 7(f) where $x = 0.4$ and the largest solidity occurs, the relation between the lift and incidence angle completely flips over for a range of σ_e 's, i. e. the lift is the highest at the lowest incidence angle.

This peculiar behavior for cavitating cascade flow observed above never happens in the cases of single lifting foils. Physically it can be understood and explained as follows. When the solidity becomes large and thus the blades are more closely packed in the cascade configuration, the adjacent blades are strongly affected by the existence of cavity thus causing significant hydrodynamic effects. This effect becomes stronger as the cavity becomes thicker and longer or as the flow incidence angles become larger and the cavitation number becomes smaller as has been seen above.

To our knowledge the above highly nonlinear cascade effect have never been incorporated into supercavitating propeller design. If the lift curves of single supercavitating foils are used for such designs, large discrepancies between the design and experimental data are to be expected. For example, increasing flow incidence angles or, equivalently, increasing blade camber at a radial location of the blade having a relatively large solidity essentially decreases the sectional lift. This results in a smaller thrust coefficient in experiments than expected by design. A totally opposite situation must sometimes be taken; blade angles and camber must be decreased to increase lift depending on the solidity and cavitation number. This may be one of the reasons why the experimental thrust and torque coefficients of NSRDC Model 3770 were found far short of the design values based on single foil predictions. More detailed discussions about this point will be made in the

next section.

It is interesting to compare the lift coefficients obtained in the present nonlinear cascade theory and those of supercavitating single foils. The latter values at $\sigma_e = 0$ are easily computed from the design lift coefficients, correction factors listed in Table C1 and angles of attack:

$$C_{LS0} = C_{L_d} \cdot K + \pi\alpha/2 \quad (47)$$

where the subscripts S and 0 in (47) designate 'single foil' and 'zero cavitation number', respectively. C_{LS0} calculated based on Equation (47) are plotted in each Figure 7(a) through 7(f). It is seen that a well known approximation for finite cavity length by a correction factor $(1 + \sigma)$, commonly used for a single foil flow, cannot be applied to the s/c flow in the cascade configuration whatsoever. It is also noted that C_{LS0} 's are much larger than those values extrapolated from the linear portions of C_L curves, again showing a remarkable supercavitating cascade effect on lifting forces.

It is also seen that the choking conditions marked in Figures 7(a) through 7(f) vary to a great degree depending on the solidity. With small solidity and a small incidence angle, the choking flow does not occur until σ_e becomes fairly small, say 0.007 (see Figure 7(a)), while a σ_e of 0.041 is enough to cause the same condition for a large solidity and a large angle of attack (see Figure 7(f)). This behavior is also attributable to the increasing cascade blockage effects with increase in solidity and incidence angle.

Figures 8(a) through (f) show drag coefficients parallel to the upstream flow direction, each corresponding to Figure 7(a) through (f), respectively. It is seen that these drag forces also exhibit a trend similar to that of the lift coefficient.

The lift and drag coefficients shown in these figures will be used later in propeller analysis to calculate thrust and torque coefficients by using the formulae in Equations (43) and (44). The information which now connect the 2-D theory to the propeller lifting line theory are those about the circulation, Γ . Using the computer outputs of the 2-D s/c cascade theory, in particular the flow deflection angle, α_2 and U_2/V_e , we calculated Γ 's and plotted them in Figures 9(a) to (f). Equations (10) and (11) are used for Γ 's of the infinite and finite cavity cases, respectively. The numbers read out from these figures are used as input data to a computer program for s/c propellers.

Finally, Figures 11(a) through 11(f) show lift-to-drag ratios (L/D) as a function of lift. It is interesting to see that the values of L/D are less sensitive to cavitation number (or $C_{L\ell}$ in the figures) and solidity as long as incidence angles and other parameters remain constant. This indicates that a blade section having a good L/D value as a single foil with an infinitely long cavity is also guaranteed to have a good L/D at finite cavity lengths in a cascade configuration. This fact also seems to explain the good correlation, obtained in the efficiency of the 3770 propeller, between experimental data and design data, while the thrust and torque coefficients are way off as already discussed.

The numerical computations presently carried out with the two-dimensional supercavitating cascade programs are a most time-consuming and difficult part during the present analysis. In particular, such flow configurations as having large solidity with large stagger angles and large incidence angles cause numerical instabilities in the functional iterative procedure as was pointed out in [4]. In the present case, for example at $x = 0.4$ and $\alpha_e = 6^\circ$, where the solidity is 0.912, the next value of σ to the choking case which could be calculated was $\sigma_e = 0.068$. For any cavitation number between these two points, the numerical procedure failed to obtain a convergent solution. However, other points, where $\sigma > 0.068$, were calculated without any difficulties and these points have been smoothly connected by a curve as shown in Figure 7(f). The error incurred in this way is not considered to be significant in the present analysis. For all other cases, convergent solutions were obtained at almost equally spaced values of σ_e . Execution time to obtain a convergent solution at each data point was about 150 seconds with CDC 6600 and about 40 seconds with CDC 7600. About sixty data points were computed to generate the present 2-D s/c cascade data, so that a total of 2400 seconds of computer time was used with the CDC 7600 or equivalently 9000 seconds with the CDC 6600.

6. CALCULATIONS OF PROPELLER PERFORMANCE FOR NSRDC MODEL 3770 SUPERCAVITATING PROPELLER

Based on the mathematical formulation and numerical procedures described in the precedent sections, a computer program has been written for calculating K_T , K_Q and (thrust, torque coefficients and efficiency) of supercavitating propellers. (A complete listing of the computer program and input-output data manual are given in Appendix D).

The 2-D s/c cascade data for the 3770 propeller have been already prepared for propeller analysis. By taking five discrete radial points on the blade, i. e., $x = 0.4, 0.6, 0.7, 0.8$ and 0.9 , the propeller hydrodynamic characteristics have been calculated. The cavitation number, σ_{Va} and speed coefficient, J , of the 3770 propeller at the design point are 0.617 and 0.44 , respectively (see Table 1 of Reference 5). First of all we calculated K_T , K_Q and η at this point and show the results in Table 2 in comparison with design and experimental data taken from Reference 5 (also see Figure 12). It is clearly seen that the present method predicts them well, in particular, thrust coefficient K_T , and efficiency η particularly, i. e. within 4 percent of the experimental data. There exists a large discrepancy in K_T and K_Q between the design data and experiment which use about 15 and 11 percent, respectively, although the η there is close to others. The reason for this discrepancy has already been explained in the previous sections; the data basis for the present method depends on the supercavitating cascade theory whereas the design method depended on an infinite cavity, single foil theory.

This point will become even more clear when we compare some of blade sectional characteristics between the two methods. Four different parameters are shown in Table 3 for comparison. These include local cavitation number, effective flow incidence angle, downwash angle and lift coefficients. The local cavitation numbers of the present method shown in the table are those corrected on the basis of the cavity thickness data from the 2-D cascade calculations (see Equation (21)), whereas those of all design methods are simply based on $V = ((\omega r)^2 + V_a^2)^{\frac{1}{2}}$.

The discrepancies shown in all these parameters of Table 3 are quite large and it is again considered that they are attributable to the differences in the force characteristics used by the two different methods as was mentioned before. Among others, it is seen that one of the most significant differences exists in downwash α_i angles and thus effective flow incidence angles α_e , the latter in the design method are all about 2 degrees whereas the former range from 6.8 degrees to 4.6 degrees. The local lift coefficients near the hub predicted by the present methods are larger than those of the design method but become smaller as one proceeds toward the propeller tip. A question now arises why the thrust and power coefficients predicted here are smaller than those of the design method. It is simply answered that lift forces near the tip are more contributory to K_T and K_Q due to the smaller pitch and larger radius as will be readily seen from Equations (34) and (36).

It is interesting to investigate the boundary between the supercavitating and partial cavitating regimes of propeller operation. According to the

2-D s/c cascade data regarding the length of cavity, shown in Figures 10(a) to (f), it reads that the propeller blade at $x = 0.4$ is partially cavitating or fully wetted if $\alpha_e = 2.06^\circ$ and $\sigma = .0656$ obtained by the design method are true (see Figure 10(f)). With $\alpha_e = 6.8^\circ$ and $\sigma = .0798$ at $x = 0.4$ predicted by the present method, the length of cavity is about 1.1 chord length which means that the propeller barely stays in a supercavitating regime. Unfortunately, no clear photographic evidence of 3770 is available for us to check this feature. In any case, it is strongly recommended that not only force data but also photographic data at each measurement point be taken for any future supercavitating propeller experiments. The former will justify the overall accuracy of a prediction method used whereas the latter will play an important role in verifying a local flow phenomena.

Figure 12 shows K_T , K_Q and η over a range of speed coefficient, J , for the design cavitation number $\sigma_{Va} = .617$. As J is taken close to about 0.5, the calculated α_e and σ_e at $x = 0.4$ become 4.5° and $.097$. Again from Figure 10(f), we can see that the blade near the hub (at $x = 0.4$) under the above conditions is in a partially cavitating region where the present supercavitating propeller theory becomes invalid. It seems this reason that all curves in Figure 12 start showing deflection around such a J .

In Figure 13 we compare the present results with experimental data for $\sigma_{Va} = .500$. It is seen that the correlation for K_T , K_Q and η at such J of 0.44 to .5 is excellent but that the discrepancy starts growing

as J becomes outside the above range of J . The same reason as above explains the discrepancy for large J 's at which a part of the propeller operates at partial cavitating condition.

The reason for the discrepancy for smaller J (say, less than 0.44) is not known at this point. Physically, a decrease of J increases the effective flow angle α_e and decreases local cavitation number σ_e , leading more and more to a local choking condition of supercavitating propeller. From certain values of α_e and σ_e on, neither of these values cannot change. It means that the lift and drag coefficients should reach constant values thus C_T and C_p in Equations (43) and (44) also approach constant values. However, K_T and K_Q are proportional to J^2 and J^3 respectively (see Equations (40) and (41)) so that these values theoretically decreases as J decreases. Experimental data in Figure 13 do not show any of this type of trend at least before $J = 0.4$ whereas the results of the present theory clearly demonstrate the above theoretical argument.

It is also considered that the discrepancy in K_T , K_Q and η for smaller J may be suggestive even for incidence angle correction due to the choking condition of the 2-D cascade theory in addition to the σ -correction. For determining which argument is true, further comparisons of the present theory with existing and possibly new experimental data from supercavitating propellers are urgent.

In order to accurately predict propeller performance for a range of larger J , say 0.51 in this case, the 2-D cascade data based on partial cavitating

conditions must be used. Although a linearized theory for partial cavitating cascade is available, it cannot be applied for the propeller analysis in which the flow there is highly nonlinear. Development of a similar nonlinear theory to that for supercavitating cascade 4 is now in order.

Figure 13 also shows results before we applied the correction method to cavitation numbers (by dotted lines). When J was set at a slightly smaller value than 0.46, in this case, a combination of such α_e and σ put us beyond the choking condition where there exists no 2-D cascade data. By forcing us to find Γ by extrapolation (which seems irrelevant, first of all) we managed to determine K_T , K_Q and η , which are plotted in Figure 13. These values are of course not valid. Without using either cavitation number correction as does the present method or possibly incidence angle correction, it is impossible to avoid this inherent 2-D choking problem in three-dimensional flow applications. It is clearly seen that an adequate treatment of this problem is most crucial in the entire supercavitating propeller analysis as long as a cascade theory is intended to be used.

For the above computations, we have used Newton's iterative procedures which showed a slow but steady convergence. For each run, it took about 30 seconds for a CDC 7600.

7. CONCLUSIONS AND RECOMMENDATIONS

The present method has incorporated a 2-D s/c cascade theory into a propeller lifting line theory with downwash angle correction and cavitation number correction made.

The results obtained from the theory have shown an excellent correlation with experimental data within a certain range of speed coefficient, J , whereas some discrepancy exists outside that range. It is quite clear that the discrepancy for larger, J , is attributable to the appearance of the partial cavitating flow near the hub so that the present theory naturally becomes invalid. That for smaller, J , cannot be clearly explained at this stage as mentioned before.

Furthermore, it has been found that there exists a significantly large difference in local flow conditions between the present theory based on cascade data and design theory based on single foil data. These include downwash flow angles, effective flow angles, cavitation numbers and lift coefficients.

In order to clarify some of the uncertainties having just arisen, the following specific recommendations for future research works to be carried out are made.

- 1) More comparisons between the theory and experiments for different types of propeller

Preceding page blank

configurations such as those in 11 are necessary for verifying the accuracy of the present prediction theory.

- 2) Slightly beyond a range of the largest efficiency or optimum design point, there exists a partially cavitating flow regime. We always have a possibility that s/c propellers sometimes operate at such a regime. In order to cover a full range of performance prediction for s/c propellers, it is advisable to develop a non-linear partially cavitating cascade theory and to incorporate the data from such a theory into the present method.
- 3) Although the two-dimensional supercavitating cascade theory [4] used here was compared well with experimental data before, such a comparison was very much limited due to the lack of experimental data. It is recommended that more experiments be conducted, in particular for a range of high solidity and high stagger angle.
- 4) A more rigorous evaluation of the effects of propeller cavity thickness on cavitation

number and possibly on local flow angle
may be necessary.

Finally, it is concluded that cascade and three-dimensional effect of supercavitating propellers plays a most crucial role in their hydrodynamic performance. In cooperation of this effect into both prediction and design methods for such propellers is unavoidable.

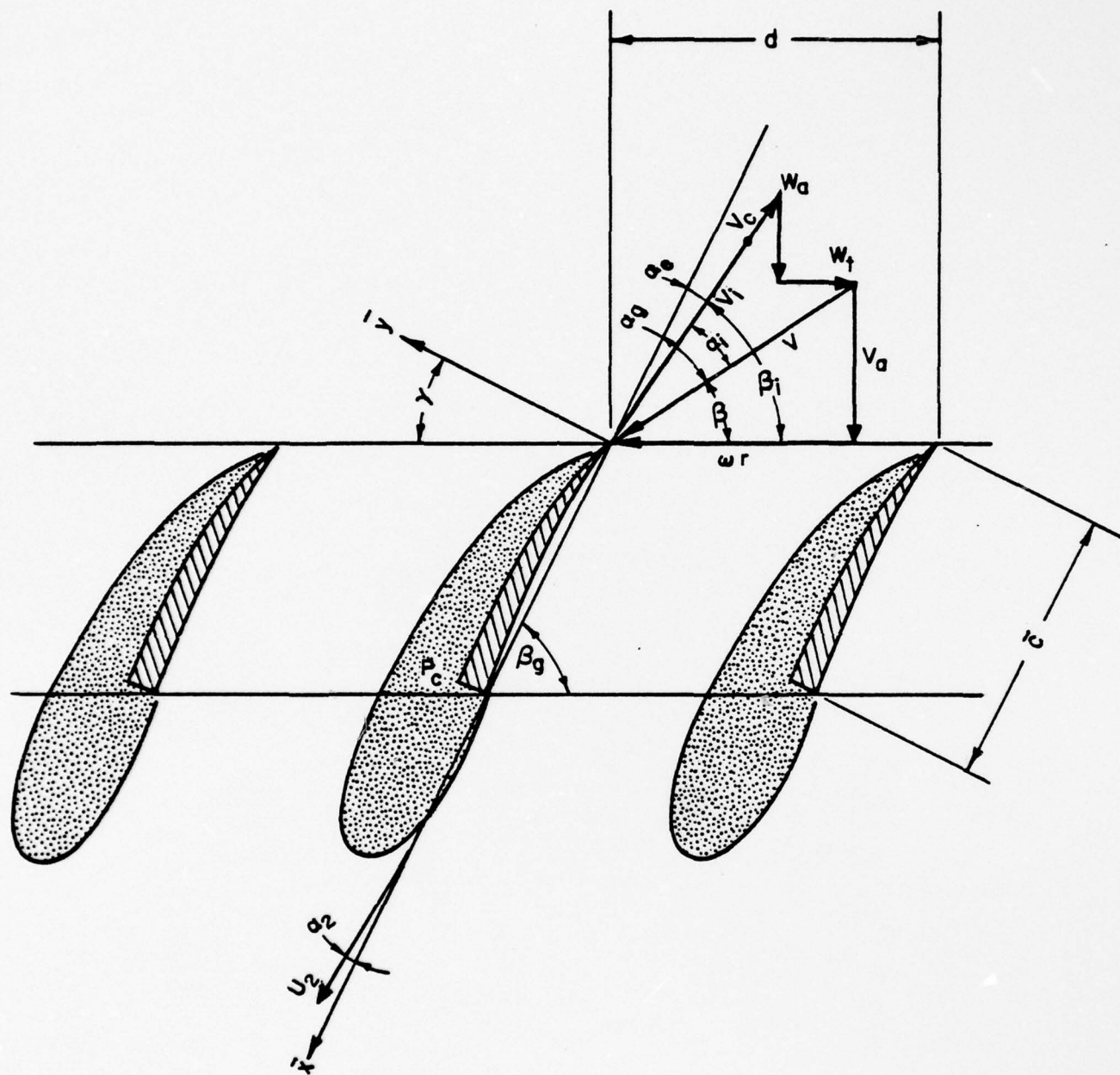


Figure 1 Flow Configuration in Cascade Geometry of Propeller at a Constant Radius r with Velocity Diagram.

Preceding page blank

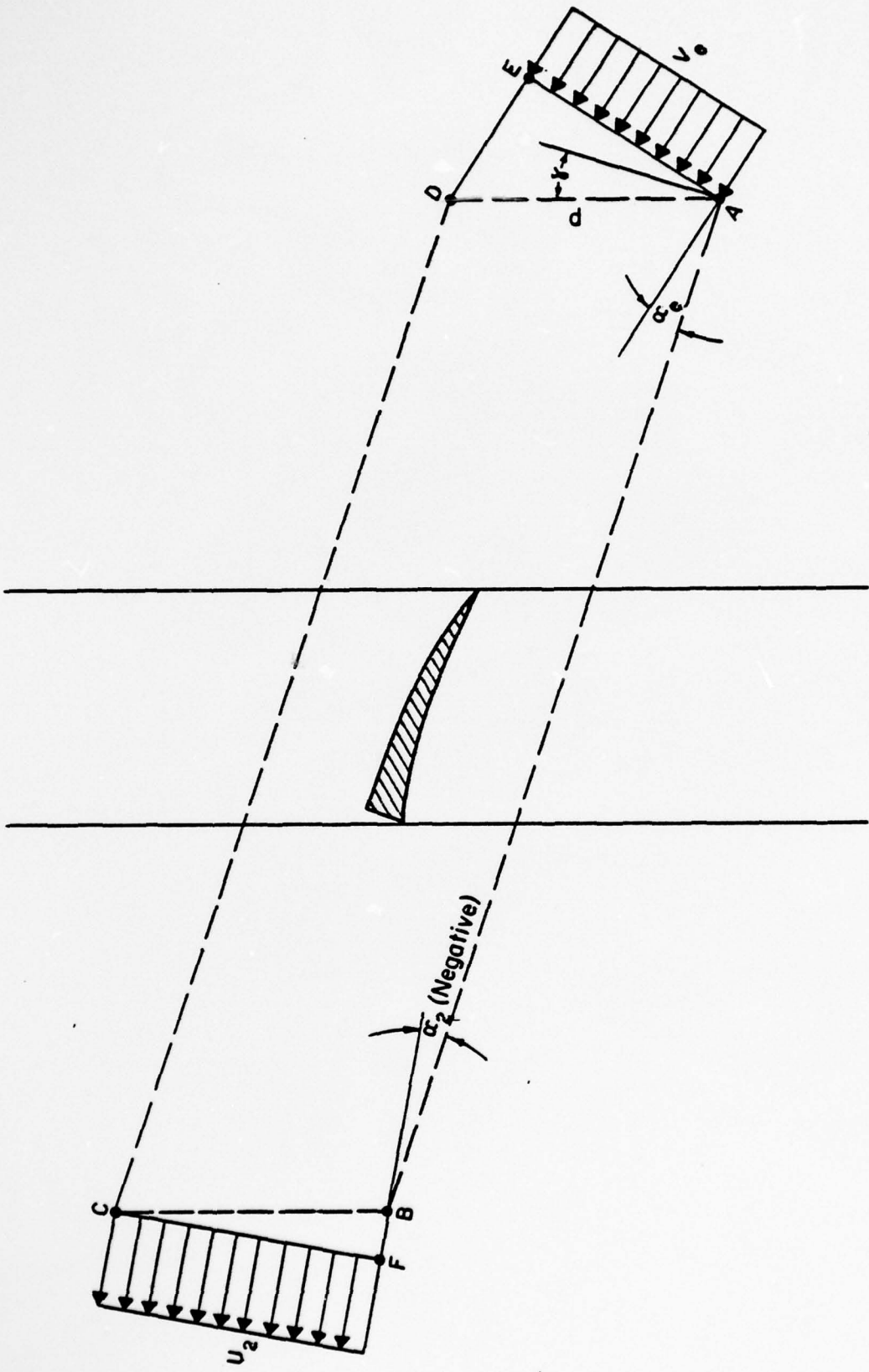


Figure 2 Change of Circulations Γ in Cascade Flow.

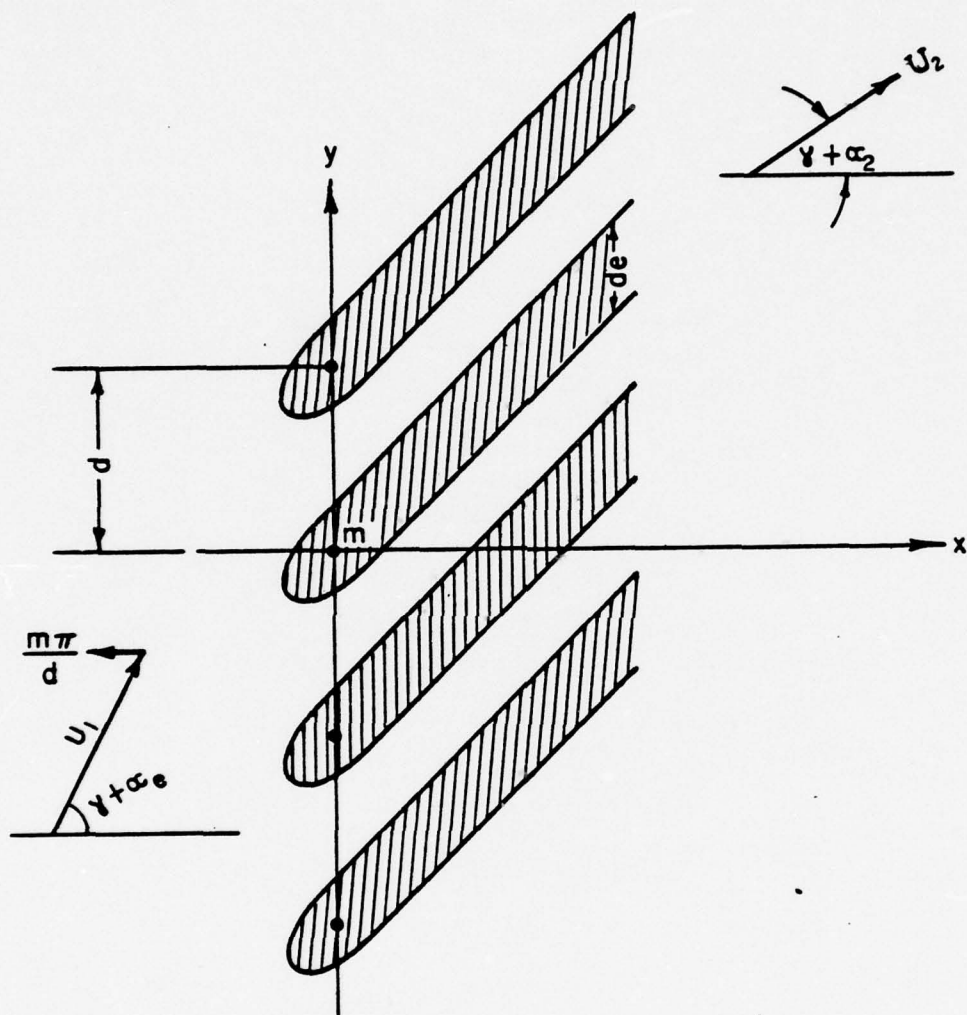


Figure 3 Representation of Cavity Thickness by Distribution of Source Singularities in a Cascade Row.

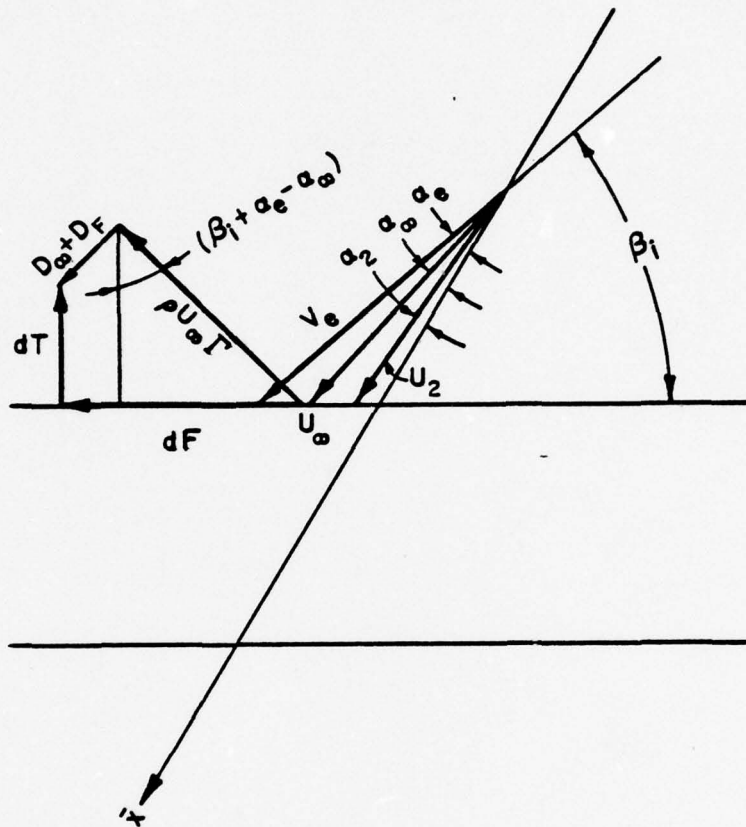


Figure 4 Geometric Mean Angle α_{∞} , Force Normal to Geometric Mean Velocity U_{∞} in Cascade Flow and Thrust and Torque Components.

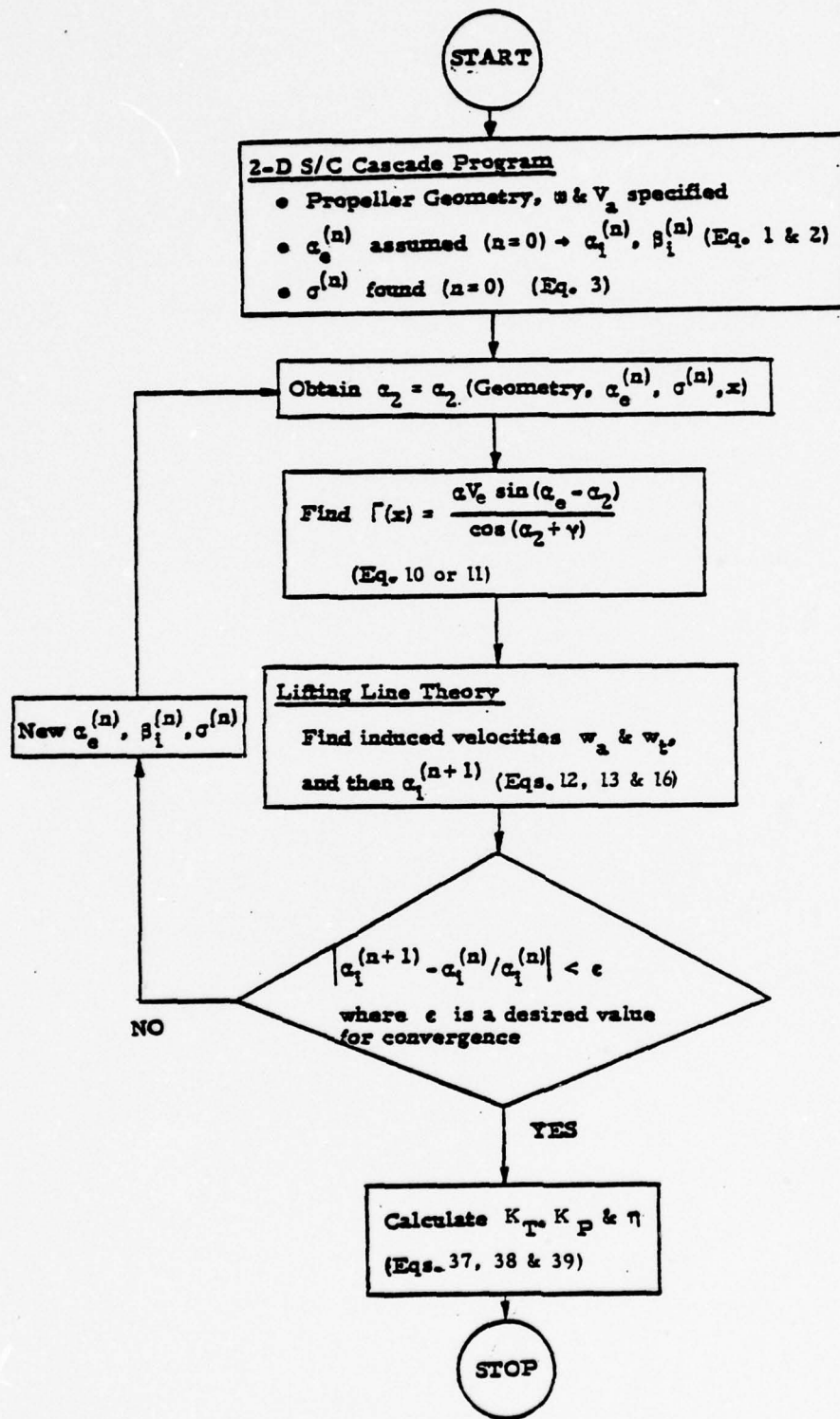


Figure 5 Flow Chart of Substitution Procedures Iterative

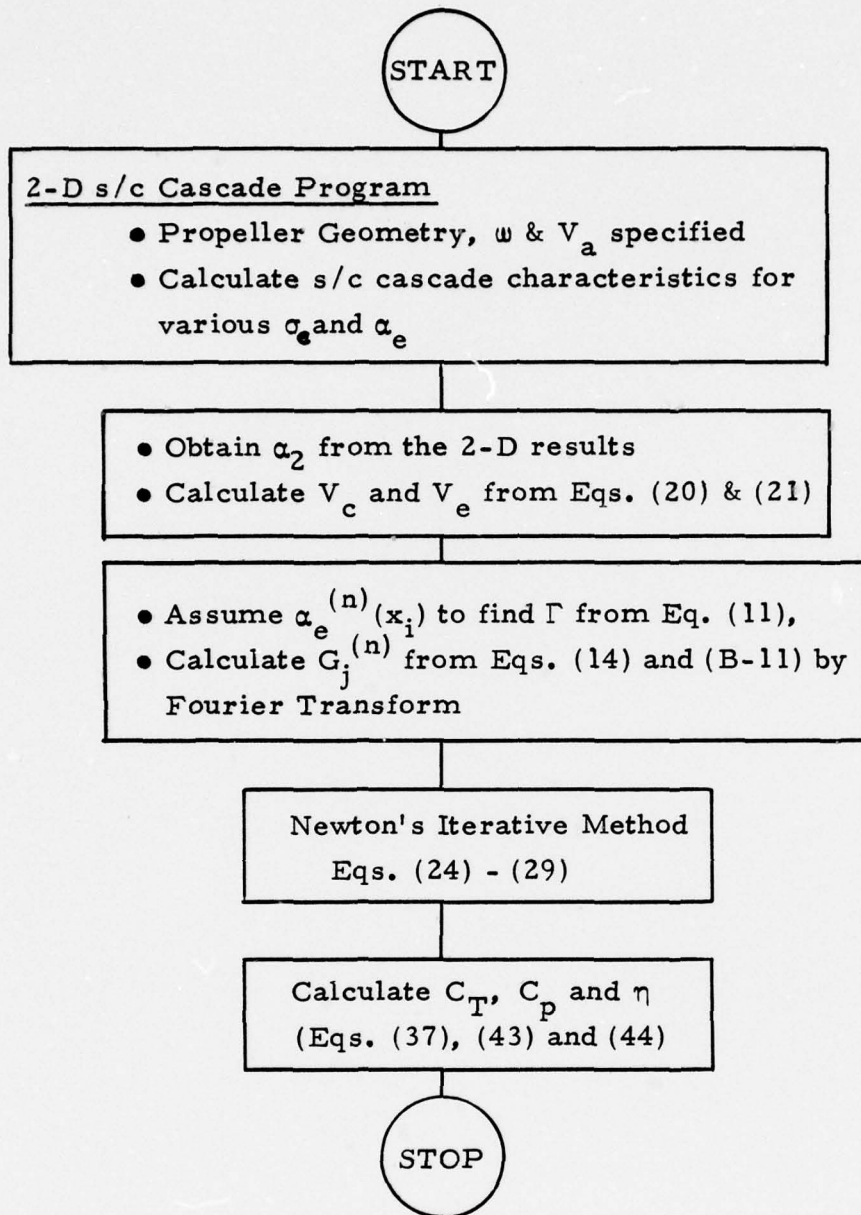


Figure 6 Flow Chart of Newton's Iterative Procedures

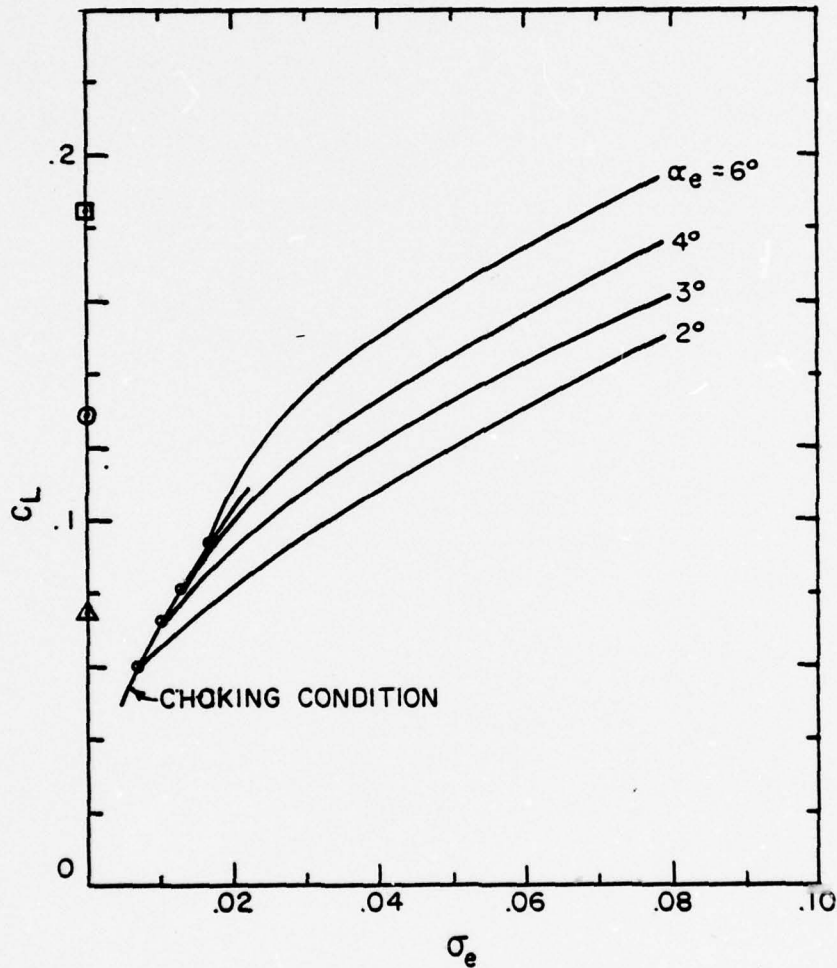


Figure 7(a) Lift Coefficient C_L Normal to the Upstream Velocity vs. Cavitation Number σ for Incidence Angles $\alpha_e = 2^\circ, 3^\circ, 4^\circ$ and 6° at the Blade Span-wise Location of $x = 0.9$ where the Solidity is 0.244 and geometric stagger angle γ is 74.03° . $\Delta \odot \square$ are C_L Values of $\alpha_e = 2^\circ, 4^\circ, 6^\circ$ Respectively Calculated from a Linearized Theory for a Single Foil (Equation 47).

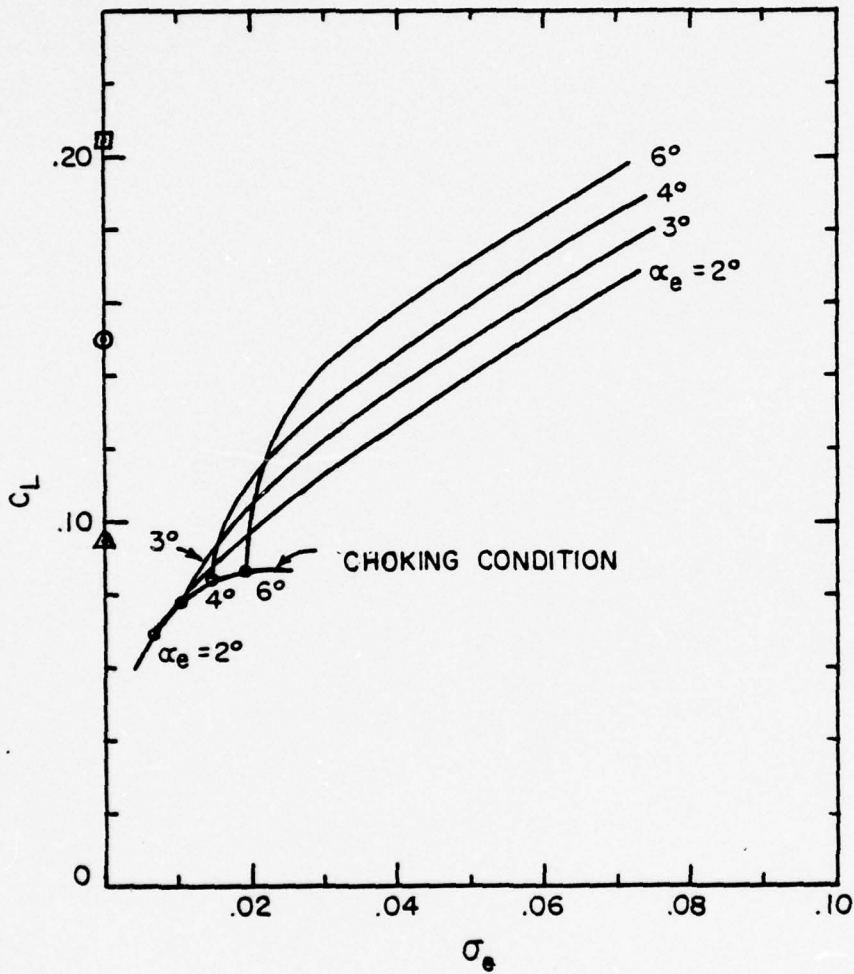


Figure 7(b) The Same as Figure 7(a) Except That $x = 0.8$ where the Solidity is 0.365 and γ is 72.40° .

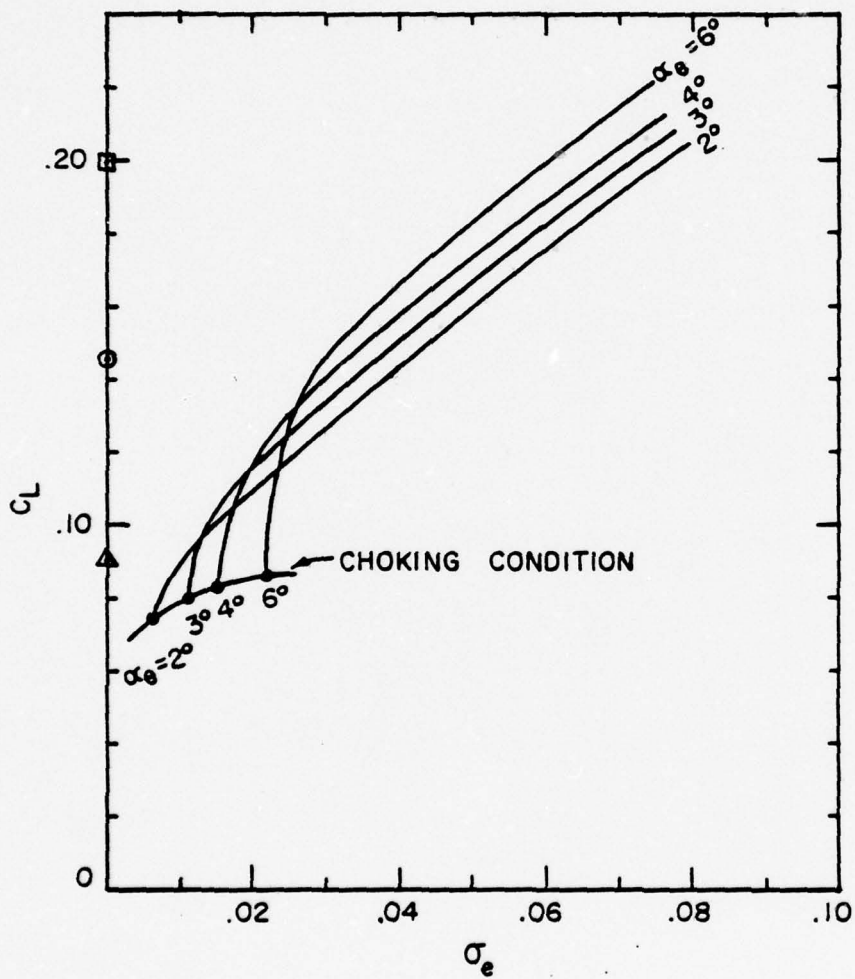


Figure 7(c) The Same as Figure 7(a) Except That $x = 0.7$ where the Solidity is 0.479 and γ is 70.33° .

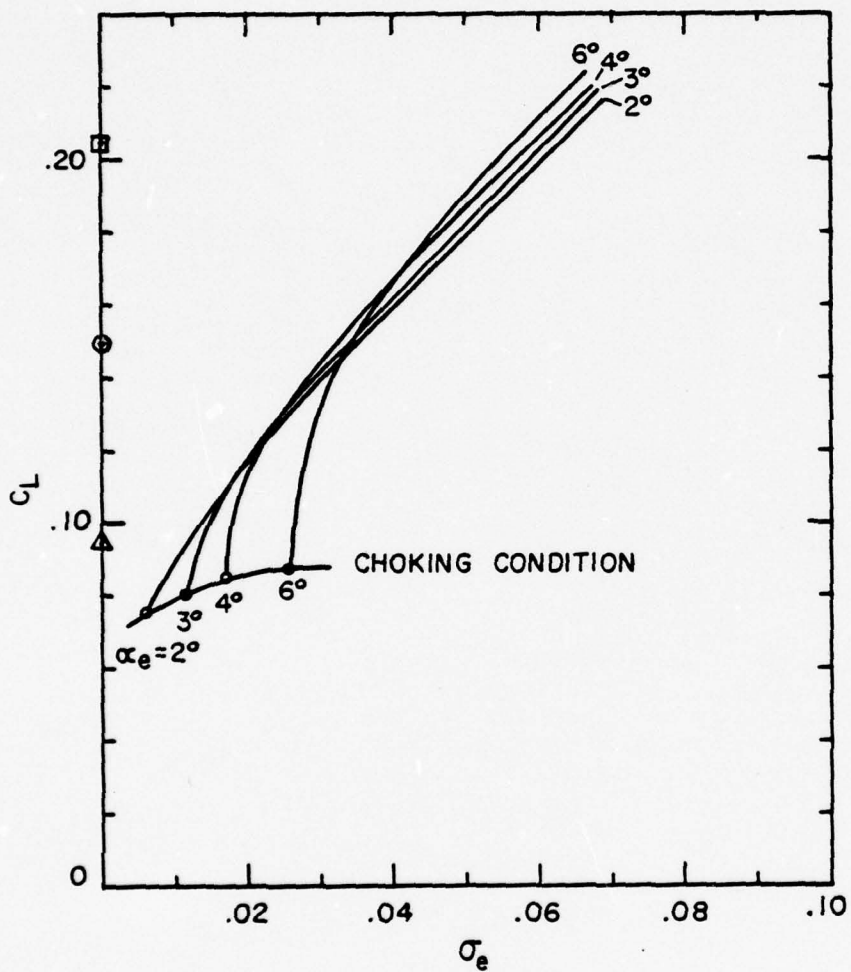


Figure 7(d) The Same as Figure 7(a) Except That $x = 0.6$ where the Solidity is 0.594 and γ is 67.61° .

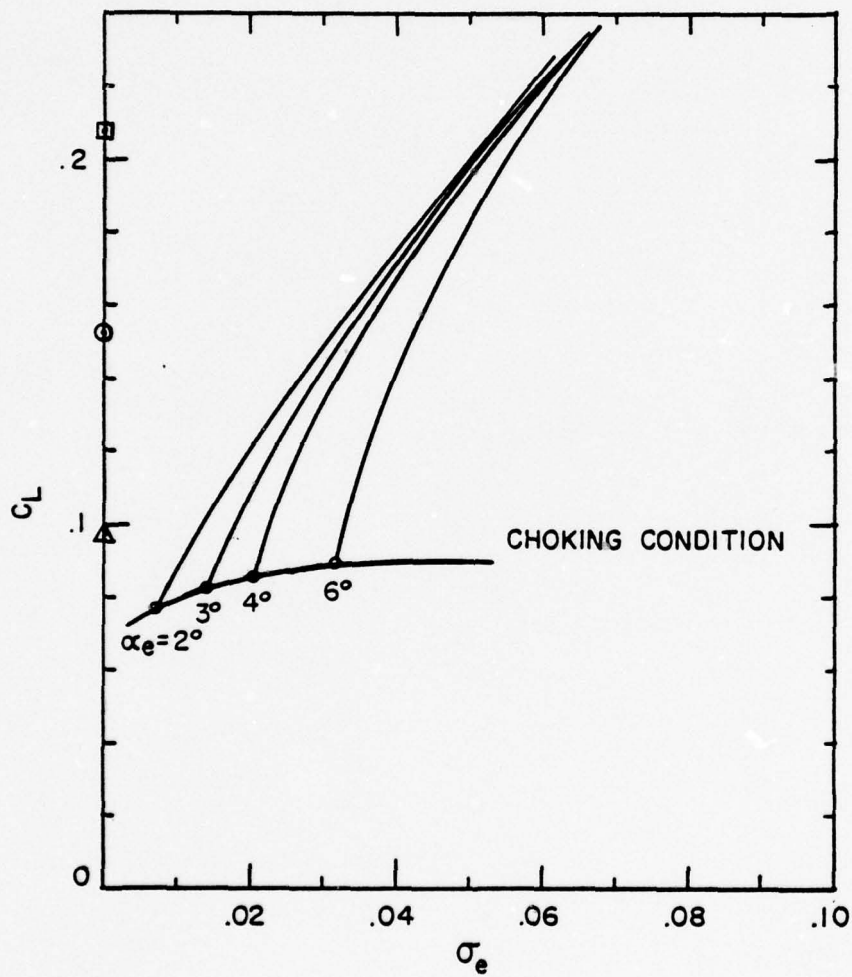


Figure 7(e) The Same as Figure 7(a) Except That $x = 0.5$ where the Solidity is 0.728 and γ is 63.94° .

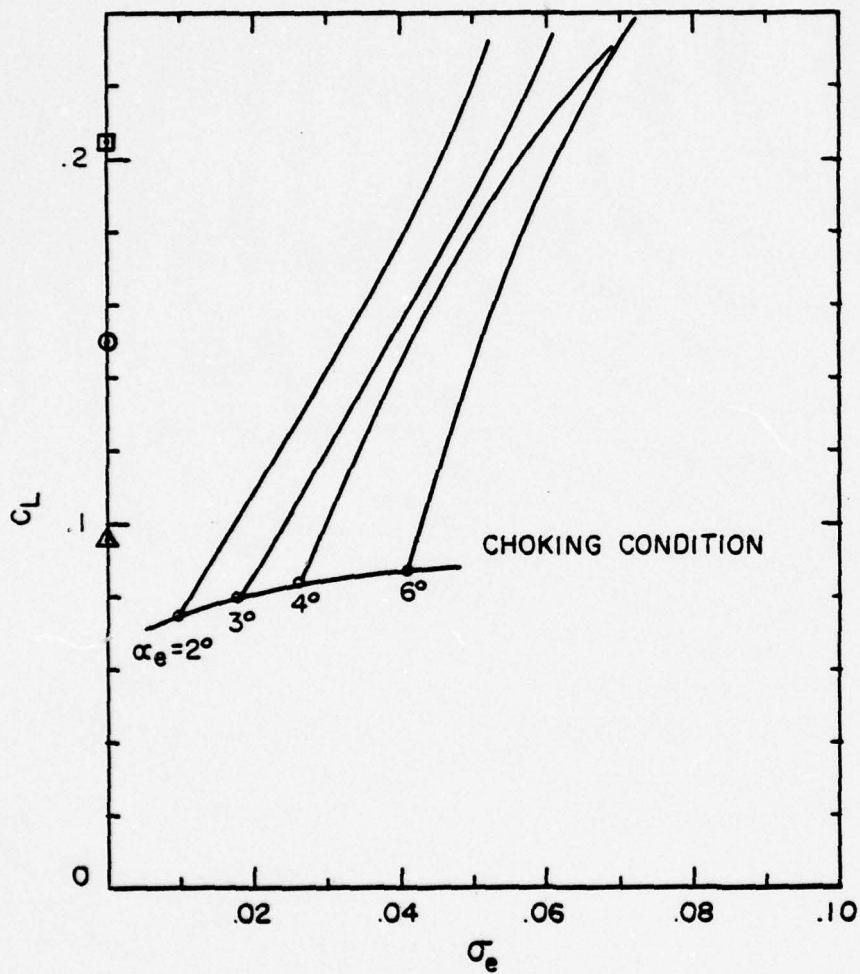


Figure 7(f) The Same as Figure 7(a) Except That $x = 0.4$ where the Solidity is 0.912 and γ is 58.77° .

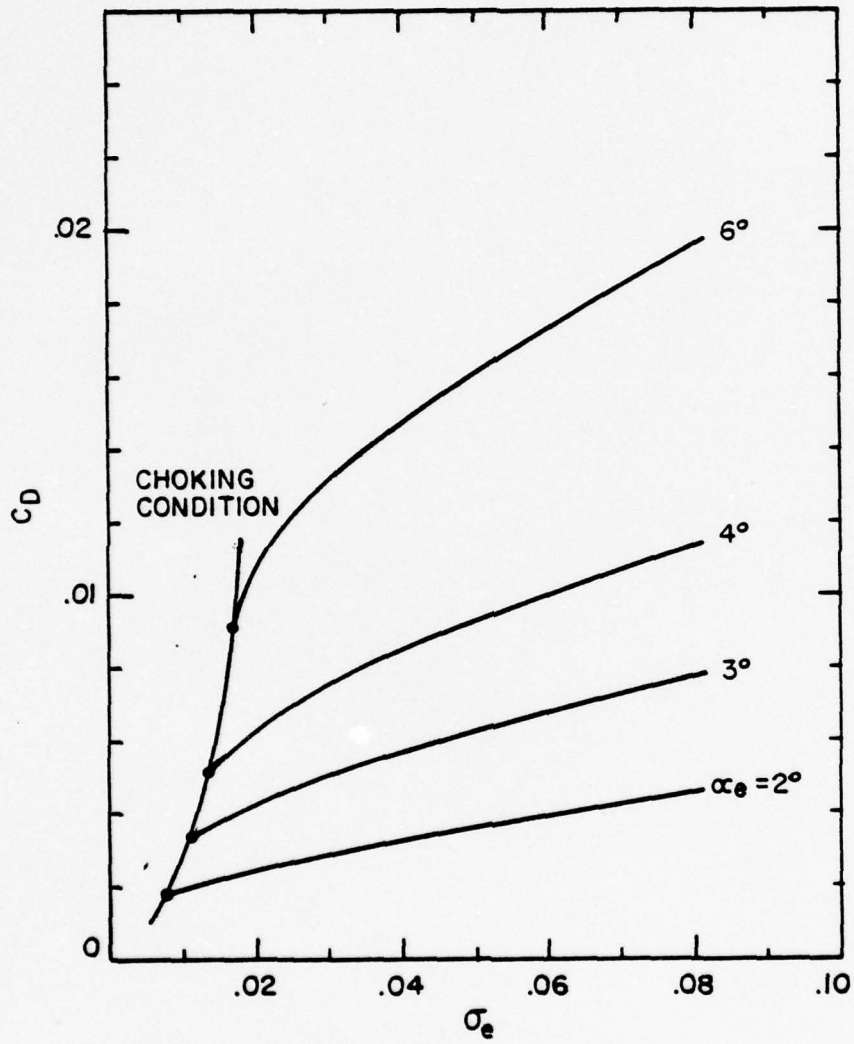


Figure 8(a) Drag Coefficient C_D Corresponding to Figure 7(a) ($x = 0.9$).

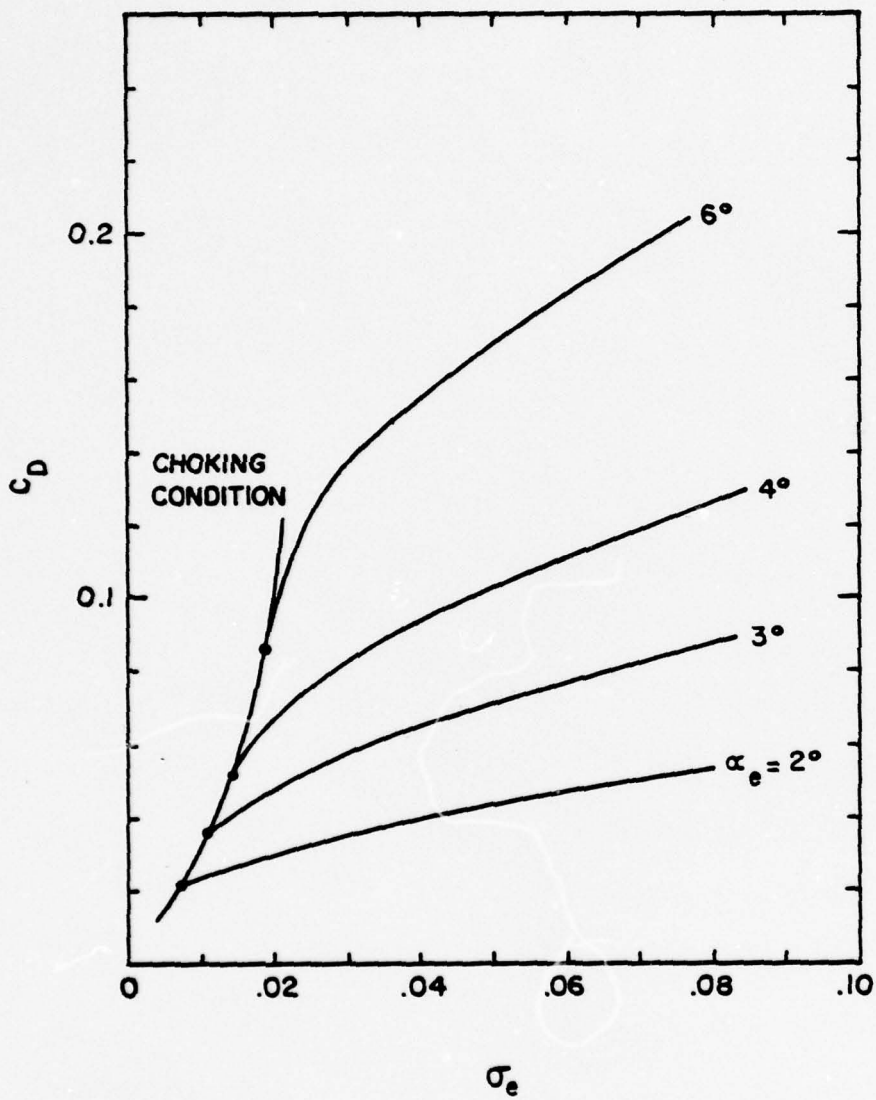


Figure 8(b) Drag Coefficient C_D Corresponding to Figure 7(b) ($x = 0.8$).

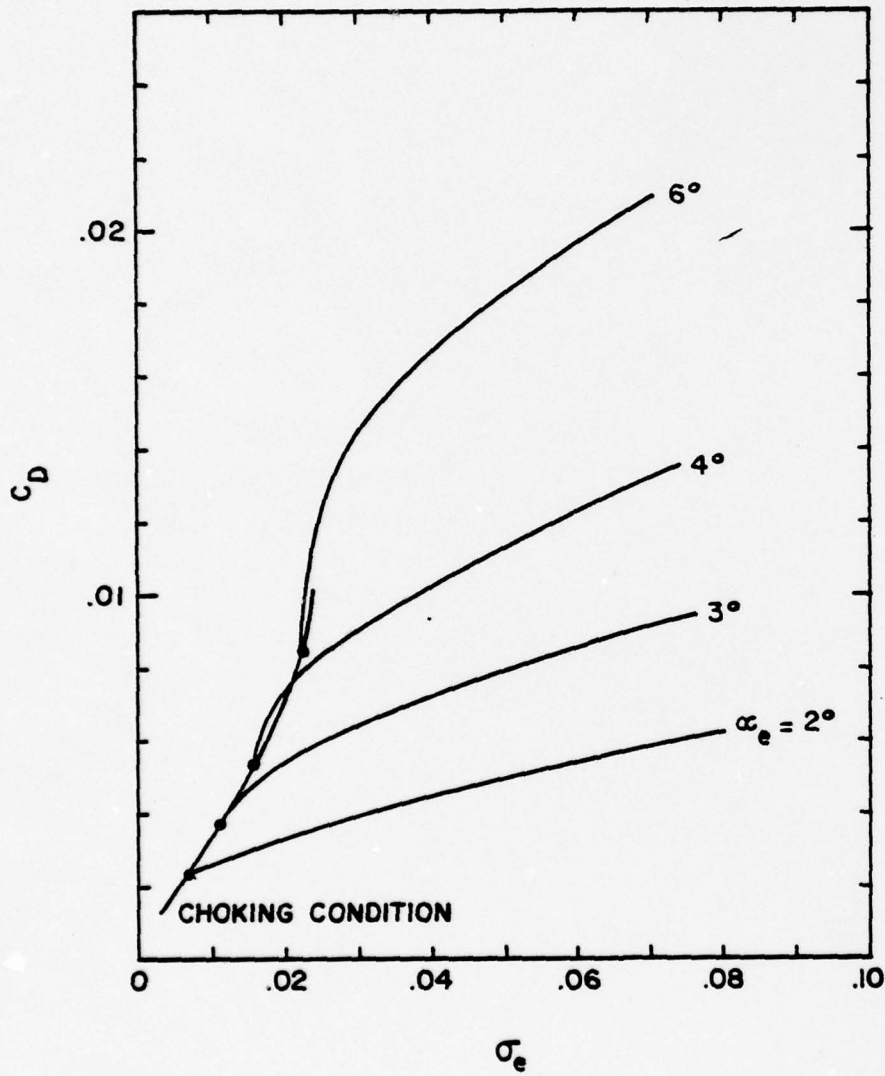


Figure 8(c) Drag Coefficient C_D Corresponding to Figure 7(c) ($x = 0.7$).

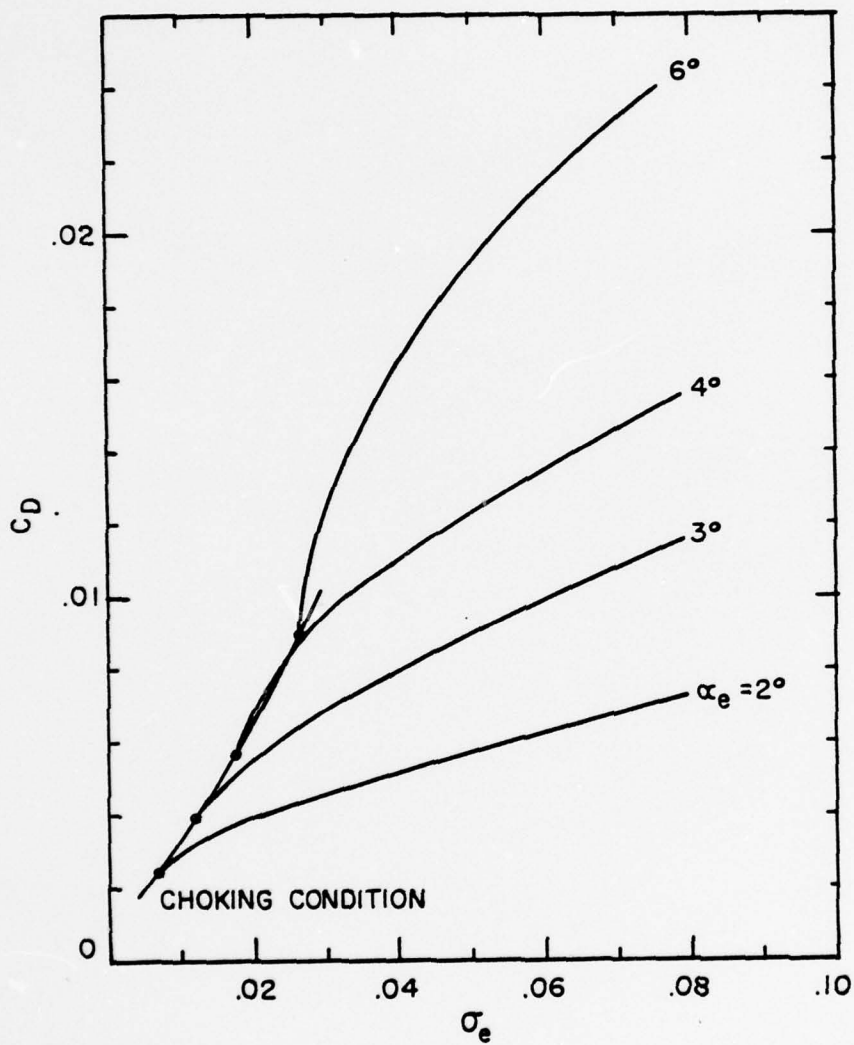


Figure 8(d) Drag Coefficient C_D Corresponding to Figure 7(d) ($x = 0.6$).

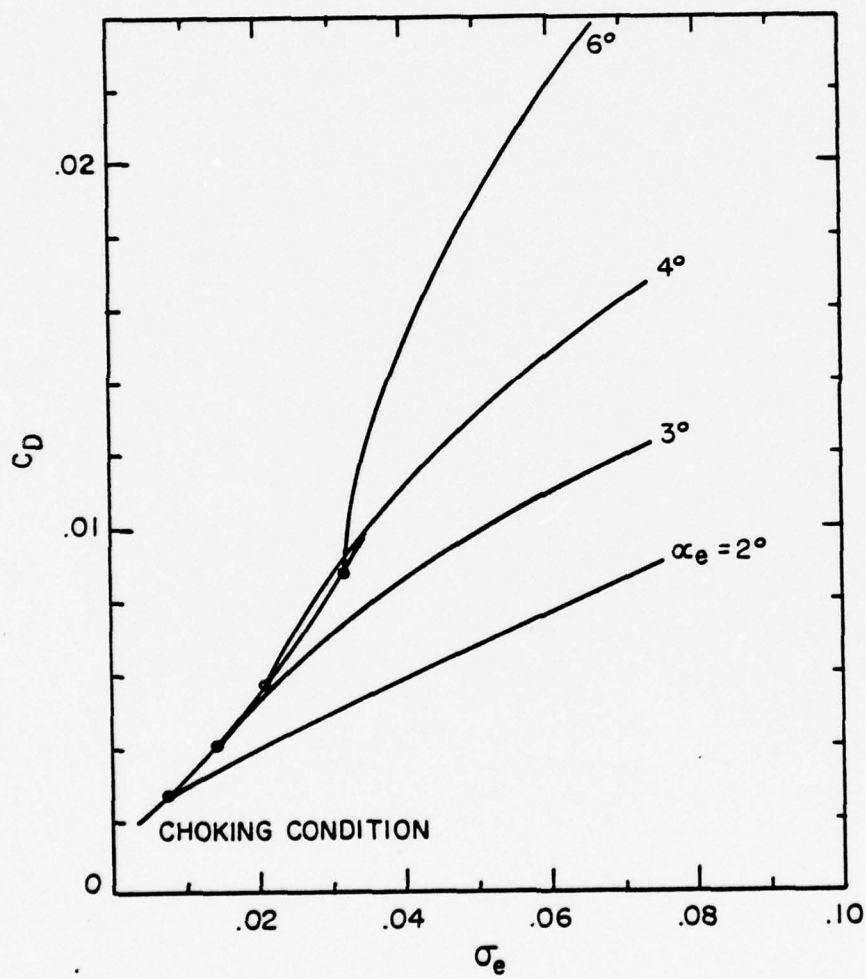


Figure 8(e) Drag Coefficient C_D Corresponding to Figure 7(e) ($x = 0.5$).

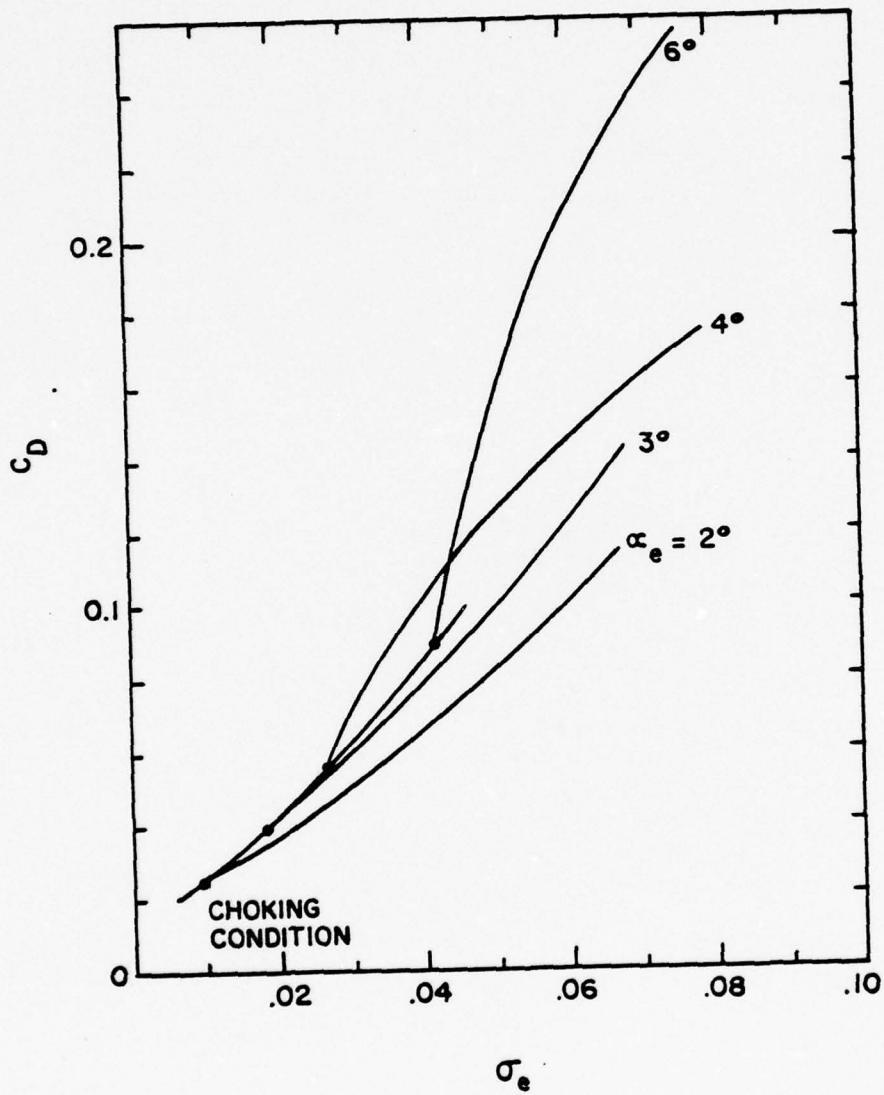


Figure 8(f) Drag Coefficient C_D Corresponding to Figure 7(f) ($x = 0.4$).

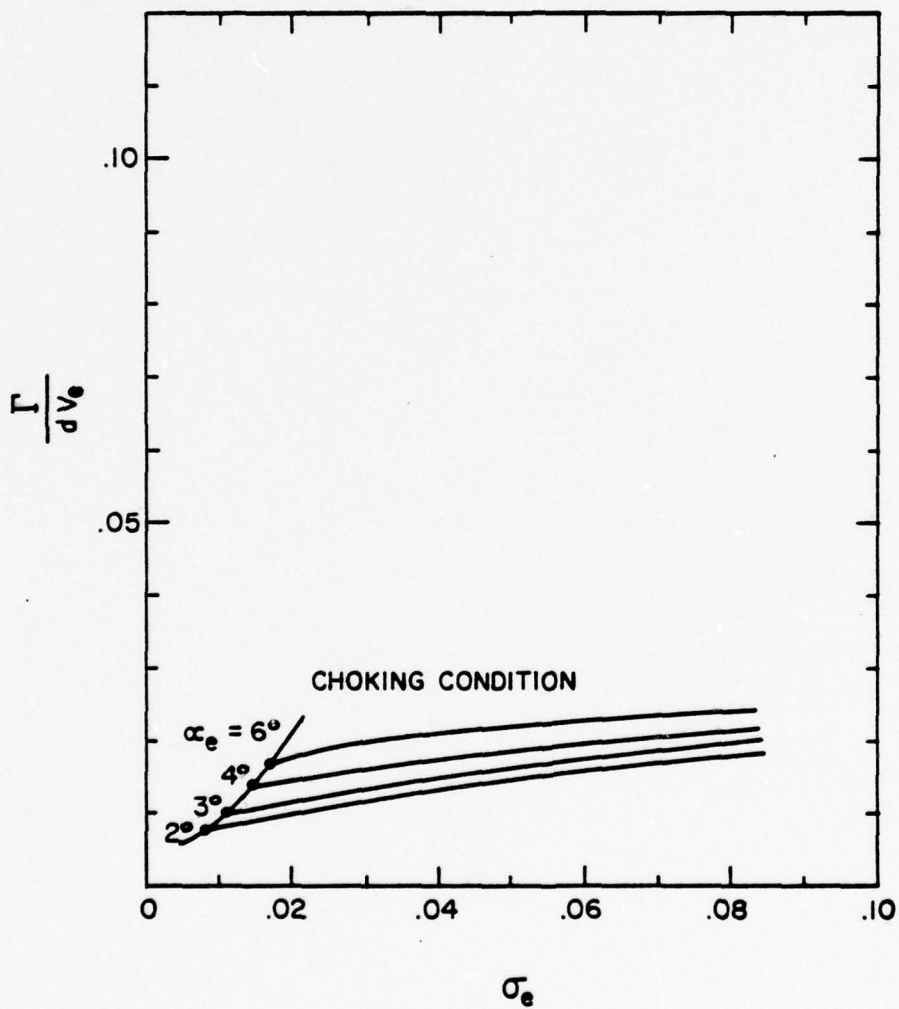


Figure 9(a) Normalized Circulation Γ/dV_e vs. σ_e
 Corresponding to Figure 7(a) ($x = 0.9$).

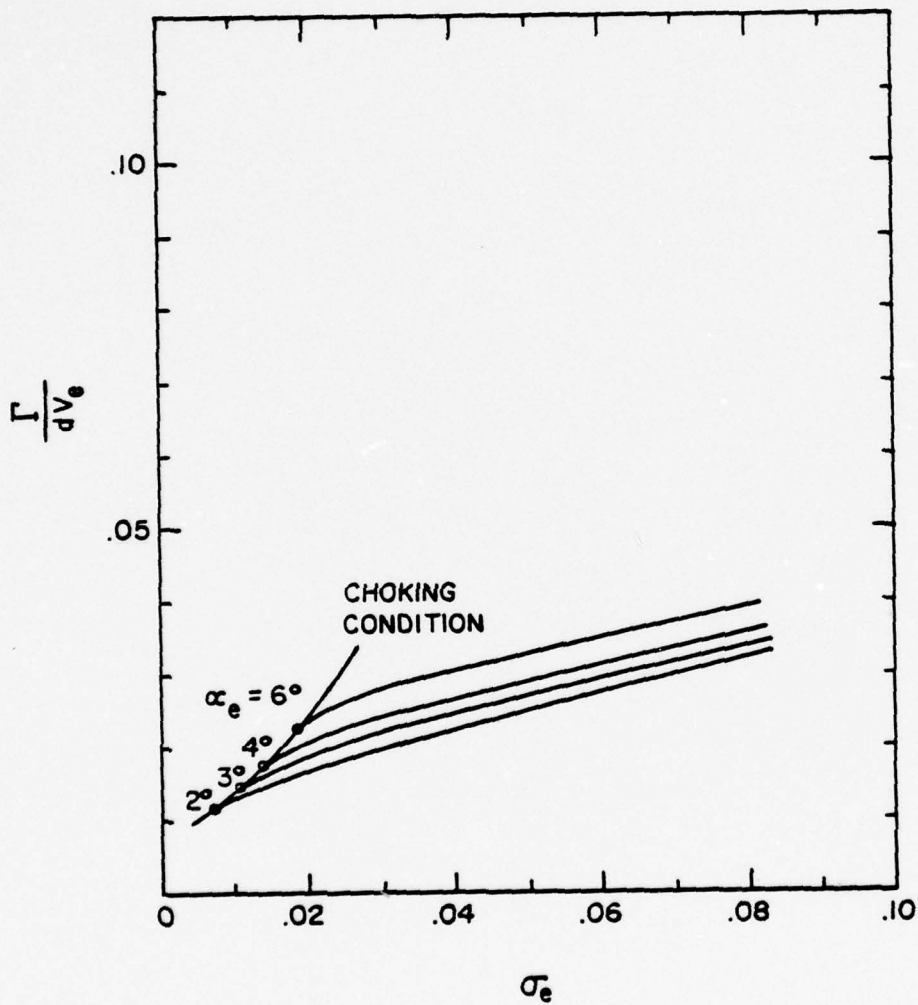


Figure 9(b) Γ/dV_e vs. σ_e Corresponding to Figure 7(b)
($x = 0.8$).

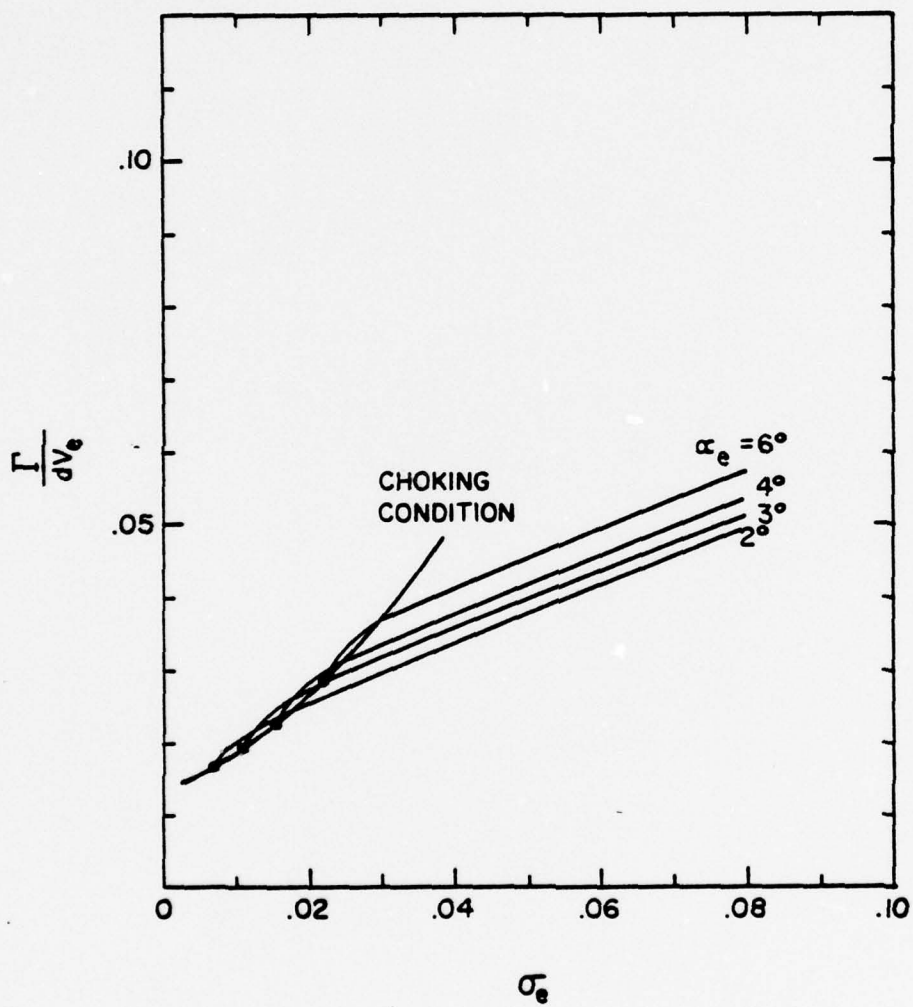


Figure 9(c) Γ/dV_e vs. σ_e Corresponding to Figure 7(c)
($x = 0.7$).

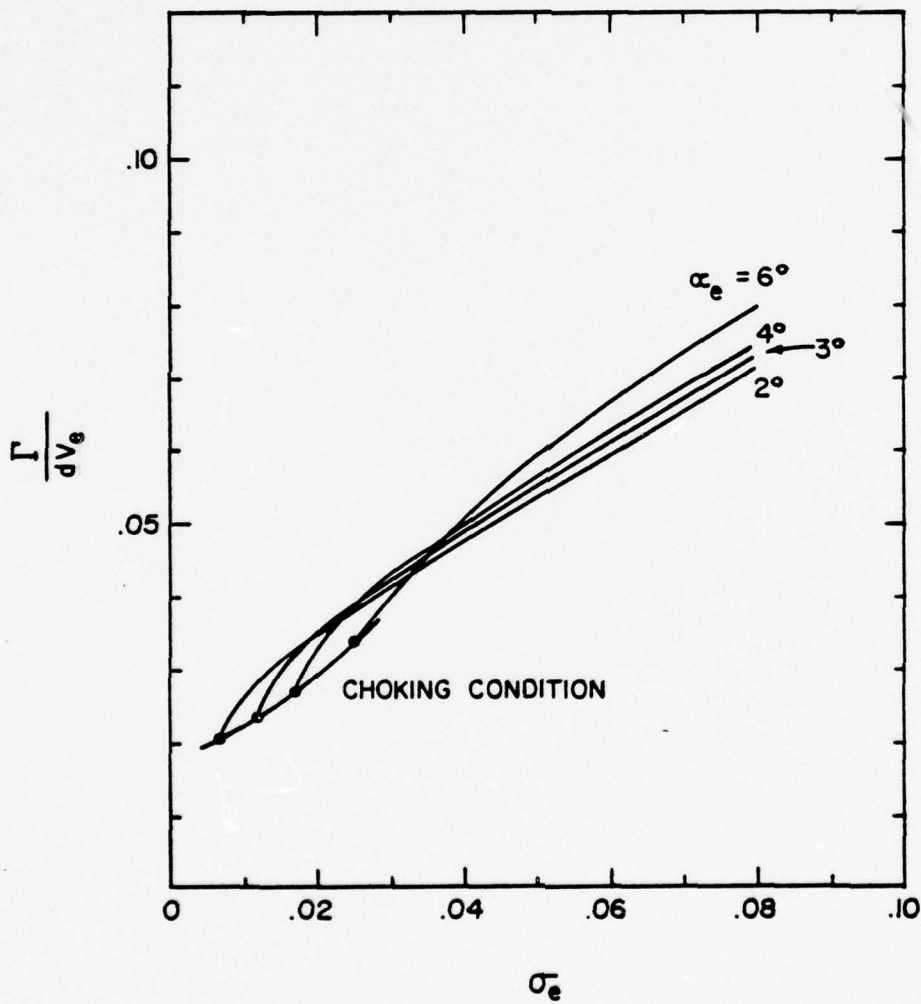


Figure 9(d) Γ/dV_e vs. σ_e Corresponding to Figure 7(d)
($x = 0.6$).

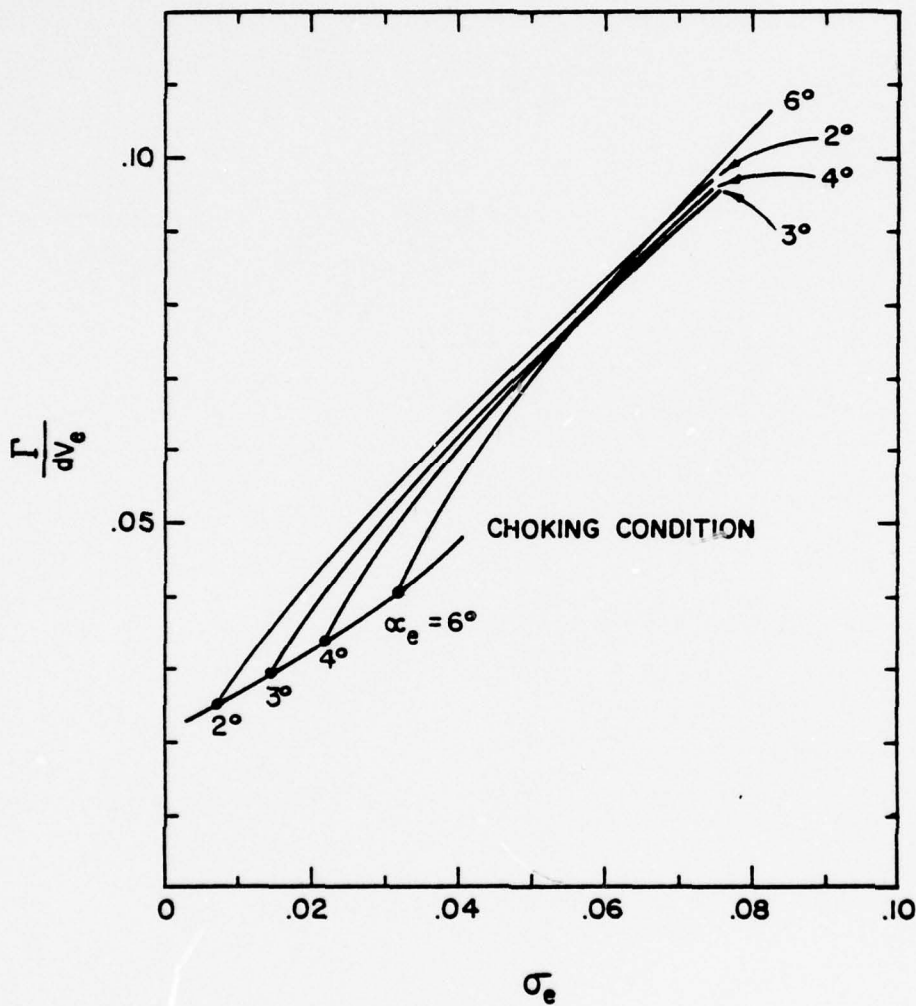


Figure 9(e) Γ/dV_e vs. σ_e Corresponding to Figure 7(e) ($x = 0.5$).

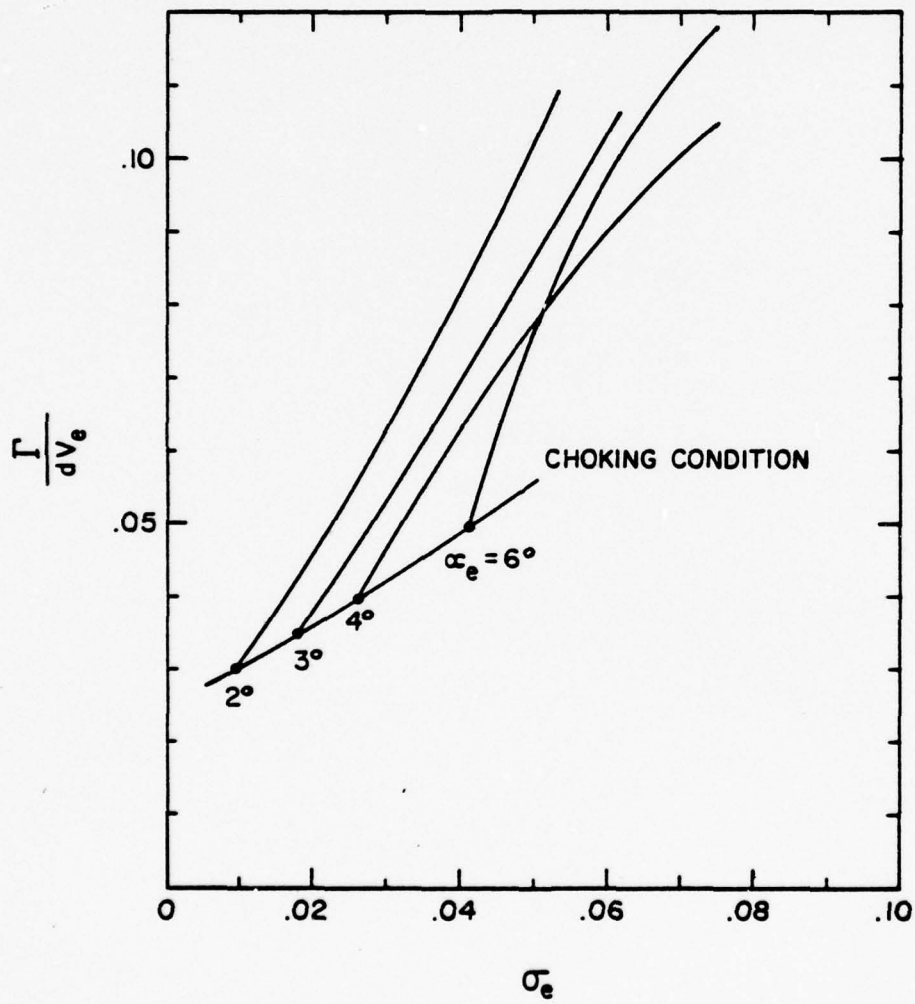


Figure 9(f) Γ/dV_e vs. σ_e Corresponding to Figure 7(f)
($x = 0.4$).

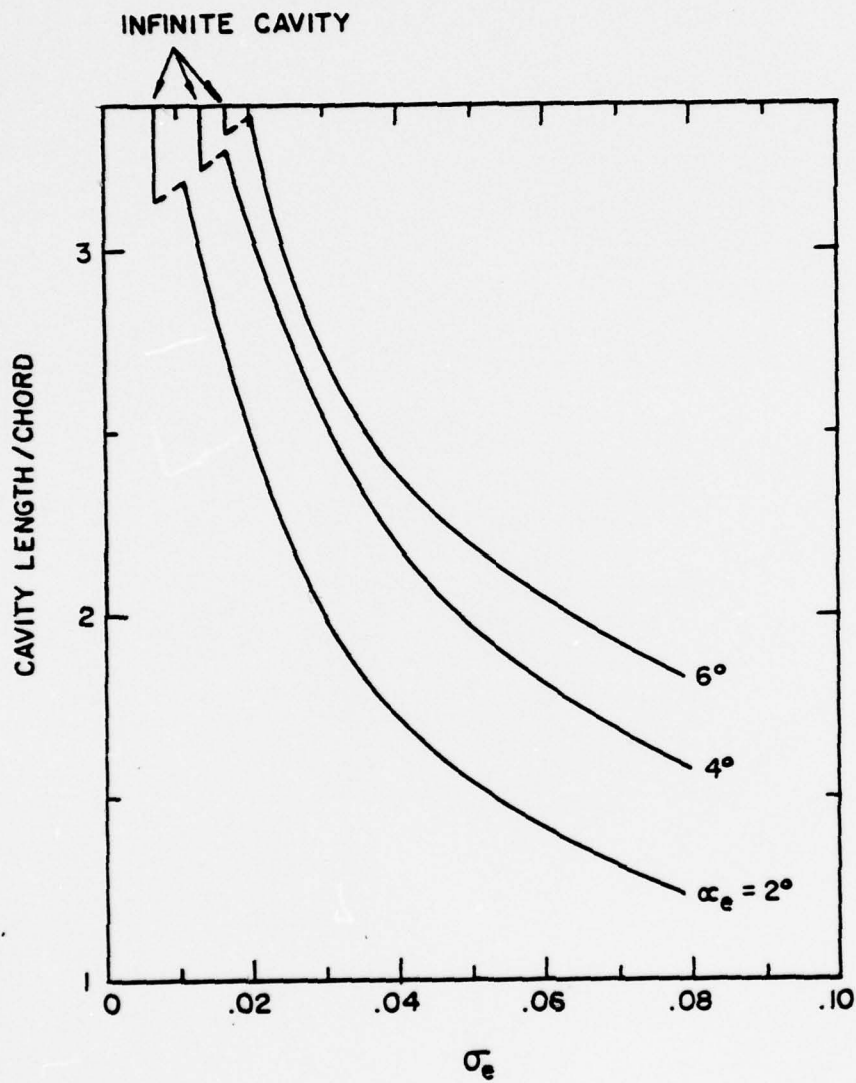


Figure 10(a) Length of Cavity vs. σ_e for Incidence Angles $\alpha_e = 2^\circ, 4^\circ$ and 6° at $x = 0.9$.

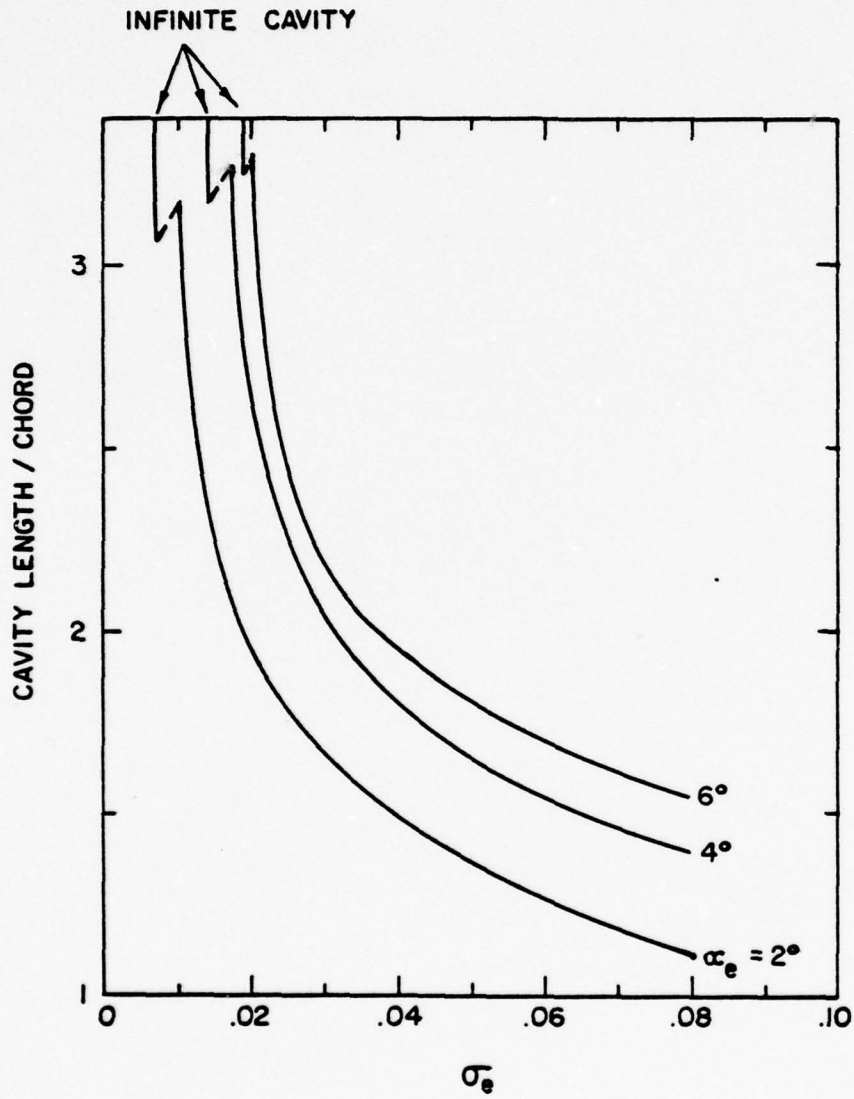


Figure 10(b) The Same as Figure 10(a) Except That $x = 0.8$.

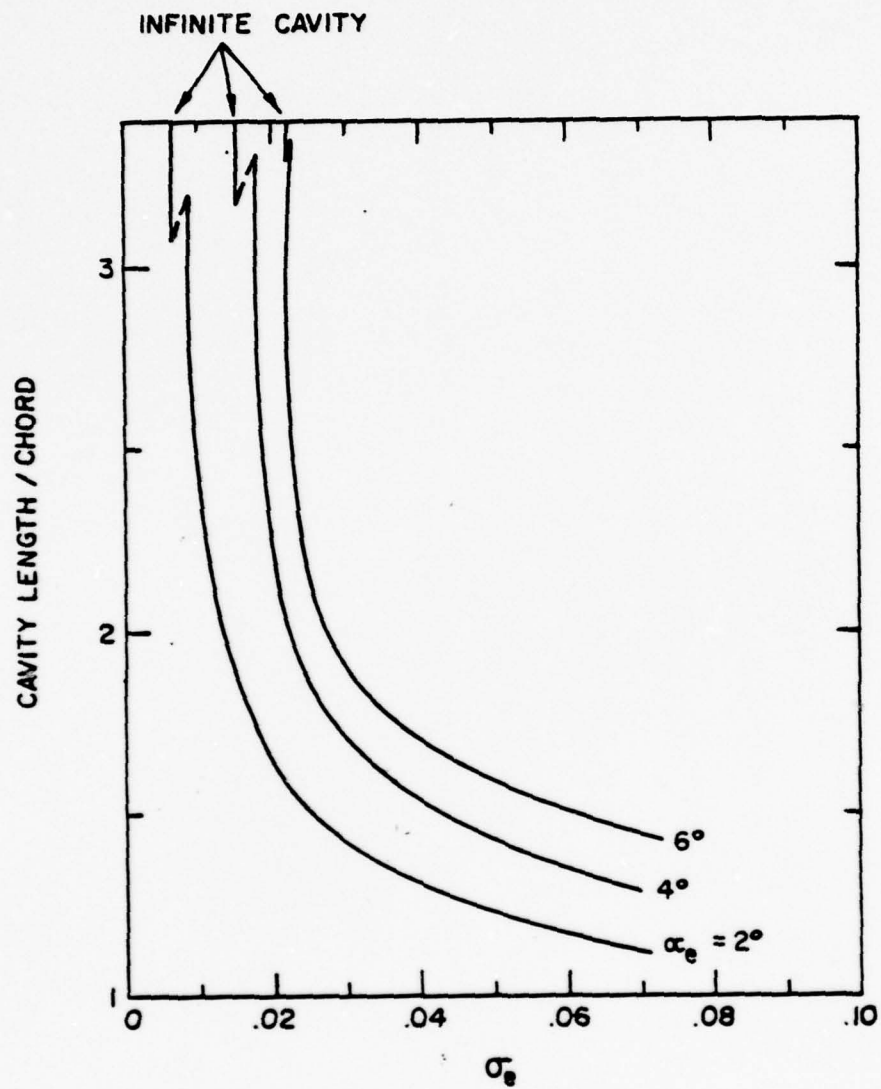


Figure 10(c) The Same as Figure 10(a) Except That $x = 0.7$.

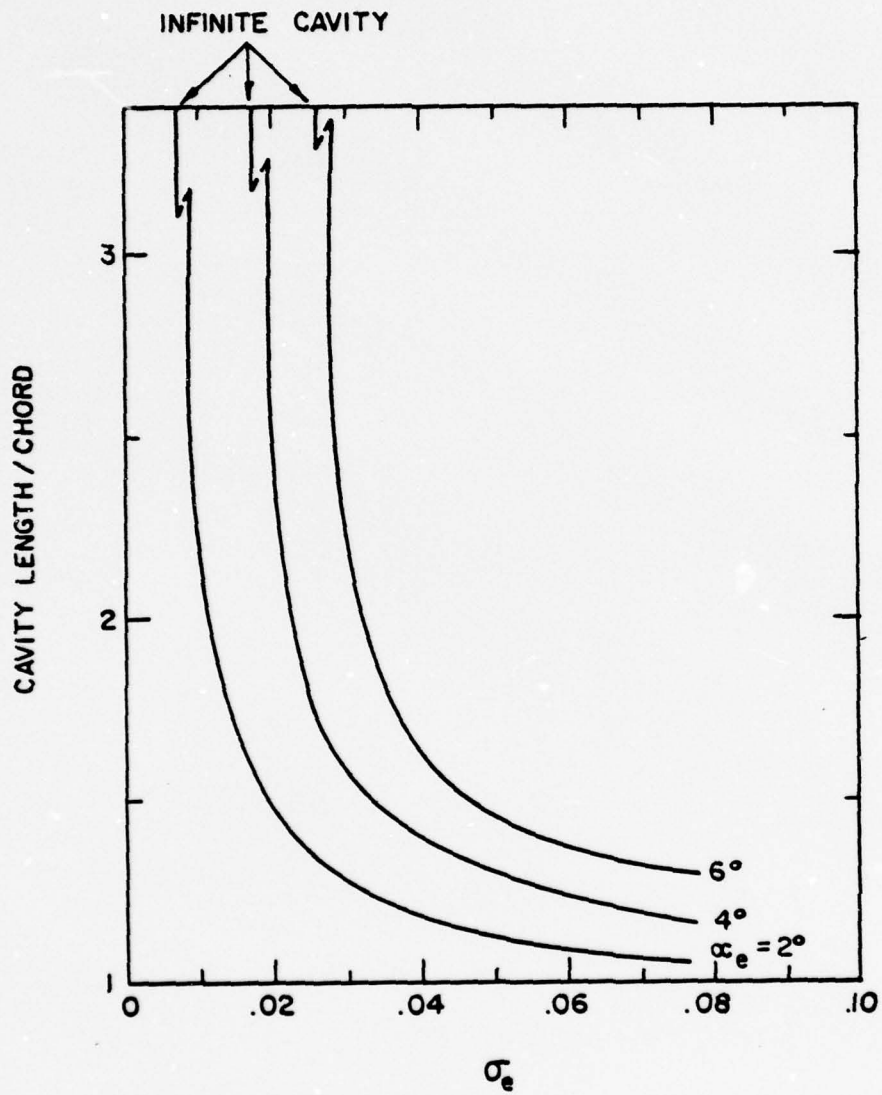


Figure 10(d) The Same as Figure 10(a) Except That $x = 0.6$.

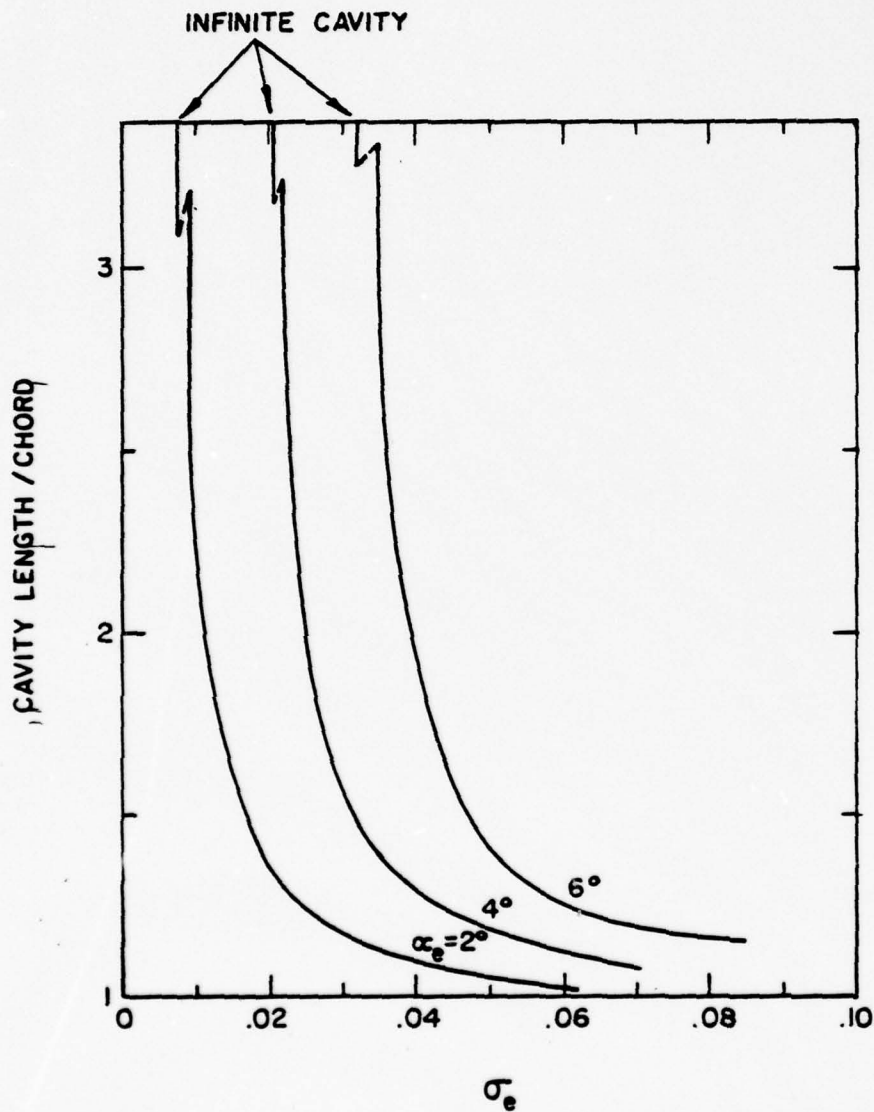


Figure 10(e) The Same as Figure 10(a) Except That $x = 0.5$.

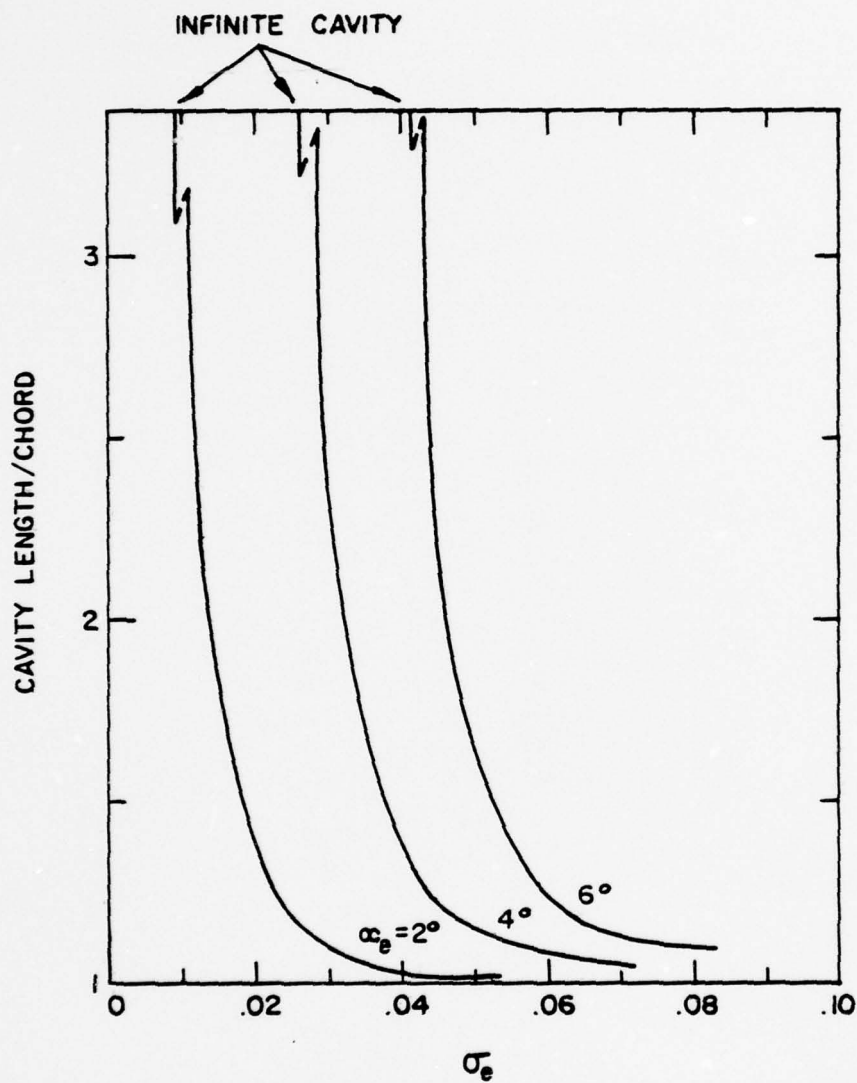


Figure 10(f) The Same as Figure 10(a) Except That $x = 0.4$.

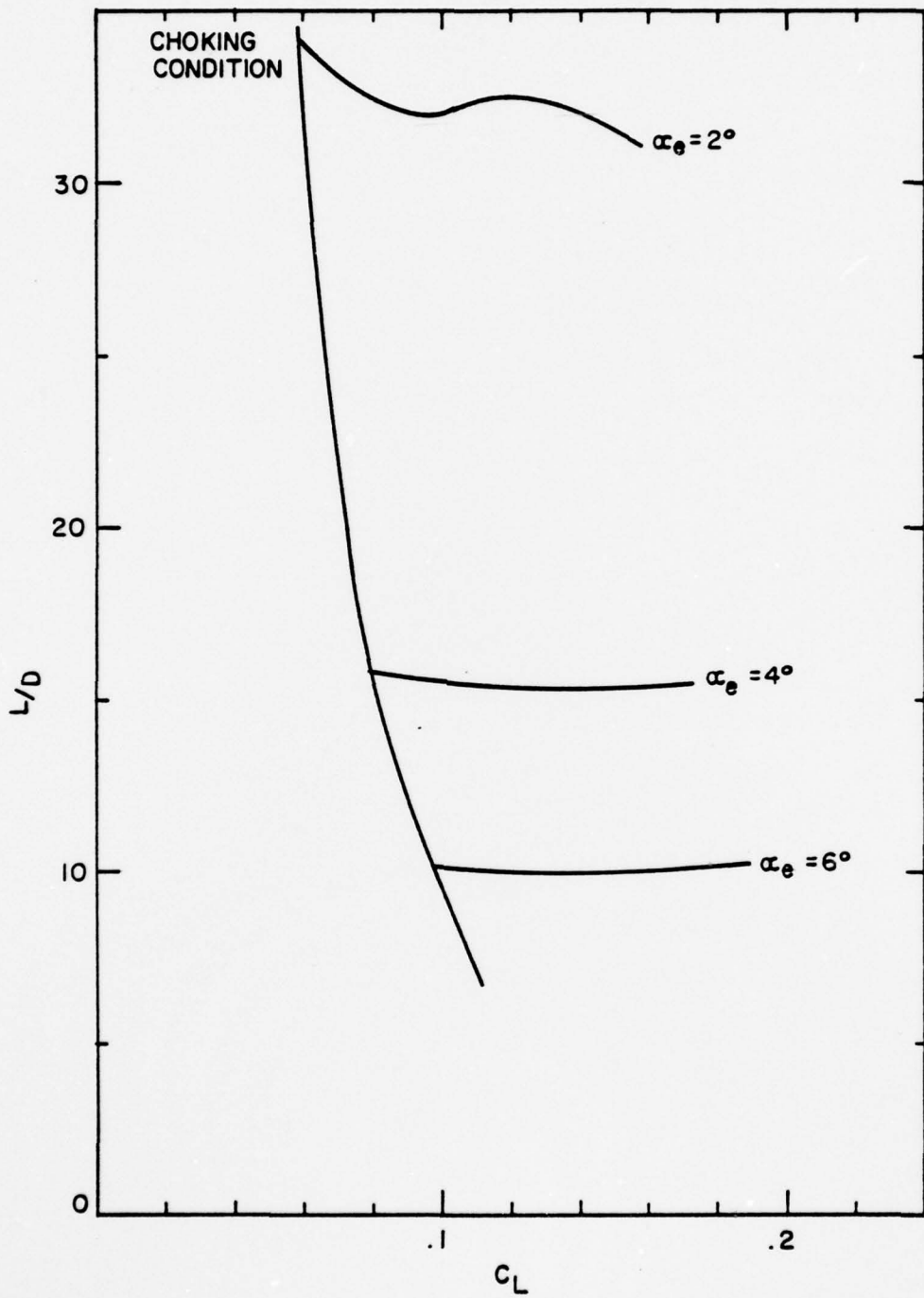


Figure 11(a) Lift-to-Drag Ratio L/D vs. C_L for Incidence Angles $\alpha_e = 2^\circ$, 4° and 6° at $x = 0.9$.

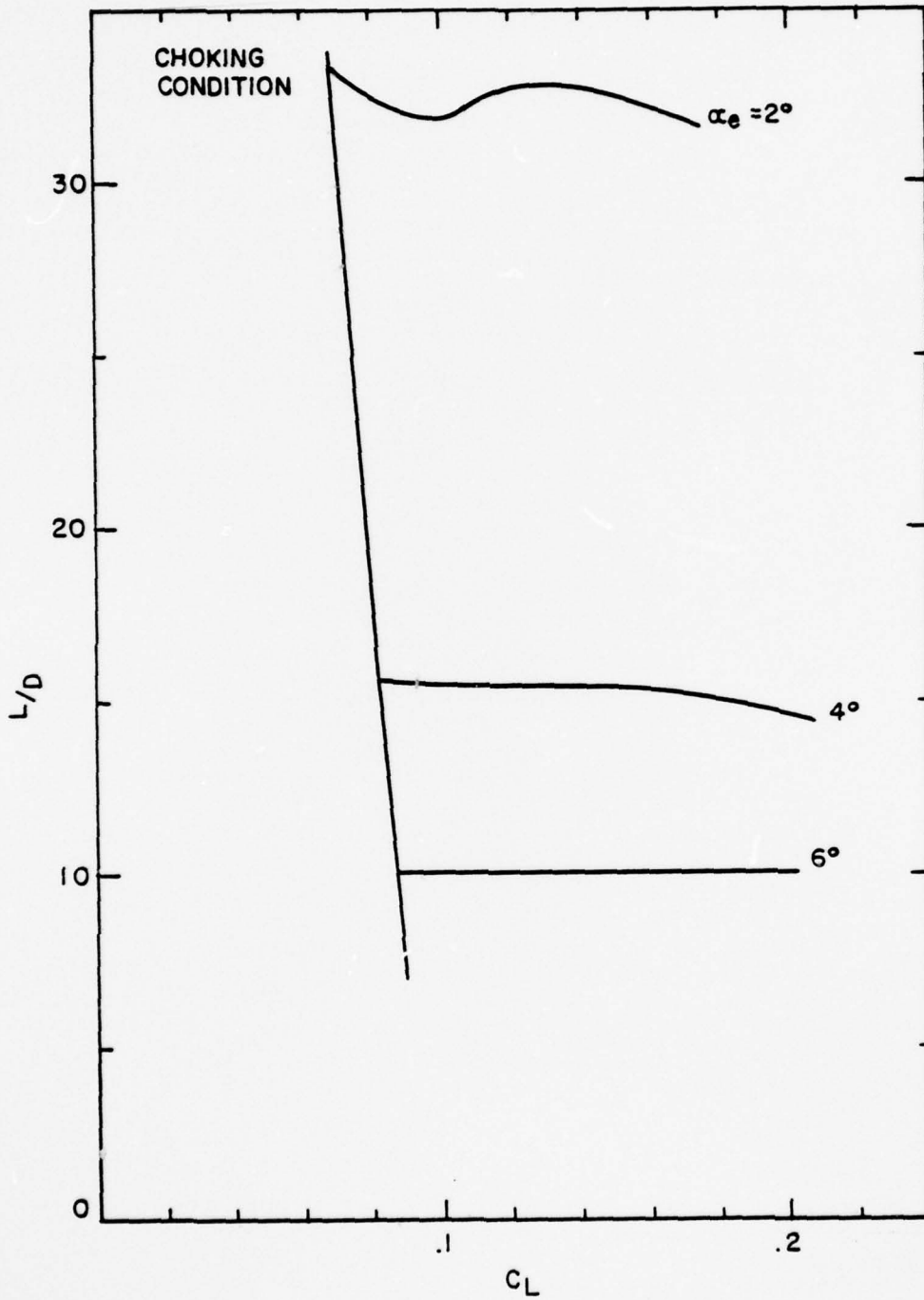


Figure 11(b) The Same as Figure 11(a) Except That $x = 0.8$.

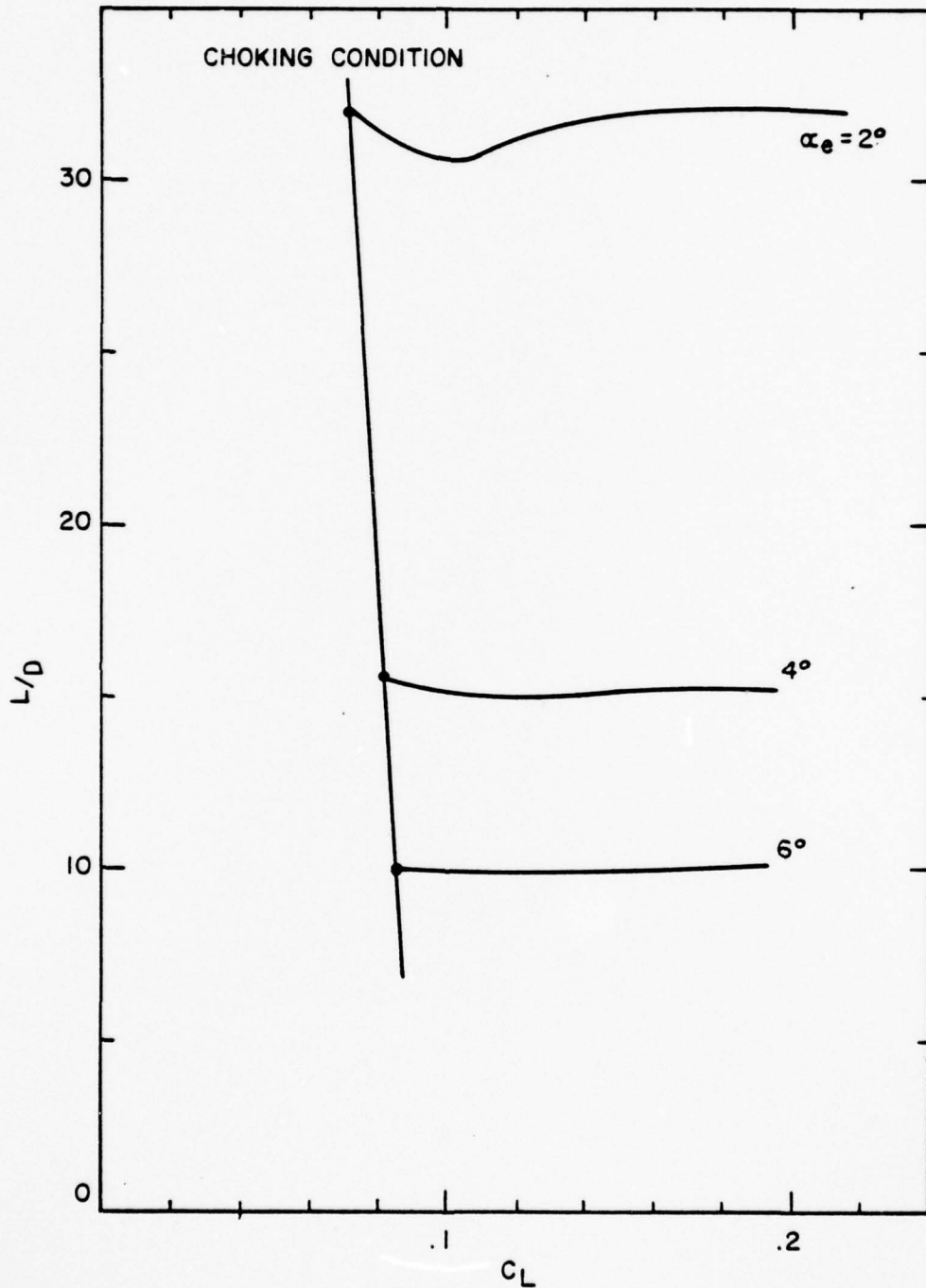


Figure 11(c) The Same as Figure 11(a) Except That $x = 0.7$.

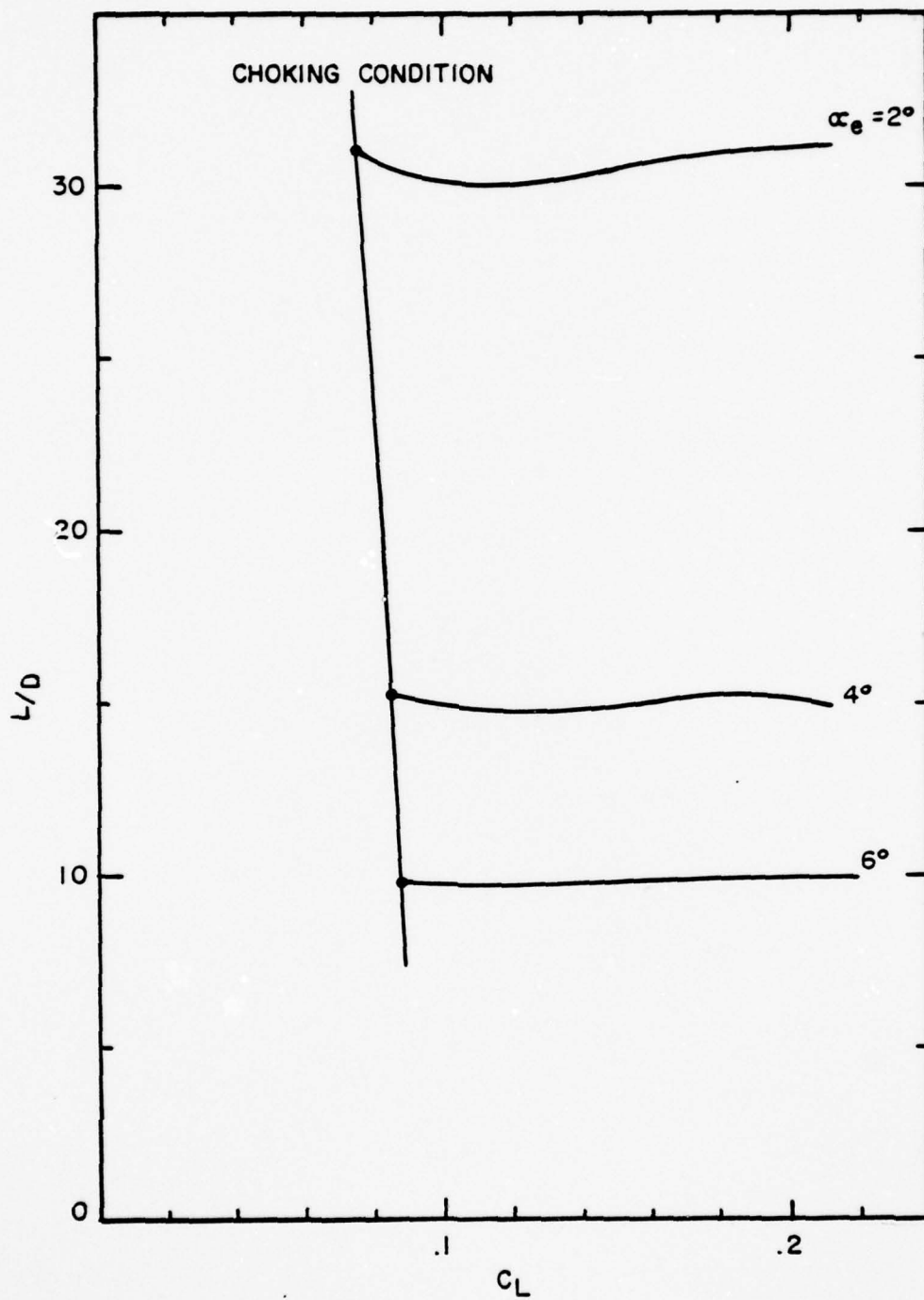


Figure 11(d) The Same as Figure 11(a) Except That $x = 0.6$.

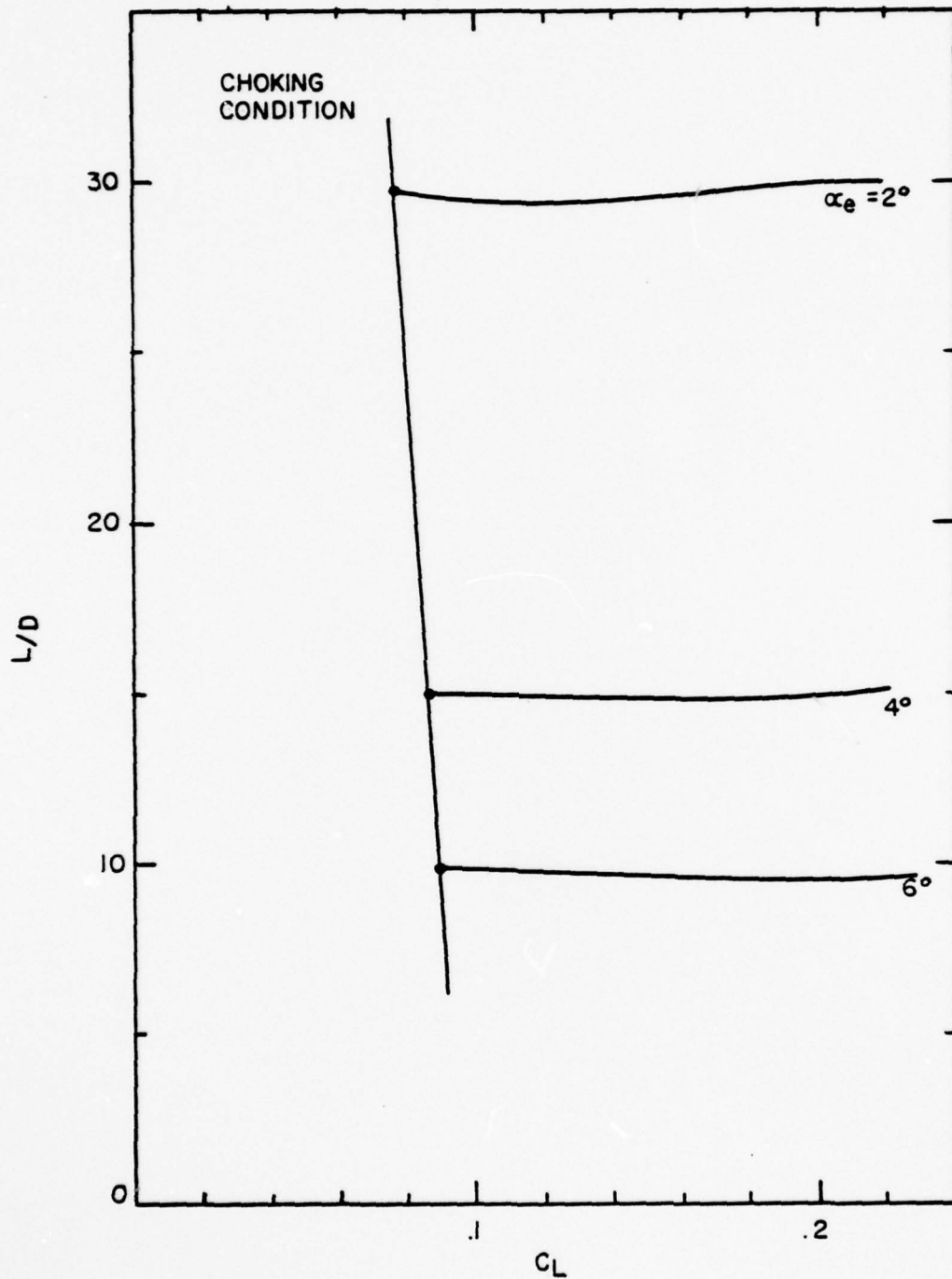


Figure 11(e) The Same as Figure 11(a) Except That $x = 0.5$.

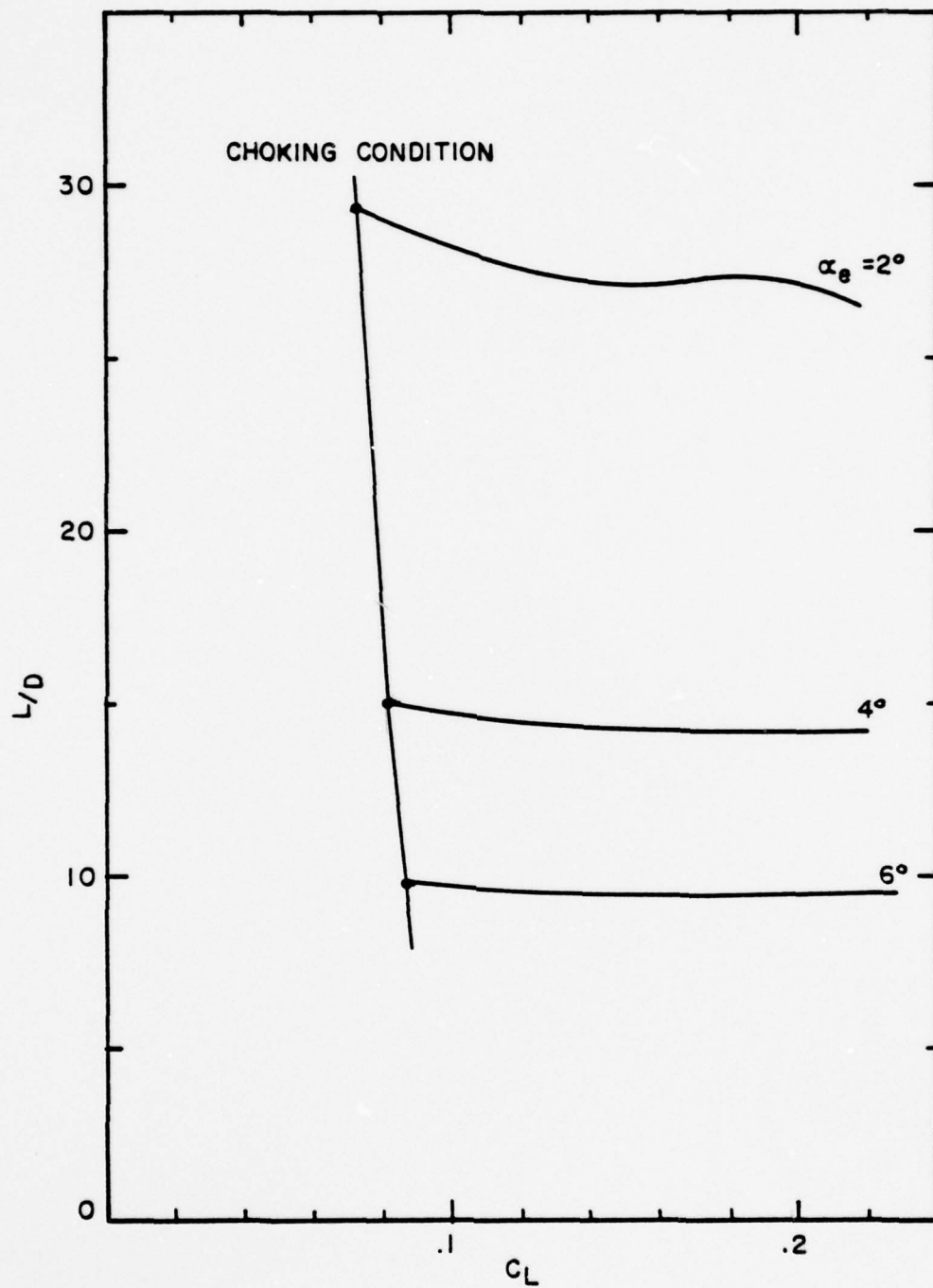


Figure 11(f) The Same as Figure 11(a) Except That $x = 0.4$.

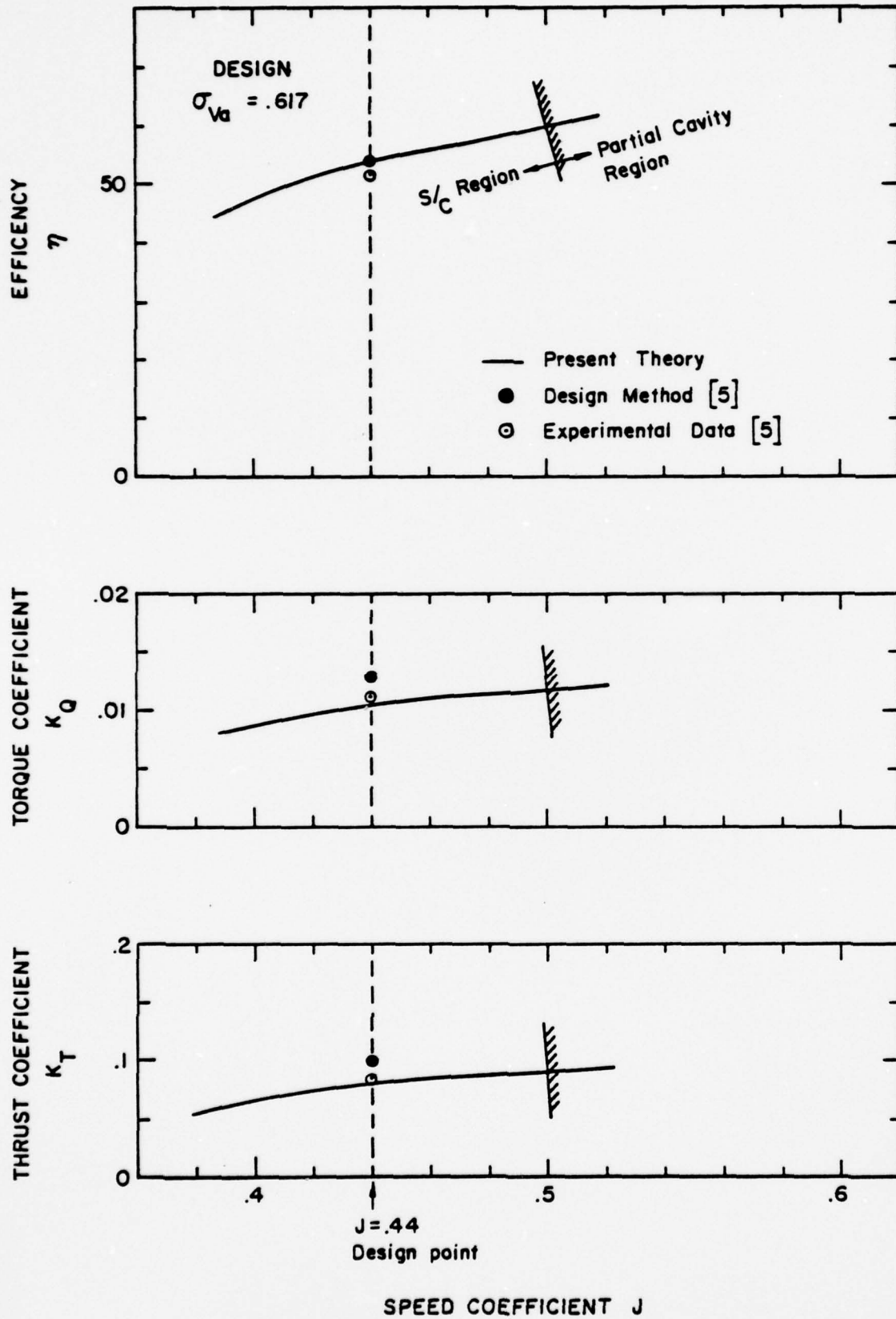


Figure 12 Performance Prediction for 3770 at Design $\sigma_{Va} = .617$.

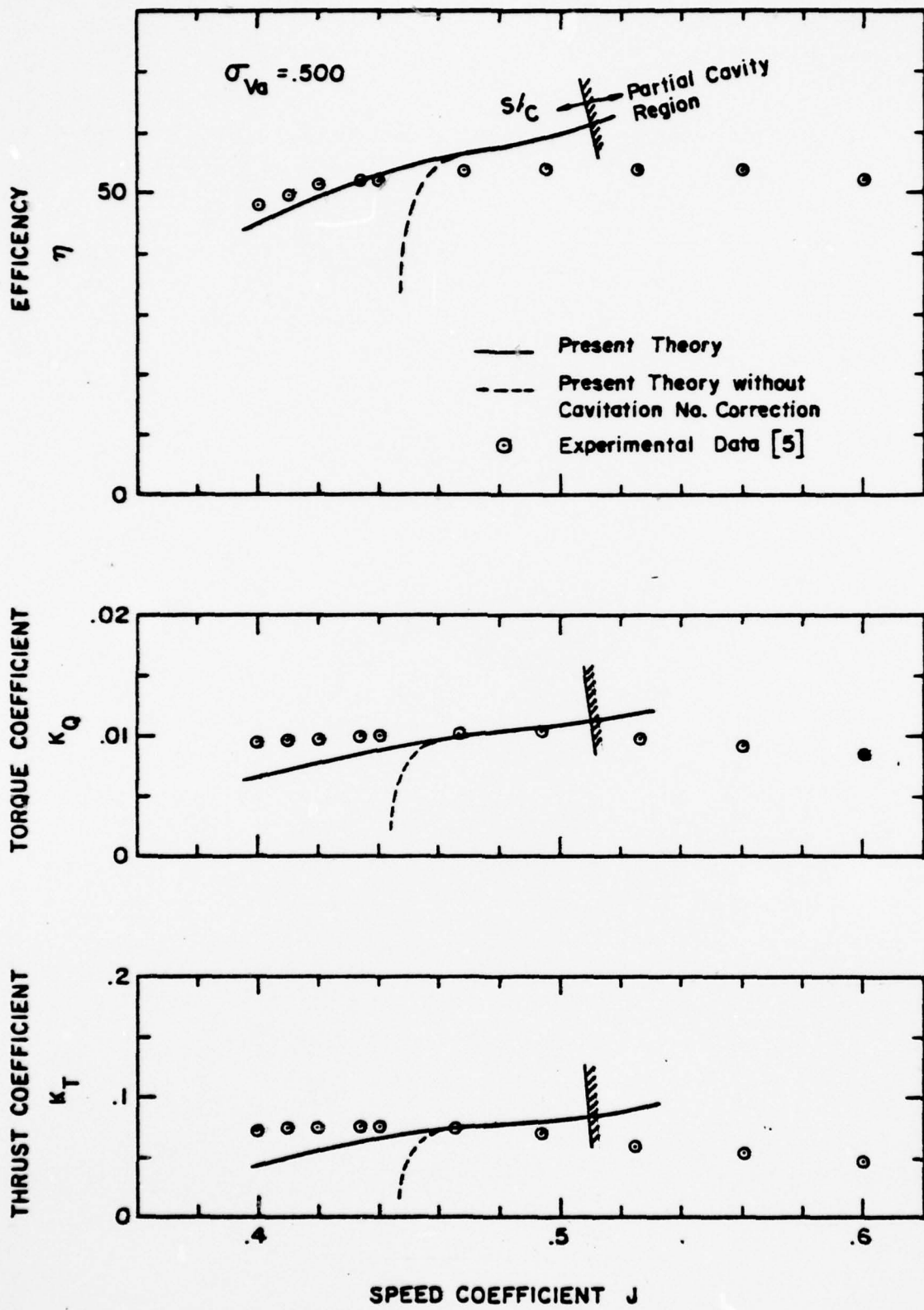


Figure 13 Comparison of 3770 Performance between the Present Theory and Experimental Data [5] at $\sigma_{Va} = .500$.

TABLE 1

Design Characteristics of NSRDC Model 3770
Supercavitating Propeller (from Reference [5])

Blade Number (g)	3
Pitch/Diameter	.786
EAR	.508
Chord/Diameter at $x = 0.7$.351
Design α_e at $x = 0.7$	2°
Design C_L at $x = 0.7$.147
Section	TMB Modif.
J	.440
σ_{Va} at $x = 0.7$.617

Note: Some more information on 3770 are given in Appendix C.

TABLE 2

Comparison of K_T , K_Q and η between the Present Result,
 Design Data and Experimental Data for 3770
 Supercavitating Propeller at Design Point,
 $\sigma_{Va} = .617$ and $J = .440$.

	Design Data (Ref. 5)	Experimental Data (Ref. 5)	Present Results
K_T	.1004	.085	.0819
K_Q	.0130	.0115	.0106
$\eta(\%)$	54.1	52.0	54.0

TABLE 3

Comparison of the Detailed Flow Characteristics of 3770
 between the Design Method [5] and Present Method
 at Design Point, $\sigma_{Va} = .617$ and $J = .440$.

Nondimensional Radius x	Local Cavitation Number σ		Effective Incidence Angle α_e		Downwash Angle α_i		Lift Coefficient C_L	
	Design Method Ref. 5	Present Method	Design Method Ref. 5	Present Method	Design Method Ref. 5	Present Method	Design Method Ref. 5	Present Method
0.4	.0656	.0798	2.06°	6.80°	9.87°	5.13°	.198	.281
0.6	.0302	.0398	1.99°	5.97°	7.23°	3.23°	.153	.168
0.7	.0223	.0290	1.91°	5.15°	6.45°	3.19°	.139	.141
0.8	.0170	.0227	1.91°	5.00°	5.76°	2.65°	.131	.118
0.9	.0134	.0173	1.91°	4.60°	5.21°	2.51°	.125	.094

REFERENCES

- [1] Tachmindji, A.J. and Morgan, W.B., "The Design and Estimated Performance of a Series of Supercavitating Propellers", Proceedings of the Second Symposium on Naval Hydrodynamics, August 1958.
- [2] Kerwin, J.E. and Leopold, R., "Propeller-Incidence Correction Due to Blade Thickness", Journal of Ship Research, Vol. 7, No. 2, October 1963, pp. 1-6.
- [3] Sutherland, C.D. and Cohen, H., "Finite Cavity Cascade Flow", Proceedings of the 3rd U. S. National Congress of Applied Mechanics, 1958, pp. 837-845.
- [4] Furuya, O., "Exact Supercavitating Cascade Theory", Journal of Fluid Eng., Vol. 97, ASME, December 1975.
- [5] Venning, E., Jr., and Haberman, W.L., "Supercavitating Propeller Performance", Trans. of SNAME, Vol. 70, p. 354, 1962.
- [6] Furuya, O., "Preliminary Report - Development of an Off-Design Predictive Method for Supercavitating Propeller Performance", Tetra Tech Report for DWTNSRDC, May 1976.
- [7] Lerbs, H.W., "Moderately Loaded Propellers with a Finite Number of Blades and an Arbitrary Distribution of Circulation", Trans. SNAME, Vol. 60, 1952.
- [8] Furuya, O., "Three-Dimensional Theory on Supercavitating Hydrofoils Near a Free Surface", Journal of Fluid Mech., Vol. 71, Part 2, pp. 339-359, 1975.
- [9] Acosta, A.J. and Sabersky, R., "Fluid Flow", Macmillan

Pub. Co., 1964, p. 334.

- [10] Morgan, W.B., et al., "Propeller Lifting Surface Corrections", Trans. SNAME, Vol. 76, pp. 309-347, 1968.
- [11] Bohn, J. and Altmann, R., "Two Supercavitating Propeller Design for Hydrofoil Ships", Hydronautics Technical Report 7607.01-1, May 1976.

APPENDIX A

Two Dimensional Nonlinear Supercavitating
Cascade Theory (Reference [4])

The detailed mathematical formulation is described in [4]. However some important features needed for the present calculations are repeated here for convenience.

$\text{Re}\{w(\zeta_1)\}$, $\text{Im}\{w(\zeta_1)\}$, g_3 , $s(-1)$ and g_5 in equations (4) through (8) are given by:

$$\begin{aligned}
 w(\zeta_1) &= \text{Re}\{w(\zeta_1)\} + i \text{Im}\{w(\zeta_1)\} \\
 &= \sqrt{(\zeta_1+1)(\zeta_1-b)} \left\{ \frac{1}{2\pi i} \int_a^{-1} \frac{-i2 \ln(\sqrt{1+\sigma}/U_2)}{\sqrt{(\xi'+1)(\xi'-b)}} \frac{d\xi'}{\xi'-\zeta_1} \right. \\
 &\quad + \frac{1}{2\pi i} \int_{-1}^b \frac{2\bar{\theta}(\xi')}{i\sqrt{(1+\xi')(b-\xi')}} \frac{d\xi'}{\xi'-\zeta_1} + \frac{1}{2\pi i} \int_0^b \frac{2\pi}{\sqrt{(1+\xi')(b-\xi')}} \frac{d\xi'}{\xi'-\zeta_1} \\
 &\quad \left. + \frac{1}{2\pi i} \int_b^c \frac{i \cdot 2 \ln(\sqrt{1+\sigma}/U_2)}{\sqrt{(\xi'+1)(\xi'-b)}} \frac{d\xi'}{\xi'-\zeta_1} \right\} \quad (\text{A-1})
 \end{aligned}$$

where

$$\begin{aligned}
 \zeta_1 &= \tilde{A} \exp\{i(\pi/2-\delta)\}, \\
 g_3 &= \frac{1}{\pi} \ln(\sqrt{1+\sigma}/U_2) \cdot \left\{ \ln \frac{-(b+1)}{2\sqrt{(a+1)(a-b)}+(a+1)+(a-b)} + \ln \frac{(b+1)}{2\sqrt{(c+1)(c-b)}+(c+1)+(c-b)} \right\} \\
 &\quad + \left(\frac{\pi}{2} - \sin^{-1} \frac{1-b}{1+b} \right) + \frac{1}{\pi} \int_{-1}^b \frac{\bar{\theta}(\xi') d\xi'}{\sqrt{(1+\xi')(b-\xi')}} \quad (\text{A-2})
 \end{aligned}$$

$$s(-1) = - \int_{\xi}^{-1} h(\xi', a, b, c, U_2(\alpha_2)) \cdot k(\xi', \tilde{A}) d\xi' \quad (A-3)$$

where

$$h(\xi, a, b, c, U_2(\alpha_2)) = \left[\exp \left\{ - \frac{\ln(\sqrt{1+\sigma}/U_2)}{\pi} \left(\pi + \sin^{-1} \frac{(1+\xi)(a-b) + (\xi-b)(1+a)}{(\xi-a)(1+b)} \right) \right. \right. \\ \left. \left. + \sin^{-1} \frac{(1+\xi)(c-b) + (\xi-b)(1+c)}{(c-\xi)(1+b)} \right) + \frac{\sqrt{(1+\xi)(b-\xi)}}{\pi} \right] \times (A-4) \\ \left[\int_{-1}^b \frac{\bar{\theta}(\xi')}{\sqrt{(1+\xi')(b-\xi')}} \frac{d\xi'}{\xi' - \xi} \right] \times \frac{2\sqrt{b}\sqrt{(1+\xi)(b-\xi)} + \xi(b-1) + 2b}{\{-\xi(1+b)\}} \cdot \frac{1}{U_2}$$

$$k(\xi, \tilde{A}) = \frac{d}{\pi} \frac{\xi \cos \delta}{(\xi - \tilde{A} \sin \delta)^2 + (\tilde{A} \cos \delta)^2} \quad (A-5)$$

and

$$\delta = \alpha_e + \gamma, \quad (A-6)$$

$$g_5 = \frac{d}{2\pi} \left\{ e^{-i\delta} \ln \frac{\zeta_1 - c}{\zeta_1 - a} + e^{i\delta} \frac{\bar{\zeta}_1 - c}{\bar{\zeta}_1 - a} \right\} \quad (A-7)$$

In these equations a, b, c are ξ -coordinates in the mapped plane (see Figure A-2), \tilde{A} is a parameter associated with the cascade mapping function and U_2 is the velocity at downstream infinity which is related to α_2 through a continuity equation:

$$U_2 = \frac{\cos(\alpha_e + \gamma)}{\cos(\alpha_2 + \gamma)}$$

where V_e is taken to be unity in the 2-D calculations and all of these values are solution parameters to be determined by Equations (4) through (8) shown in the text. The potential plane from which the ζ -plane is mapped and the definition of s and β are shown in Figures A1 and A3.

APPENDIX B

Calculations of Induced Velocities w_a and w_t by
a Lifting Line Theory

The following calculation method of the induced velocities w_a and w_t is based on the work of Lerbs [7]. The equations for w_a and w_t are written again:

$$\frac{w_a(x)}{V_a} = \frac{1}{2} \int_{x_h}^1 \frac{dG(x')}{dx'} \frac{1}{x-x'} i_a(\beta_i, x', x) dx' \quad (B-1)$$

$$\frac{w_t(x)}{V_a} = \frac{1}{2} \int_{x_h}^1 \frac{dG(x')}{dx'} \frac{1}{x-x'} i_t(\beta_i, x', x) dx' \quad (B-2)$$

where

$$G(x) = \frac{\Gamma}{2\pi R V_a} \quad (B-3)$$

$$i_a(\beta_i) = \left\{ \begin{array}{ll} g \frac{x}{x' \tan \beta_i} \left(\frac{x'}{x} - 1 \right) (1+B_2), & x < x' \\ -g \frac{x}{x' \tan \beta_i} \left(\frac{x'}{x} - 1 \right) B_1, & x > x' \end{array} \right\} \quad (B-4)$$

$$i_t(\beta_i) = \left\{ \begin{array}{ll} g \left(\frac{x'}{x} - 1 \right) B_2, & x < x' \\ -g \left(\frac{x'}{x} - 1 \right) (1+B_1), & x > x' \end{array} \right\} \quad (B-5)$$

$$B_{1,2} = \left(\frac{1+y^2}{1+y'^2} \right)^{\frac{1}{4}} \left[\frac{1}{e^{gA_{1,2}-1}} \mp \frac{1}{2g} \frac{y'^2}{(1+y'^2)^{1.5}} \ln \left(1 + \frac{1}{e^{gA_{1,2}-1}} \right) \right] \quad (\text{B-6})$$

$$A_{1,2} = \pm \left(\sqrt{1+y^2} - \sqrt{1+y'^2} \right) \mp \frac{1}{2} \ln \frac{(\sqrt{1+y'^2}-1)(\sqrt{1+y^2}+1)}{(\sqrt{1+y'^2}+1)(\sqrt{1+y^2}-1)} \quad (\text{B-7})$$

$$y' = \frac{1}{\tan \beta_1} \quad (\text{B-8})$$

$$y = \frac{x}{x' \tan \beta_1} \quad (\text{B-9})$$

where Nicholson's asymptotic formulae have been applied in obtaining B_1 and B_2 from the original integrals of vortex sheets.

By introducing φ for a change of variables:

$$x = \frac{1}{2} (1+x_h) - \frac{1}{2} (1-x_h) \cos \varphi, \quad (\text{B-10})$$

thus $x = x_h$ and 1 correspond to $\varphi = 0$ and π .

We also write $G(x)$ and i in Fourier sine and cosine series, respectively:

$$G(\varphi) = \sum_{m=1}^{\infty} G_m \sin m \varphi \quad (\text{B-11})$$

$$i(\varphi, \varphi') = \sum_{n=0}^{\infty} I_n(\varphi) \cos n \varphi'. \quad (\text{B-12})$$

The coefficients G_m and $I_n(\varphi)$ in (B-11) and (B-12) are obtained by using the orthogonality of sine and cosine function:

$$G_m = \frac{2}{\pi} \int_0^{\pi} G(\varphi') \sin m\varphi' d\varphi' \quad (\text{B-13})$$

$$I_n^a(\varphi) = \frac{k}{\pi} \int_0^{\pi} i_a(\varphi, \varphi') \cos n\varphi' d\varphi' \quad (\text{B-14})$$

$$I_n^t(\varphi) = \frac{k}{\pi} \int_0^{\pi} i_t(\varphi, \varphi') \cos n\varphi' d\varphi' \quad (\text{B-15})$$

$$\left. \begin{array}{l} k=1, n=0 \\ k=2, n \geq 1 \end{array} \right\}$$

where x and x' are replaced by φ and φ' by using the relation of equation (B-10).

Now w_a and w_t are written in the following forms:

$$\frac{w_a(\varphi)}{V_a} = \frac{1}{1-x_h} \sum_{m=1}^{\infty} m G_m h_m^a(\varphi) \quad (\text{B-16})$$

$$\frac{w_t(\varphi)}{V_a} = \frac{1}{1-x_h} \sum_{m=1}^{\infty} m G_m h_m^t(\varphi) \quad (\text{B-17})$$

where

$$h_m^{a,t}(\varphi) = \frac{\pi}{\sin \varphi} \left[\sin m\varphi \sum_{n=0}^m I_n^{a,t}(\varphi) \cos n\varphi + \cos m\varphi \sum_{n=m+1}^{\infty} I_n^{a,t}(\varphi) \sin n\varphi \right] \quad (\text{B-18})$$

It must be noted that, at $\varphi=0$ and $\varphi=\pi$:

$$h_m^{a,t}(0) = \pi \left[m \sum_{n=0}^{\infty} I_n^{a,t}(0) + \sum_{n=m+1}^{\infty} n I_n^{a,t}(0) \right] \quad (\text{B-19})$$

$$h_m^{a,t}(\pi) = -\pi \cos m \pi \left[m \sum_{n=0}^m I_n^{a,t}(\pi) \cos n \pi + \sum_{n=m+1}^{\infty} n I_n^{a,t}(\pi) \cos n \pi \right] \quad (\text{B-20})$$

where L' Hospital's rule has been used.

APPENDIX C

Geometric and Hydrodynamic Configurations of
Supercavitating Propeller Model TMB(NSRDC) 3770

Sectional profiles of supercavitating propeller Model TMB(NSRDC) 3770 are made up by Tulin-Barkart two-terms camber sections at zero cavitation number, modified with a lifting surface correction factor. The equations of such profiles are given by:

$$\frac{\bar{y}}{\bar{c}} = \frac{8C_{Ld}}{5\pi} K \left\{ \frac{4}{3} \left(\frac{\bar{x}}{\bar{c}} \right) + \frac{8}{3} \left(\frac{\bar{x}}{\bar{c}} \right)^{3/2} - 4 \left(\frac{\bar{x}}{\bar{c}} \right)^2 \right\} \quad (C1)$$

where

C_{Ld} = design lift coefficient

\bar{c} = chord length

K = correction factor of a lifting line surface theory .

In Table C1 the y -coordinates of the blade pressure sides at several radial locations are shown with appropriate values of C_{Ld} and K . Also shown in the same Table are the pitch-to-diameter ratio, P/D , blade setting angle, β_g , geometric stagger angle γ and solidity, including the number of propeller blades, diameter of propeller and hub-to-tip diameter ratio.

Table C2 shows the geometric flow angles β (see Figure 1) and the geometric flow incidence angles α_g at various radius locations for various speed coefficients, J . It is noted that the sum of β and α_g is equal to the geometric blade setting angles β_g at any location for all J 's.

The local cavitation numbers based on $V = \left\{ (wr)^2 + V_a^2 \right\}^{1/2}$ are calculated by equation (45), for various J 's and are shown in Table C3. This table

roughly shows a range of the cavitation number over which the super-cavitating propeller hydrodynamics are to be calculated.

++++PROPELLER GEOMETRY OF NSRDC MODEL 3770++++

NUMBER OF BLADE = 3
 DIAMETER OF PROPELLER = 14.0" (.424m)
 HUB/TIP DIAMETER RATIO = .20

Y-COORDINATES OF 2-TERM CAMBER OF NSRDC 3770

	.30	.40	.50	.60	.70	.80	.90
CHORDWISE POSITION							
0.00000	0.00000000	0.00000000	0.00000000	0.00000000	0.00000000	0.00000000	0.00000000
.00750	.00203174	.00241544	.00245443	.00233171	.00207683	.00169733	.00118757
.01250	.00349041	.00414959	.00421657	.00400574	.00356787	.00291592	.00204017
.05000	.01526949	.01815320	.01844621	.01752390	.01560833	.01275626	.00892513
.10000	.03136865	.03724275	.03789469	.03599996	.03206474	.02620564	.01833520
.20000	.06094677	.07245683	.07362636	.06994504	.06224922	.05091546	.03562383
.30000	.06442945	.10037432	.10199446	.09689474	.08630300	.07053309	.04934963
.40000	.10028047	.11921888	.12114519	.11508603	.10250578	.08377518	.05661467
.50000	.10761200	.12793500	.13000000	.12350000	.11000000	.08900000	.06290000
.60000	.16582498	.12581049	.12784120	.12144914	.10817332	.08840711	.06185547
.70000	.09447964	.11232253	.11413557	.10842675	.09657622	.07892911	.05522404
.80000	.07323523	.08706602	.08847135	.08404779	.07486038	.06118134	.04280652
.90000	.04181761	.04971505	.05051750	.04799162	.04274558	.03493479	.02444270
.95000	.02222150	.02641812	.02684454	.02550231	.02271461	.01856403	.01296863
1.00000	0.00000000	0.00000000	0.00000000	0.00000000	0.00000000	0.00000000	0.00000000

DESIGN CL	.20050000	.19860000	.17980000	.16080000	.14670000	.13860000	.13280000
K FACTOR	.1751943	.2102732	.2360084	.2507002	.2447577	.2117241	.1546060
P/D=	.757	.762	.768	.776	.786	.797	.809
BETAG(DFG)	38.77	31.23	26.06	22.36	19.67	17.60	15.97
STAG(DEG)	51.23	58.77	63.54	67.64	70.33	72.40	74.03
SOLIDITY	1.216	.912	.728	.594	.479	.365	.244

NOTF

K IS A CORRECTION FACTOR FOR CAMBER CLD
 P/D IS PITCH TO DIAMETER RATIO
 BETAG IS GEOMETRIC BLADE ANGLE
 STAG IS GEOMETRIC STAGGER ANGLE

Table C-1 Geometric and Hydrodynamic Configurations
 of Supercavitating Propeller Model TMB(NSRDC) 3770.

J	.3		.4		.5		.6		.7	
	BETA	ALFG	BETA	ALFG	BETA	ALFG	BETA	ALFG	BETA	ALFG
X= .3	17.66°	21.11°	23.00	15.77	27.95	10.82	32.48	6.29	36.60	2.17
X= .4	13.43	17.80	17.66	13.57	21.70	9.53	25.52	5.71	29.12	2.11
X= .5	10.81	15.25	14.29	11.77	17.66	8.43	20.91	5.15	24.02	2.04
X= .6	9.04	13.32	11.98	10.38	14.86	7.50	17.66	4.70	20.37	1.99
X= .7	7.77	11.90	10.31	9.36	12.81	6.86	15.26	4.41	17.66	2.01
X= .8	6.81	10.79	9.04	8.56	11.25	6.35	13.43	4.17	15.56	2.04
X= .9	6.06	9.91	8.05	7.92	10.03	5.94	11.98	3.99	13.91	2.06

Table C-2 Geometric Flow Angles β and Geometric Flow Incidence Angles α_g at Various Radial Locations of the Propeller 3770 for Various J's.

X	LOCAL CAVITATION NUMBER BASED ON V						
	J	.3	.4	.5	.6	.7	
X= .3		.0568	.0942	.1355	.1779	.2194	
X= .4		.0333	.0568	.0843	.1145	.1461	
X= .5		.0217	.0376	.0568	.0786	.1022	
X= .6		.0152	.0266	.0406	.0568	.0748	
X= .7		.0113	.0194	.0303	.0427	.0568	
X= .8		.0087	.0152	.0255	.0333	.0444	
X= .9		.0069	.0121	.0187	.0266	.0356	

Table C-3 Local Cavitation Numbers σ Based on $V(= \left\{ (\omega r)^2 + V_a^2 \right\}^{\frac{1}{2}})$ for Various J's.

for $\sigma_V = 0.617$ based on V_a

APPENDIX D

Computer Program Listing and
Input and Output Data Setup

1. INTRODUCTION

The computer program called 'SCSCREW' (listed below) calculates the hydrodynamic characteristics of supercavitating propellers with sectional two-dimensional s/c cascade data given as input data. Therefore, the computer program developed in [4] must be used to generate these 2-D s/c cascade data prior to the use of 'SCSCREW'. The method of preparing these input data will be explained later.

In what follows we describe the structure of the program 'SCSCREW' including functions of subroutines, input data set-up and type of output data obtained as the result of calculations.

2. STRUCTURE OF SCSCREW

SCSCREW consists of a main program and several subroutines, brief descriptions of which will be given as follows;

1) MAIN PROGRAM SCSCREW

- Specify the dimensions for data.
- Read input data.
- Exercise Newton's iterative procedure (see Figure 6).
- Calculate C_T , C_p , K_T , K_Q and η with and without drag forces.
- Calculate local flow conditions including downwash flow angle, effective incidence angle, cavitation number, lift and drag coefficients.

2) FUNCTION CLCD (I, S, B, ILD)

- Interpolate lift, drag and circulation with input data passed on to this program through common statement.

I: Index for radial or spanwise position on blade

S: Cavitation number for which CLCD to be calculated

B: Flow incidence angle for which CLCD to be calculated

ICLCD: Control Index

ICLCD = 0 for lift

ICLCD = 1 for drag

ICLCD = 2 for circulation

Preceding page blank

3) SUBROUTINE FITCAV (MM1, SE, EE, M1, I1, ACC)

- Curve-fitting for cavity thickness by polynomials.

MM1: Index for radial or spanwise position on blade

SE: Cavitation number at which cavity thickness data are available

EE: Cavity thickness data

M1: Number of flow incidence angles for which cavity thickness data are available

I1: Number of cavitation numbers for which cavity thickness data are available

ACC: Coefficients of polynomials fitted for cavitation number as a function of cavity thickness, calculated in FITCAV.

4) SUBROUTINE CAVINO (NG, SC, AE, ACC, A2, I1, SCN, EE, M1)

- Correct a local cavitation number for the effect of cavity thickness (see Equation's (17) through (21)).

NG: Index for radial or spanwise position on blade

SC: Cavitation number before correction

AE: Flow incidence angle

ACC: Coefficients for polynomials with which cavitation number is fitted as a function of cavity thickness in Subroutine FITCAV

A2: Flow incidence angles at which cavity thickness data are available

I1: Number of cavitation numbers for which cavity thickness data are available

SCN: Corrected cavitation number

- EE: Cavity thickness data
- M1: Number of flow incidence angles for which cavity thickness data are available

5) SUBROUTINE FANC (F, FE, SC, ACC, NG, KI, I1)

- Provides a functional relation for cavitation number as a function of cavity thickness;

$$f \equiv (SC \cdot U_1^2 / V_e^2) - (\text{Polynomials in FITCAV})$$

where U_1/V_e is given in Equation (21) of the text.

- F: f given above
- EE: Cavity thickness (e in Equation (21))
- SC: Cavitation number
- ACC: Coefficients of polynomial in FITCAV
- NG: Index for a radial position on the blade
- KI: Index for an incidence angle
- I1: Dummy index (to be neglected)

6) SUBROUTINE MOSEC (A, B, ER1, ER2, X, J, NG, K1, SC, ACC, I1)

- Find a root for $f(x) = 0$ where x must lie between A and B and $f(A) > 0$, $f(B) < 0$.

- A, B: A root of $f(x) = 0$ lies between A and B
- ER1, ER2: Accuracy control valuables with which $|x_{\text{real}} - x| < ER1$
and $|f(x_{\text{real}}) - f(x)| < ER2$
- x: A root for $f(x) = 0$ found in this subroutine
- J: Number of iterations executed in MOSEC
- NG, KI, SC, ACC, I1: The same as those in FANC.

7) SUBROUTINE DETERM (A, N, D)

- Calculate determinant of a matrix A of rank N.

A: Matrix input, requiring dimension (50, 2N+3)

N: Rank of the matrix

D: Calculated determinant of A

8) SUBROUTINE LSQUAR (DATA, NUMBER, N, A, CHISQ, XM)

- Least square fitting for DATA with polynomials of order N.

DATA: DATA(1, NUMBER) \equiv x

DATA(2, NUMBER) \equiv y

DATA(3, NUMBER) = Error in data

NUMBER: Number of input data

N: Order of polynomials

A: Coefficients of polynomials

CHISQ: Chi-square error to be specified

XM: Dimension of (20, 43) needed, but neglect data in XM (not used here)

9) FUNCTION FALF(X), FGAM(X) & FBET(X)

- Calculate α , β , γ at x in Filon's integration formula (see Equations (25.4.47) to (25.4.57) in "Handbook of Mathematical Functions", National Bureau of Standard).

10) SUBROUTINE SPLINE (X, Y, DY, S2, S3, T, SS, SS1, SS2, LIM, N, C1).

- Cubic spline curve fitting for Y(X) and evaluate SS(T)

Y(X): Dimensional Data of order N

T: Points for which Y to be evaluated

SS: Evaluated data a T

OTHER PARAMETERS: Disregard (not used)

3. INPUT DATA SET-UP

The following describes set-ups for input data cards. Typical input data are also listed at the end of the computer program listing.

Card No.	Symbol	Description	FORMAT
1	NGAUS	Number of points for Gauss Quadrature	8I10
2	T(I)	Nondimensional positive half coordinates for Gauss Quadrature	4F20.10
3	W(I)	Weighting factors for Gauss Quadrature	4F20.10
4	EP	Increment for a finite difference method to obtain partial differentials in Newton's method	8F10.5
5	MAXIT	Maximum iteration number in Newton's method	8I10
	MM	Number of discrete control points on the propeller blade	
	MF, NF	Number of terms used for Filon integration method	
	NFILON	Number of increments in Filon integration method	
	IOLD	If not equal to 0, VIVA of old calculations are fed in as input data. If 0, it is approximately calculated in the program ($VIVA \equiv U_1/V_a$)	
	IWRITE	Number of the last iterations for which output printing is made.	

Card No.	Symbol	Description	FORMAT
6	DIA	Propeller diameter in inches.	8F10.5
	VASHIP	Propeller axial speed in feet/sec ($= V_a$)	
7	XJJ	Advance coefficient (J)	8F10.5
	ZZ	Number of blades (g)	
	SIGVA	Cavitation number based on V_a ($= \sigma_{Va}$)	
	XH	Propeller hub diameter/propeller tip diameter ($= x_h$)	
	XXM	Weighting factor in iterative procedure	
8	XX(I)	Nondimensional radial or spanwise position ($= x$) where I from 2 to MM-1	8F10.5
9	BETAG(I)	Geometric blade angle (see Figure 1) in degree ($= \beta_g$)	8F10.5
10	ALFE(I)	Effective flow incidence angle in degree ($= \alpha_e$)	8F10.5
11	SOLI(I)	Solidity ($= SOL$)	8F10.5
12	VIVA(I)	U_1/V_a data only if IOLD $\neq 0$	8F10.5

Repeat for IXX from 2 to MM-1

13	XXX	Nondimensional radial position ($= x$) for lift, drag and circulation data	F10.3
	MANGLE	Number of incidence angles ($= \alpha_e$) for which the data are available	I10
	ISIG	Number of points for σ_e for which the data are available	I10
	SIGMIN(IXX)	Not used, disregard	F10.5

Repeat MANG1 times

14	ANG1(LANG)	Incidence angle at which the data are read-in.	8F10.5
15	SIGD(IXX, LANG, I)	σ_e for which the data are read-in at IXX & LANG	8F10.5
16	CL1(IXX, LANG, I)	Data for lift coefficients (= C_L)	8F10.5
17	CDL(IXX, LANG, I)	Data for drag coefficients (= C_D)	8F10.5
18	GGGI(IXX, LANG, I)	Data for circulation (= Γ/dV_e)	8F10.5

Repeat for IXX = 2 to MM-1

19	XXX	} The same as before	8F10.5
	MANG1		
	ISIG1		

Repeat for LANG = 1 to MANG1

20	ANG2(LANG)	Incidence angle at which cavity thickness data are read-in	8F10.5
21	SIGE(IXX, LANG, I)	Cavitation number at which cavity thickness data are read-in	8F10.5
22	EE(IXX, LANG, I)	Cavity thickness at IXX and LANG	8F10.5

4. TYPICAL OUTPUT DATA

Typical output data are also listed at the end of the program listing.

Most of them are self-explanatory. Those not explained in output data are described as follows:

XN(I) :	solution parameters
	$\left. \begin{aligned} \text{XN(I)} &= \alpha_e, \quad I = 1, \quad \text{MM} \\ &= G_m, \quad I = \text{MM} + 1, \quad 2 \times \text{MM} \end{aligned} \right\}$
F(I):	Residues of each function in Equation (22)
P(I, J):	Partial derivatives of Jacobian <u>J</u> in Equation (25)
ALFG(I):	α_g
BETAI(I):	β_i
ALFI(I):	α_i
VIVA(I):	U_1/V_a
SIGV(I):	local cavitation number

5 COMPUTER PROGRAM LISTING OF 'SCSCREW'

```

PROGRAM SCSCREW(INPUT,OUTPUT,TAPE5=INPUT,TAPE6=OUTPUT)
C LIFTING LINE PROPELLER THEORY IN COMBINATION WITH 2-D S/C CASCADE THEORY.
C PROGRAMMED BY N. FURUYA, 5-27-76.
  DIMENSION BETA(10), BETAI(10), ALFE(10), VIVA(10), GGAM(10)
  DIMENSION GGG(99), SOLI(10), ALFINF(10), XX(10), ALFEO(10)
  DIMENSION PHI(12), T(100), W(100), SOUT(150), GM(100)
  DIMENSION S(150), OFTD(100), OFPD(100), OFCP(100), ALFI(10)
  DIMENSION CLS(10), CDS(10), ALFG(10), FTD(10), FPD(10)
  DIMENSION XALF(10), XBET(10), SINA(10,150), SINT(10,150), BETAG(10)
  DIMENSION HMA(10,100), HMT(10,100), WAVA(10), WTVA(10), SIGV(10)
  DIMENSION UIVI(10), FCT(12), FCP(12), XCT(12), OFCT(100), UIVA(10)
  DIMENSION DY(150), S2(150), S3(150), SS1(150), SS2(150)
  DIMENSION XIA(8,150), XIT(8,150), ALFIND(10)
  DIMENSION GMU(20), P(50,20), Q(50,20), F(20), XN(20), RGA(20), TBG(20)
  DIMENSION DFTE(20), PXJ(20), STGVU(20), VIVAU(20), CDLIM(10,10)
  DIMENSION ANG2(10), STGE(10,5,5), EE(10,5,5), ACC(10,5,5)
  DIMENSION SHI(10)
  COMMON PAI, CONV, CONVI, SIGM,N(10)
  COMMON SIGD(10,5,15), CL1(10,5,15), ANG1(5), CD1(10,5,15)
  COMMON MANGLE, ISIG,GGGI(10,5,15)
  PAI=3.141592654
  CONV=PAI/180.
  CONVI=180./PAI

C DATA FOR CUBIC SPLINE METHOD AND GAUSS QUADRATURE. ARE ALREADY IN.
  READ(5,100) NGAUS
  NGAUS1=NGAUS+1
  N2=NGAUS/2
  NGAUS2=N2+1
  READ(5,560) (T(I),I=NGAUS2,NGAUS)
  READ(5,560) (W(I),I=NGAUS2,NGAUS)
  DO 25 IQ=1,N2
  T(IQ)=-T(NGAUS1-IQ)
  25 W(IQ)=W(NGAUS1-IQ)
  WRITE(6,561) (T(I),I=NGAUS2,NGAUS)
  WRITE(6,562) (W(I),I=NGAUS2,NGAUS)
  560 FORMAT(4F20.10)
  561 FORMAT(1X,*T(I)=*,10(F10.8,1X))
  562 FORMAT(1X,*W(I)=*,10(F10.8,1X))

C READ-IN DATA*****
C MM=NUMBER OF CONTROL POINTS ON THE BLADE RADIAL LOCATIONS TO BE EVALUATED. *
C (MUST BE AN ODD NUMBER) *
C MAXIT= MAXIMUM NO. OF ITERATIONS AT WHICH THE ITERATION IS STOPPED. *
C XH=HUB RADIUS/TIP RADIUS RATIO. *
C XTJ= SPEED COEFFICIENT(=VA/(N*D)). *
C LZ=NUMBER OF BLADES.
C STGV=CAVITATION NUMBER BASED ON THE SHIP SPEED VA.
C XX(I)=NORMALIZED RADIAL POINTS TO BE EVALUATED.
C BETAG(I)=GEOMETRIC BLADE SETTING ANGLES IN DEGREES.
C ALFE(I)=ASSUMED EFFECTIVE FLOW INCIDENCE ANGLES.
C MF IS NO. OF TERMS IN FOURIER SINE SERIES FOR GM,MF TO BE GREATER THAN MF.
C NF IS NO. OF TERMS IN FOURIER COSINE SERIES FOR IN.
C NFILON IS NUMBER OF TERMS (EVEN NO.) FOR FILON FORMULA.
C VASHTP IS AN ADVANCE SPEED IN FEET/SEC.
C DTA IS PROPELLER DIAMETER IN INCH.
C INLD=0 FOR NO DATA FOR VIVA(I), JOLD.NE.0 FOR USING PREVIOUS DATA.
C IWRITE IS NO. OF LAST ITERATIONS FOR WHICH THE RESULTS ARE PRINTED.
C EP IS INCREMENT RATIO FOR PARTIAL DERIVATIVES FO D(CL)/D(ALFE).

```

Preceding page blank

C GGGI(I,J,K) IS NORMALIZED CIRCULATION AS FUNCTIONS OF XX,SIGMA, AND ALFA
 C ----(T= GAMMA/(VE*D)).

C GGG=GGGI/(2.*PAI*R*VA)
 READ(5,101) EP
 READ(5,100) MAXIT,MM,MF,NF,NFILON,IOLD,IWRITE
 READ(5,101) DIA,VASHIP
 READ(5,101) XJJ,ZZ,SIGVA,XH,XXM
 MM1=MM+1
 MM2=MM+2
 MMX=MM*2
 READ(5,101) (XX(I),I=2,MM1)
 READ(5,101) (BETAG(I),I=2,MM1)
 READ(5,101) (ALFE(I),I=2,MM1)
 READ(5,101) (SOLI(I),I=2,MM1)
 IF(IOLD.EQ.0) GO TO 722
 READ(5,101) (VIVA(I),I=2,MM1)

722 CONTINUE

100 FORMAT(8I10)

101 FORMAT(8F10.5)

C LIST THE READ-IN DATA.

WRITE(6,188) MAXIT,MM,MF,NF,IOLD
 WRITE(6,715) DIA
 WRITE(6,716) VASHIP
 WRITE(6,339) NFILON
 WRITE(6,119) ZZ
 WRITE(6,185) XH
 WRITE(6,111) XJJ
 WRITE(6,112) SIGVA
 WRITE(6,113) (XX(I),I=2,MM1)
 WRITE(6,114) (BETAG(I),I=2,MM1)
 WRITE(6,115) (ALFE(I),I=2,MM1)
 WRITE(6,177) (SOLI(I),I=2,MM1)
 IF(IOLD.EQ.0) GO TO 724
 WRITE(6,723) (VIVA(I),I=2,MM1)

724 CONTINUE

110 FORMAT(13X,*NUMBER OF BLADES=*,F3.0)

111 FORMAT(17X,*SPEED COEFF.=*,F8.4)

112 FORMAT(3X,*CAVITATION NO. BASED ON VA=*,F8.5)

113 FORMAT(5X,*XX(I)=*,8(F10.5,1X))

114 FORMAT(2X,*BETAG(I)=*,8(F10.5,1X))

115 FORMAT(3X,*ALFE(I)=*,8(F10.5,1X))

177 FORMAT(3X,*SOLI(I)=*,8(F10.5,1X))

185 FORMAT(3X,*HUB/TIP=*,F6.3)

188 FORMAT(18I,10X,*MAXIT=*,I3,1X,*MM=*,I2,1X,*MF=*,I2,1X,*NF=*,I2,1X,
 X,IOLD=*,I2)

339 FORMAT(10X,*NFILON=*,I3)

715 FORMAT(5X,*PROPELLER DIAMETER IN INCH=*,F10.5)

716 FORMAT(5X,*ADVANCE SPEED IN FEET/SEC.=*,F10.5)

723 FORMAT(3X,*VIVA(I)=*,8(F10.5,1X))

C THIS IS A ROUTINE FOR FINDING CIRCULATION FROM 2-D CASCADE DATA.*****

C ISIG=NUMBER OF DATA POINTS IN ONE CL-SIGMA CURVE(LESS THAN 14). *

C SIGMIN IS MIN. SIGMA AT WHICH ALFA=6, IN THIS CASE IS CALCULATED. *

C MANGLE=NUMBER OF INCIDENCE ANGLES AT ONE BLADE SECTION(LESS THAN 5). *

C THESE NUMBERS MUST BE THE SAME FOR ALL XX(I). *

DO 120 IXX=2,MM1

READ(5,102) XXX,MANGLE,ISIG,SIGMIN(IXX)

102 FORMAT(F10.3,2I10,F10.5)

WRITE(6,116) XXX,MANGLE,ISIG

```

WRITE(6,665) SIGMIN(IXX)
116 FORMAT(/,5X,*X=*,F5.3,5X,*NO. OF INCIDENCE ANGLES =*,I2,5X,*NO. OF
X DATA POINTS ON ONE CL CURVE=*,I2)
665 FORMAT(5X,*MIN. SIGMA FOR USE (IF THE MAX. ALFA(IN THIS CASE 6 DEGR
XFEES) =*,F7.4)
C SIGD(I,J,K)= DATA POINTS FOR SIGMA WHERE CL DATA ARC READ IN.
C IN ORDER FROM SMALL SIGD TO LARGE ONES.
C ANGI(I)=INCIDENCE ANGLES USED IN 2-D.
C CL1(I,J,K)=2D LIFT COEFFICIENTS NORMAL TO VI.
C CD1(I,J,K)=2D DRAG COEFFICIENTS PARALLEL TO VI.
DO 120 IANG=1,MANG1
READ(5,101) ANGI(IANG)
READ(5,101) (SIGD(IXX,IANG,I),I=1,ISIG)
READ(5,101) (CL1(IXX,IANG,I),I=1,ISIG)
READ(5,101) (CD1(IXX,IANG,I),I=1,ISIG)
READ(5,101) (GGGI(IXX,IANG,I),I=1,ISIG)
WRITE(6,119) ANGI(IANG)
WRITE(6,117) (SIGD(IXX,IANG,I),I=1,ISIG)
WRITE(6,118) (CL1(IXX,IANG,I),I=1,ISIG)
WRITE(6,173) (CD1(IXX,IANG,I),I=1,ISIG)
WRITE(6,840) (GGGI(IXX,IANG,I),I=1,ISIG)
840 FORMAT(1X,*GGGI(I,J,K)=*,8F10.5)
117 FORMAT(1X,*SIGD(I,J,K)=*,8F10.5)
118 FORMAT(1X,* CL1(I,J,K)=*,8F10.5)
119 FORMAT(5X,*ANGI=*,F5.2)
173 FORMAT(1X,* CD1(I,J,K)=*,8F10.5)
120 CONTINUE
C READ IN THE DATA FOR CAVITY THICKNESS.
DO 360 IXX=2,MM1
IF(IXX.EQ.2) WRITE(6,364)
READ(5,102) XXX,MANG1,ISIG1
DO 360 IANG=1,MANG1
READ(5,101) ANG2(IANG)
READ(5,101) (SIGE(IXX,IANG,I),I=1,ISIG1)
READ(5,101) (FE(IXX,IANG,I),I=1,ISIG1)
WRITE(6,361) ANG2(IANG)
WRITE(6,362) (SIGE(IXX,IANG,I),I=1,ISIG1)
360 WRITE(6,363) (FE(IXX,IANG,I),I=1,ISIG1)
361 FORMAT(5X,*ANG2=*,F5.2)
362 FORMAT(1X,*SIGE(I,J,K)=*,8F10.5)
363 FORMAT(3X,*FE(I,J,K)=*,8F10.5)
364 FORMAT(/,1X,*-----DATA FOR CAVITAION THICKNESS-----*)
C CURVE FITTING OF CAVITY THICKNESS BY POLYNOMIALS.
CALL FITCAV(MM1,SIGE,FE,MANG1,ISIG1,ACC)
DO 731 I=2,MM1
DO 731 J=1,4
731 WRITE(6,730) (ACC(I,J,K),K=1,3)
730 FORMAT(10X,*ACC(I,J,K)=*,10F10.5)
C 2-D DATA READ IN ARE PASSED ON TO FUNCTION CLCD(IMM,SIGV,ANGLE,ICLCD).

C CALCULATE BETA=ATAN(VA/OMEGA*SMALLR)=ATAN(XJJ/(PAI*XX(I)))*
C CALCULATE ALFI=BETAG-ALFE-BETA.
C CALCULATE GGAM=90-BETAG.
DO 125 KI=2,MM1
GGAM(KI)=90.-HETAG(KI)
PSI=XJJ/(PAI*XX(KI))
RET=ATAN(PSI)
RETA(KI)=HET*CONV1
ALFG(KI)=HETAG(KI)-RETA(KI)

```

```

125 ALFI(K1)=BETAG(K1)-BETA(K1)-ALFE(K1)
WRITE(6,156) (BETA(I),I=2,MM1)
126 FORMAT(/,3X,*BETA(I)=*,8(F10.5,1X))
WRITE(6,157) (ALFI(I),I=2,MM1)
127 FORMAT(3X,*ALFI(I)=*,8(F10.5,1X))

C CALCULATE SIGV FROM AN ASSUMPTION FOR THE THE FIRST ITERATION.*****
C VTVA(I) FOR ITERA NU. GREATER THAN AND EQUAL TO 2 WAS CALCULATED
C AFTER EACH ITERATION.
C VTVA(I) FOR ITERA=1 IS CALCULATED BY AN ASSUMPTION OF VI=V* $\cos(\text{ALFI})$ .
DO 126 IS=2,MM1
XALF(IS)=CONV*ALFI(IS)
XBET(IS)=CONV*BETA(IS)
VIVA(IS)= $\cos(\text{XALF}(\text{IS}))/\sin(\text{XBET}(\text{IS}))$ 
VVI=1./VIVA(IS)
VVI2=VVI**2
126 SIGV(IS)=STGVA*VVI2
WRITE(6,128) (SIGV(I),I=2,MM1)
128 FORMAT(3X,*SIGV(I)=*,8(F10.5,1X))

C FIND GAMMA(GGG(I)) DISTRIBUTION.(NORMALIZED TO GGG/(D*VI)).
C FOR THE FIRST ITERATION.
MAN=MANGLE
MANA=MAN-1
MANB=MAN-2
DO 130 NG=2,MM1
AE=ALFE(NG)
SC=SIGV(NG)
WRITE(6,365) SC
C ---CAVITATION NUMBER CORRECTIONS-----
CALL CAVING(NG,SC,AE,ACC,ANG2,ISIG1,SCN,EE,MANG1)
WRITE(6,366) SCN
SR=SC/SCN
SR=SQRT(SR)
SC=SCN
ICLCD=0
CLS(NG)=CLCD(NG,SC,AE,ICLCD)
ICLCD=1
CDS(NG)=CLCD(NG,SC,AE,ICLCD)
C C SUBROUTINE CLCD ALSO INTERPOLATES NORMALIZED GAMMA(CIRCULATION).
ICLCD=2
130 GGG(NG)=CLCD(NG,SC,AE,ICLCD)*XX(NG)*VIVA(NG)*SR/ZZ
WRITE(6,193) (CLS(I),I=2,MM1)
WRITE(6,194) (CDS(I),I=2,MM1)
WRITE(6,131) (GGG(I),I=2,MM1)
131 FORMAT(2X,*GAMMA(I)=*,10(F8.4,1X))
224 CONTINUE
GGG(1)=0.
GGG(MM2)=0.

C FIND COEFFICIENTS OF FOURIER SINE TRANSFORMATION FOR GAMMA DISTRIBUTION.
C PHI(T)=TRANSFORMED COORDINATES FOR XX(I).
PHI(1)=0.
PHI(MM2)=PAI
XAL=1.-XH
XH1=0.5*(1.+XH)
XHA=0.5*XAI
DO 132 IPH=2,MM1
AL=(XH1-XX(IPH))/XHA

```

```

132 PHI(IPH)=ACOS(AL)
C USE CUBIC SPLINE METHOD IN COMBINATION WITH FILON INTEGRATION FORMULA****
C FOR INTEGRATION.
NFIH1=NFILOH/2+1
SPACL=PAI/NFILOH
NFI1=NFILOH+1
DO 134 ICH=1,NFI1
134 S(ICH)=SPACE*(ICH-1)
C1=1.E-7
CALL SPLINE(PHI ,GGG,DY,S2,S3,S,SOUT,SSI,SS2,MM2,NFI1 ,C1)
DO 145 ISEK=1,MM
ARG=ISEK*SPACE
AMH=FALF(ARG)
RMH=FRET(ARG)
GMH=FGAM(ARG)
AFF=AMH*(SOUT(1)-SOUT(NFI1))*COS(ISEK*PAI)
S2K=0.
S2KA=0.
DO 510 K2=1,NFIH1
I2A=K2*2
I2=K2*2-1
S2K=S2K+SIN(I2)*SIN(ISEK*S(I2))
IF(K2.EQ.NFIH1) GO TO 510
S2KA=S2KA+SOUT(I2A)*SIN(ISEK*S(I2A))
510 CONTINUE
RS2K=BMH*S2K
GS2KA=GMH*S2KA
GM(ISEK)=SPACE*(AFF+RS2K+GS2KA)
146 CONTINUE
GM(ISEK)= GM(ISEK)*2./PAI
WRITE(6,147) ISEK,GM(ISEK)
147 FORMAT(5X,3HG(,I2,2H)=,E14.7)
225 CONTINUE
145 CONTINUE

C CALCULATE INDUCTION FACTORS.*****
C CALCULATE SMALL IA AND IN.
C THEN CALCULATE INA AND INT.
DO 150 ID=2,MMJ
XRE=(BLTAG(ID)-ALFE(ID))*CONV
TRI=1./TAN(XRE)
TRI2=TRI**2
C PHI(I)---XX(I) HAS BEEN DONE BEFORE.
NFI=NFI+1
DO 151 NX=1,NFI
NXA=NX-1
IF(NX.GE.2) GO TO 329
DO 326 NI=1,NFI1
C CHANGE OF VARIABLES FROM S(I) TO XXP(I).
XXP=XH1-XHA*COS(SINT)
XIND=XXP/XI(ID)
XII=1./XIND
AB1=ZZ*(XIND-1.)
AB2=AB1*TRI*XII
C CALCULATE A1 AND A2, THEN B1 AND B2.
YPP=XII*TH1
YPP2=YPP**2
QC=1.+YPP2
RD=1.+TRI2

```

```

RCS=SQRT(BC)
RDS=SQRT(BD)
RK1=BDS-BDS
RK2=(BDS-1.)*(RCS+1.)
RK3=(BDS+1.)*(RCS-1.)
ADK=0.5*ALOG(RK2/RK3)
AA1=DK1-ADK
AA2=-AA1
RF1=B0/BC
RF1D=DF1**0.25
RF2=TB12/R0**1.5
FGA1=EXP(ZZ*AA1)
FGA2=EXP(ZZ*AA2)
E1I=1./(FGA1-1.)
E2I=1./(FGA2-1.)
IF(XIND.LT.1.) GO TO 327
AEG2=ALOG(1.+E2I)
RB2=DF1D*(E2I+0.5*DF2*AEG2/ZZ)
XIA(ID,NI)=AB2*(1.+BB2)
XIT(ID,NI)=AB1*BB2
GO TO 326
327 AEG1=ALOG(1.+E1I)
RB1=DF1D*(E1I+0.5*DF2*AEG1/ZZ)
XIA(ID,NI)=-AB2*BB1
XIT(ID,NI)=-AB1*(1.+BB1)
326 CONTINUE
329 CONTINUE
C2KA=0.
C2KT=0.
C2KAA=0.
C2KAT=0.
DO 350 ICB=1,NFIH1
I2=ICB*2-1
I2A=ICB*2
CNT1=COS(NXA*S(I2))
C2KA=C2KA+XIA(ID,I2)*CNT1
C2KT=C2KT+XIT(ID,I2)*CNT1
IF(ICB.EQ.NFIH1) GO TO 350
CNT2=COS(NXA*S(I2A))
C2KAA=C2KAA+XIA(ID,I2A)*CNT2
C2KAT=C2KAT+XIT(ID,I2A)*CNT2
350 CONTINUE
C2KA=C2KA-.5*(XIA(ID,NFI1)*COS(NXA*PAI)+XIA(ID,1))
C2KT=C2KT-.5*(XIT(ID,NFI1)*COS(NXA*PAI)+XIT(ID,1))
ARG=NXA*SPACE
BNH=FBET(ARG)
GNH=FGAM(ARG)
SINA(ID,NX)=SPACE*(BNH*C2KA+GNH*C2KAA)/PAI
SINT(ID,NX)=SPACE*(BNH*C2KT+GNH*C2KAT)/PAI
IF(NX.GE.2) SINA(ID,NX)=2.*SINA(ID,NX)
151 IF(NX.GE.2) SINT(ID,NX)=2.*SINT(ID,NX)
150 CONTINUE

C FIND HMA(I) AND HMT(I).*****
DO 169 MA=2,MMI *
SP=SIN(PHI(MA)) *
DO 160 MB=1,MM *
PH=MB*PHI(MA) *
SPH=SIN(PH) *
CPH=COS(PH) *

```

```

HMA(MA,MB)=0.
HMT(MA,MB)=0.
MB1=MB+1
DO 161 MC=1,MB1
MCA=MC-1
PMI=MCA*PHI(MA)
CPMI=CUS(PMI)
161 HMA(MA,MB)=HMA(MA,MB)+SINA(MA,MC)*CPMI
HMT(MA,MB)=HMT(MA,MB)+SINT(MA,MC)*CPMI
HMA(MA,MB)=HMA(MA,MB)*SPH
HMT(MA,MB)=HMT(MA,MB)*SPH
MB2=MB+2
DO 162 MP=MB2,NFI
MPA=MP-1
SNP=SIN(MPA*PHI(MA))
CPS=CPM*SNP
162 HMA(MA,MB)=HMA(MA,MB)+CPS*SINA(MA,MP)
HMT(MA,MB)=HMT(MA,MB)+CPS*SINT(MA,MP)
PSP=PAI/SP
HMA(MA,MB)=PSP*HMA(MA,MB)
HMT(MA,MB)=PSP*HMT(MA,MB)
160 CONTINUE
169 CONTINUE

```

```

C NEWTON ITERATION LOOP*****
C READY TO EXECUTE NEWTON METHOD. *
C REWRITE ALFE(I) AND GM(I) BY A NEW SET OF VARIABLES, *
C XN(I)=ALFE(I), I=1,MM AND XN(I)=GM(I),I=MM1,MMX. *
ITERA=1
ITERAM=MAXIT-1WRITE
987 CONTINUE
WRITE(6,661) ITERA
661 FORMAT(///,10X,'-----ITERATION NUMBER-----',13)
DO 525 INE=1,MM
INE1=INE+1
ALFE0(INE1)=ALFE(INE1)
GMU(INE)=GM(INE)
SIGVO(INE1)=SIGV(INE1)
VIVAO(INE1)=VIVA(INE1)
525 XN(INE)=ALFF(INE1)
DO 526 INE=MM1,MMX
INEP=INE-MM
526 XN(INE)=GM(INEP)
WRITE(6,534) (XN(I),I=1,MMX)
534 FORMAT(1X,'XN(I)=',12(F9.5,1X))
DO 170 LQ=2,MM1
WAVA(LQ)=0.
WTVA(LQ)=0.
DO 171 LP=1,MM
XPAG=LP*GM(LP)
WAVA(LQ)=WAVA(LQ)+XPAG*HMA(LQ,LP)
171 WTVA(LQ)=WTVA(LQ)+XPAG*HMT(LQ,LP)
WAVA(LQ)=WAVA(LQ)/XAL
170 WTVA(LQ)=WTVA(LQ)/XAL
IF(ITERA.LT.ITERAM) GO TO 226
WRITE(6,254) (WAVA(I),I=2,MM1)
WRITE(6,255) (WTVA(I),I=2,MM1)
226 CONTINUE
254 FORMAT(10X,'WAVA(I)=',8(E10.3,1X))

```

295 FORMAT(10X, *WTVA(I)=*, 8(E10.3, 1X))

C F(I) IS AN ARRAY OF FUNCTION AND P(I,J) IS PARTIAL DERIVATIVES.*****

```
DO 530 IFN=1,MM *
  TFN1=IFN+1 *
  BGA(IFN)=(BGTAG(IFN1)-ALFE(IFN1))*CUNV *
  TBG(IFN)=TAN(BGA(IFN)) *
  PXJ(IFN)=PA1*XX(IFN1)/XJJ *
530 F(IFN)=TBG(IFN)*(PXJ(IFN)-WTVA(IFN1))-(1.+WAVA(IFN1))
  DO 531 IFN=MM1,MMX
    GMA=0.
    TFN1=IFN-MM+1
    DO 532 IFM=1,MM
      AG=IFM*PHI(IFN1)
532 GMA=GMA+GM(IFM)*SIN(AG)
531 F(IFN)=GMA-GGG(IFN1)
  WRITE(6,533) (F(I), I=1,MMX)
533 FORMAT(1X, *F(I)=*, 12(F9.5, 1X))
```

L COMPUTATION OF PARTIAL DERIVATIVES.*****

```
DO 535 IPA=1,MM *
  DO 535 IPB=1,MM *
  TFL(IPA.EQ.,IPB) GO TO 536 *
  P(IPA,IPB)=0. *
  GO TO 535 *
536 TPAJ=IPA+1
  CBGA=COS(BGA(IPA))
  CBGA2=CBGA**2
  AXY =-(PXJ(IPA)-WTVA(IPA1))/CBGA2
  P(IPA,IPB)=AXY
535 CONTINUE
  DO 537 IPA=1,MM
    TPAJ=IPA+1
    DO 537 IPB=MM1,MMX
      TPBS=IPB-MM
      SSL =-(HG(IPA) *HMT(IPA1,IPBS)*IPBS/XAL
537 P(IPA,IPB)=SSL-HMA(IPA1,IPBS)*IPBS/XAL
```

C TRG(T) AND PXJ(I) ARE ALREADY CALCULATED.

```
DO 538 IPAS=MM1,MMX
  TPAS=IPAS-MM
  DO 538 IPB=1,MM
    TFL(IPAS.EQ.,IPB) GO TO 538
  P(IPA,IPB)=0.
```

538 CONTINUE

C D(CL)/D(ALFE) NEEDS A FINITE DEFERENCE METHOD.

```
DO 539 ICL=2,MM1
  DIF=EP*ABS(ALFE(ICL))
  AFX=ALFE(ICL)+DIF
  AFY=ALFE(ICL)-DIF
  SC=SIGV(ICL)
  CALL CAVINQ(ICL,SC,ACX,ACC,ANG2,ISIG1,SCNX,EE,MANG1)
  CALL CAVINQ(ICL,SC,ALY,ACC,ANG2,ISIG1,SCNY,EE,MANG1)
  SCX=SCNX
  SCY=SCNY
  SRX=SC/SCX
  SRY=SC/SCY
  SRX=SQRT(SRX)
  SRY=SQRT(SRY)
  TCLCD=2
  GGGX=CLCD(TCL,SCX,ACX,ICLCD)*SRX
```

```

GGY=CLCD(ICL,SCY,AEY,ICLCD)*SRY
TCLA=ICL-1
TCLAM=ICLA+MM
XVI=XX(ICL)*VIVA(ICL)/ZZ
539 P(ICLAM,ICLA)=- (GGGX-GGGY)*XVI/(2.*DIF)
NO 540 IG=1,MM
TG1=IG+1
PHN=PHI(IG1)
NO 540 IK=1,MM
YKP=IK*PHN
GXK=SIN(XKP)
TGM=IG+MM
TKM=IK+MM
540 P(IGM,IKM)=SXX
NO 541 IPT=1,MMX
IF(ITERA-LT.ITERAW) GO TO 582
541 WRITE(6,542) (P(IPT,I),I=1,MMX)
542 FORMAT(1X,*P(I,J)=*,12(F9.5,1X))
542 CONTINUE
CALL DETERM(P,MMX,DETBO)
NO 543 IPF=1,MMX
NO 544 IPG=1,MMX
Q(IPG,IPF)=P(IPG,IPF)
544 P(IPG,IPF)=-F(IPG)
CALL DETERM(P,MMX,DETE(IPF))
NO 545 IPG=1,MMX
545 P(IPG,IPF)=Q(IPG,IPF)
543 CONTINUE
NO 546 LS=1,MMX
546 XN(LS)=XN(LS)+DETE(LS)/DETBO
IF(ITERA-LT.ITERAW) GO TO 580
WRITE(6,548) (XN(I),I=1,MMX)
548 FORMAT(1X,*XN(I)=*,12(F9.5,1X))
548 CONTINUE
NO 547 LA=2,MM1
LAA=LA-1
ALFE(LA)=XN(LAA)
LAAM=LAA+MM
547 CM(LAA)=XN(LAAM)

C CALCULATE BETA1,ALF1,ALF2,VIVA AND SIGV.*****
C NEW WAVA AND WTVA-----
NO 550 MAT=2,MM1
WAVA(MAT)=0.
WTVA(MAT)=0.
NO 551 MAS=1,MM
XPAG=MAS*GM(MAS)
WAVA(MAT)=WAVA(MAT)+XPAG*HMA(MAT,MAS)
551 WTVA(MAT)=WTVA(MAT)+XPAG*HMT(MAT,MAS)
WAVA(MAT)=WAVA(MAT)/XAL
550 WTVA(MAT)=WTVA(MAT)/XAL
NO 180 KF=2,MM1
XK1=PAI*XY(KF)/XJJ
RETB=(1.+WAVA(KF))/(XK1-WTVA(KF))
BETA1(KF)=CONV1*ATAN(RETB)
ALF1(KF)=BETA1(KF)-BETA(KF)
XR=BETA(KF)*CONV
XBI=BETA1(KF)*CONV
CB=COS(XB)/SIN(XR)
CHI=1./COS(XBI)

```

```

VIVA(KF)=(CB-WTVA(KF))*CBI
180 SIGV(KF)=SIGVA/VIVA(KF)**2
  IF(ITERA.LT.ITERAW) GO TO 227
  WRITE(6,181)
  WRITE(6,196) (ALFG(I),I=2,MM1)
  WRITE(6,197) (BETA(I),I=2,MM1)
  WRITE(6,189) (ALFI(I),I=2,MM1)
  WRITE(6,183) (VIVA(I),I=2,MM1)
  WRITE(6,184) (SIGV(I),I=2,MM1)
227 CONTINUE
181 FORMAT(10X,*---NEW VALUES OF ALFE, VIVA,ETC,---*)
183 FORMAT(3X,*VIVA(I)=*,8(F10.5,1X))
184 FORMAT(3X,*SIGV(I)=*,8(F10.5,1X))
189 FORMAT(3X,*ALFI(I)=*,8(F10.5,1X))
196 FORMAT(3X,*ALFG(I)=*,8(F10.5,1X))
197 FORMAT(2X,*BETA(I)=*,8(F10.5,1X))

C CALCULATION OF PROPELLER FORCES AND EFFICIENCY.*****
C CALCULATE UNIFVA, ALFINF AND GGG.
  DO 190 KI=2,MM1
  AE=ALFC(KT)
  SC=SIGV(KT)
  CALL CAVING(KT,SC,AE,ACC,ANG2,ISIG1,SCN,EE,MANG1)
  SRI(KT)=SC/SCN
  SRI(KT)=SQRT(SRI(KT))
  IF(ITERA.LT.ITERAW) GO TO 775
  WRITE(6,365) SC
  WRITE(6,366) SCN
365 FORMAT(5X,*CAVITATION NO. BEFORE CORRECTION=*,F10.5)
366 FORMAT(5X,*CAVITATION NO. AFTER CORRECTION=*,F10.5)
775 CONTINUE
  SC=SCN
  ICLCD=0
  CLS(KT)=CLCD(KT,SC,AE,ICLCD)
  ICLCD=1
  CDS(KT)=CLCD(KT,SC,AE,ICLCD)
  ICLCD=2
  GGG(KT)=XX(KT)*VIVA(KT)*CLCD(KT,SC,AE,ICLCD)*SRI(KT)/ZZ
190 CONTINUE
  IF(ITERA.LT.ITERAW) GO TO 228
  WRITE(6,198) (GGG(I),I=2,MM1)
  WRITE(6,193) (CLS(I),I=2,MM1)
  WRITE(6,194) (CDS(I),I=2,MM1)
193 FORMAT(5X,*CL(I)=*,8(F10.5,1X))
194 FORMAT(5X,*CD(I)=*,8(F10.5,1X))
198 FORMAT(2X,*GGG(I)=*,8(F10.5,1X))
228 CONTINUE
C DATA FOR CUBIC SPLINE METHOD AND GAUSS QUADRATURE.
  XCT(1)=1.
  XCT(MM2)=1.
  FCT(1)=0.
  FCP(1)=0.
  FCT(MM2)=0.
  FCP(MM2)=0.
  FTD(1)=0.
  FPD(1)=0.
  FTD(MM2)=0.
  FPD(MM2)=0.
  RES=0IA*.5/12.*VASHIP*.LE5
  RE1=1.E6

```

```

RE2=1.E8
N0 310 ICT=2,MM1
XCT(ICT)=(XX(ICT)-XH1)/XHA
XCUN=XH1+XHA*XC(ICT)
R1E1=BE(PI(1CT))*CONV
CBIE=CUS(B1FI)
SBIE=SIN(B1FI)
FC=VIVA(1CT)**2*SOLI(1CT)*XCON*XHA *SRI(1CT)**2
FCT(1CT)=FC*(LBIE*CLS(1CT)-SBIE*CDS(1CT))
FCP(1CT)=FC*XCON*(SBIE*CLS(1CT)+CBIE*CDS(1CT))
C REYNOLDS NUMBER BASED ON PROPELLER(RES) *****FRICTION DRAG*****
C REYNOLDS NUMBER BASED ON PROPELLER RADIUS AND ADVANCE SPEED--- *
C ----RES=R*VASHIP/NU. *
C REX IS A LOCAL REYNOLDS NUMBER. *
VIVA2=VIVA(1CT)**2 *
PSD=VIVA2*SOLI(1CT)*XX(1CT)*.5/ZZ *
REX=VIVA(1CT)*SOLI(1CT)*2.*PI/ZZ *
REX=REX*XX(1CT)*RES*SRI(1CT) *
TF(REX.LE.RE1) CF=0.664/SQRT(REX) *
TF(REX.GE.RE2) CF=0.030/REX**0.142857 *
CF=0.040/REX**0.166666667 *
PSDF=PSD*CF*XHA *
RETAGR=RETAG(1CT)*CONV *
SBG=SIN(BETAGR) *
CBG=CUS(BETAGR) *
FTD(1CT)=FC*CF*SBG *
310 FPD(1CT)=FC*XCON*CF*CBG *
CALL SPLINE(XLT,FCT,DY,S2,S3,T,UFCT,SS1,SS2,MM2,NGAUS,C1)
CALL SPLINE(XCT,FCP,DY,S2,S3,T,OFCP,SS1,SS2,MM2,NGAUS,C1)
CALL SPLINE(XCT,FTD,DY,S2,S3,T,OFD,SS1,SS2,MM2,NGAUS,C1)
CALL SPLINE(XLT,FPD,DY,S2,S3,T,OFD,SS1,SS2,MM2,NGAUS,C1)
CT=0.
CP=0.
CTD=0.
CPD=0.
N0 311 ICP=1,NGAUS
CT=CT+UFCT(ICP)*W(ICP)
CP=CP+OFCP(ICP)*W(ICP)
CTD=CTD+UFD(ICP)*W(ICP)
311 CPD=CPD+OFD(ICP)*W(ICP)
XLAM=XJJ/PAI
CT=2.*CT
CP=2.*CP/XLAM
EFF=CT/CP
CTD=CT-2.*CTD
CPD=CP+2.*CPD/XLAM
EFFD=CTD/CPD
XJJ2=XJJ**2
XJJ3=XJJ2*XJJ
XKT=CT*XJJ2*PAI/8.
XPT=CP*XJJ3/16.
XKTD=CTD*XJJ2*PAI/8.
XPTD=CPD*XJJ3/16.
TF(ITERA.LT.ITERAW) GO TO 585
WRITE(6,312) CT ,XKT,CTD,XKTD
WRITE(6,313) CP ,XPT,CPD,XPTD
WRITE(6,314) EFF,EFFD
312 FORMAT(15X,*THRUST COEFFICIENT=*,F10.5,5X,*KT=*,F10.5,3X,*CT WITH
*FRICTION DRAG=*,F10.5,2X,*KTD=*,F10.5)
313 FORMAT(16X,*POWER COEFFICIENT=*,F10.5,5X,*KP=*,F10.5,3X,*CP WITH F

```

```

XDRIFTION DRAG=*,F10.5,2X,*KPD=*,F10.5)
314 FORMAT(22X,*EFFICIENCY CT/CP=*,F10.5,5X,*EFFICIENCY WITH FRICTION
XDRAG=*,F10.5)
505 CONTINUE
IF(ITERA.EQ.MAXIT) GO TO 999
ITERA=ITERA+1
DO 755 IUK=2,MM1
IUKA=IUK-1
GM(IUKA)=XXM*GMU(IUKA)+(1.-XXM)*GM(IUK)
ALFE(IUK)=XXM*ALFEU(IUK)+(1.-XXM)*ALFE(IUK)
ALFI(IUK)=BFTAG(IUK)-BETA(IUK)-ALFE(IUK)
755 RETAI(IUK)=BETA(IUK)-ALFI(IUK)
IF(ITERA.LE.ITERAW) GO TO 230
WRITE(6,182) (ALFE(I),I=2,MM1)
182 FORMAT(3X,*ALFE(I)=*,8(F10.5,1X))
230 CONTINUE
GO TO 987
999 STOP
END

```

```

FUNCTION CLCD(I,S,B,ILD)
C THIS SUBROUTINE INTERPOLATES CL,CD AND CIRCULATION FROM INPUT DATA AT X, SIGMA
C AND ALFA, DEPENDING ON ICLCD=0,1,2.
COMMON PAI, CONV, CONVI, SIGM1N(10)
COMMON SIGD(10,5,15), CL1(10,5,15), ANGI(5), CD1(10,5,15)
COMMON MANGLE, ISIG, GGGI(10,5,15)
DIMENSION P( 3,10), Q( 3,10), STOR(10,23), ALE2(10), A(10)
C I SPECIFIES XX(I).
C S IS CAVITATION NO. FOR ALG2 TO BE EVALUATED.
C A IS EFFECTIVE FLOW INCIDENCE ANGLE FOR ALG2 TO BE EVALUATED.
CHISO=0.01
ISIG=ISIG-1
M=MANGLE-1
MM=MANGLE
IF(S.LE.SIGM1N(I)) MM=MI
DO 1 K=1,MM
IT=3
IF(S.LE.SIGD(I,K,1)) GO TO 10
IF(S.GE.SIGD(I,K,ISIG)) GO TO 11
IF(S.LE.SIGD(I,K,2)) GO TO 10
IF(S.GE.SIGD(I,K,ISIGA)) GO TO 11
21 D=SIGD(I,K,IT)-S
IF(D.GE.0.) GO TO 20
IT=IT+1
IF(IT.GE.ISIG) STOP
GO TO 21
20 ISC=IT-2
ISB=IT-1
ITT=IT
ISI=IT+1
22 P(1,1)=SIGD(I,K,ISC)
P(1,2)=SIGD(I,K,ISB)
P(1,3)=SIGD(I,K,ITT)
P(1,4)=SIGD(I,K,ISI)
IF(ILD.EQ.1) GO TO 30
IF(ILD.EQ.2) GO TO 32
P(2,1)=CL1(I,K,ISC)
P(2,2)=CL1(I,K,ISB)
P(2,3)=CL1(I,K,ITT)
P(2,4)=CL1(I,K,ISI)
GO TO 31
30 P(2,1)=CD1(I,K,ISC)
P(2,2)=CD1(I,K,ISB)
P(2,3)=CD1(I,K,ITT)
P(2,4)=CD1(I,K,ISI)
GO TO 31
32 P(2,1)=GGGI(I,K,ISC)
P(2,2)=GGGI(I,K,ISB)
P(2,3)=GGGI(I,K,ITT)
P(2,4)=GGGI(I,K,ISI)
31 CONTINUE
DO 55 KS=1,4
55 P(3,KS)=0.002
N=4
M=3
CALL LSQUAR(P,N,M,A,CHISO,STOR)
ALE2(K)=A(1)
MM=MM-1
DO 56 KM=1,MM
KM1=KM-1

```

```

56 ALE2(K)=ALEZ(K)+A(KM1)*S**KM
GO TO 1
10 ISC=1
ISB=2
ITT=3
IS1=4
GO TO 22
11 ISC=ISIG-3
ISB=ISIG-2
ITT=ISIG-1
IS1=ISIG
GO TO 22
1 CONTINUE
C NOW FOUND ALE2(MANGLE) CORRESPONDING TO ANG1(MANGLE).
C THUS DETERMINE CLCD AND CIRCULATION CORRESPONDING TO A.
DO 57 KL=1,3
DO 57 KN=1,MAN
IF(KL.EQ.1) Q(KL,KN)=ANG1(KN)
IF(KL.EQ.2) Q(KL,KN)=ALEZ(KN)
57 IF(KL.EQ.3) Q(KL,KN)=0.002
MANA=MAN-1
MANB=MAN-2
CALL LSQUAR(G,MAN,MANA,A,CHISO,STOR)
CLCD=A(1)
DO 58 KT=1,MANB
KT1=KT+1
58 CLCD=CLCD+A(KT1)*B**KT
RETURN
END

```

```

SUBROUTINE FITC4V(MM1,SE,EE,M1,I1,ACC)
DIMENSION SE(10,5,5),EE(10,5,5),ACC(10,5,5),P(50,5),Q(50,5)
DO 1 I=2,MM1
DO 1 J=1,M1
DO 2 K=1,I1
DO 2 L=1,I1
IF(L.EQ.1) P(K,L)=EE(I,J,K)
IF(L.EQ.2) P(K,L)=1.
2 IF(L.EQ.3) P(K,L)=-SE(I,J,K)
CALL DETERM(P,I1,DB)
DO 3 IU=1,I1
DO 4 LP=1,I1
Q(LP,IU)=P(LP,IU)
4 P(LP,IU)=SE(I,J,LP)*EE(I,J,LP)
CALL DETERM(P,I1,DC)
ACC(I,J,IU)=DU/DB
DO 5 LP=1,I1
5 P(LP,IU)=Q(LP,IU)
3 CONTINUE
1 CONTINUE
RETURN
END

```

vv

```

SUBROUTINE CAVINO(NG,SC,AE,ACC,A2,I1,SCN,EE,M1)
DIMENSION ACB(5)
DIMENSION ACC(10,5,5),A2(10),EE(10,5,5),XX(5),P(50,5),Q(50,5)
ER1=1.E-3
ER2=ER1
IFL=0
M1A=M1-1
I=1
2 IF(AE.LE.A2(I)) GO TO 1
IF(I.GE.M1) GO TO 1
I=I+1
GO TO 2
1 CONTINUE
K=I-2
IF(I.EQ.1.OR.I.EQ.2) K=1
IF(I.EQ.M1A.UR.I.EQ.M1) K=M1-2
K3=K+2
C FIND EEX.
DO 3 KI=K,K3
C A MUST BE LESS THAN ONE.
A=:S
10 B=A-0.001
IF(IFL.EQ.1) WRITE(6,40)
40 FORMAT(1X,-----E BECAME NEGATIVE-----)
IF(IFL.EQ.1) STOP
CALL FANC(PF,B,SC,ACC,NG,KI,I1)
IF(PF.GE.0.) GO TO 11
A=B
GO TO 10
11 CONTINUE
AAR=A
A=B
R=AAR
CALL MOSEC(A,B,ER1,ER2,X,J,NG,KI,SC,ACC,I1)
C CONVERT E(OR X) INTO SIGMA.
PS1=2.-X
PS2=2.-2.*X
PS3=PS1/PS2
PS4=PS3**2
SIGMA=SC*PS4
3 XX(KI)=SIGMA
C WE HAVE CAVITATION NO. AS A FUNC. OF ANG2.
C PUT IN A POLYNOMIAL FORM.
DO 20 IS=1,3
DO 20 IT=1,3
20 P(IS,IT)=A2(K+IS-1)**(IT-1)
CALL DETERM(P,3,DB)
DO 21 ID=1,3
DO 22 IE=1,3
Q(IE,ID)=P(IE,ID)
22 P(IE,ID)=XX(K+IE-1)
CALL DETERM(P,3,DC)
ACH(ID)=UC/DB
DO 23 IE=1,3
23 P(IE,ID)=Q(IE,ID)
21 CONTINUE
SCN=ACB(1)
DO 24 IL=1,2
IL1=IL+1
24 SCN=SCN+ACB(IL1)*AE**IL
RETURN
END

```

```
SUBROUTINE FANC(F,CE,SC,ACC,NG,KI,II)
DIMENSION ACC(10,5,5)
RHS1=ACC(NG,KI,1)*EE+ACC(NG,KI,2)
RHS2=EL+ACC(NG,KI,3)
RHS=RHS1/RHS2
AA1=2.-EE
AA2=2.-2.*EF
AA3=AA1/AA2
AA4=AA3**2
XLHS=SC*AA4
F=XLHS-RHS
F=-F
RETURN
END
```

```

SUBROUTINE MOSEC(A,B,ER1,ER2,X,J,NG,KI,SC,ACC,I1)
DIMENSION ACC(10,5,5)
J=0
X1=A
X2=B
4 J=J+1
IF(J.GE.800) GO TO 8
CALL FANC(PFX1,X1,SC,ACC,NG,KI,I1)
CALL FANC(PFX2,X2,SC,ACC,NG,KI,I1)
X3=X1+(X2-X1)*PFX1/(PFX1-PFX2)
CALL FANC(PFX3,X3,SC,ACC,NG,KI,I1)
IF(PFX3)1,2,3
1 X2=X3
X1=X1
IF(A=B)10,10,11
10 Y=X3-ER1
IF(Y.LE.0.) Y=0.
GO TO 12
11 Y=X3+ER1
12 CALL FANC(PFY,Y,SC,ACC,NG,KI,I1)
IF(PFY) 5,2,2
3 X1=X3
X2=X2
IF(A=B) 20,20,21
20 Z=X3+ER1
GO TO 22
21 Z=X3-ER1
22 CALL FANC(PFZ,Z,SC,ACC,NG,KI,I1)
IF(PFZ)2,2,5
5 GO TO 4
2 PP=ABS(PFX3)
IF(PP-ER2) 6,6,4
6 X=X3
GO TO 7
8 WRITE(6,9) J
9 FORMAT(1X,2HJ=,I3)
STOP
7 RETURN
END

```

```

SUBROUTINE DETERM (A,N,D)
C  DETERM  REVISED 02-28-73
REAL M
DIMENSION A(50,50),SAVEA(50,50)
IF (N .EQ. 1)GO TO 46
C = 1.
NN = N
DO 9 J = 1,NN
DO 9 I = 1,NN
9  SAVEA(I,J) = A(I,J)
K = 1
GO TO 13
12  K = K + 1
13  I = K + 1
L = K
GO TO 17
16  I = I + 1
17  IF (ABS(SAVEA(I,K)) .GT. ABS(SAVEA(L,K))) L = I
IF (I .NE. NN)GO TO 16
IF (L .EQ. K)GO TO 28
J = K
C  ROW INTERCHANGE
GO TO 23
22  J = J + 1
23  SAVEKJ = SAVEA(K,J)
SAVEA(K,J) = SAVEA(L,J)
SAVEA(L,J) = SAVEKJ
IF (J .NE. NN)GO TO 22
C = -C
28  I = K + 1
GO TO 31
30  I = I + 1
31  CONTINUE
IF (SAVEA(K,K) .EQ. 0.) GO TO 48
M = SAVEA(I,K) / SAVEA(K,K)
SAVEA(I,K) = 0.
J = K + 1
GO TO 36
35  J = J + 1
36  SAVEA(I,J) = SAVEA(I,J) - M * SAVEA(K,J)
IF (J .NE. NN)GO TO 35
IF (I .NE. NN)GO TO 30
IF (K .NE. (NN-1))GO TO 12
D = 1.
DO 43 I = 1,NN
J = I
D = D * SAVEA(I,J)
IF (ABS(D) .LT. 1.E-36) GO TO 48
43  CONTINUE
D = D * C
RETURN
46  D = A(1,1)
RETURN
48  D = 0.
WRITE (6,51)
RETURN
51  FORMAT(/SX, #ERROR MESSAGE FROM DETERM. #/
! SX, #MATRIX IS SINGULAR. DETERMINANT SET = 0. # //)
END

```

```

SUBROUTINE LSQUAR(DATA,NUMBER,N,A,CHISQ,XM)
C LSQUAR DATE OF OBJECT DECK 06-09-72
C LSQUAR PROVIDES A POLYNOMIAL FIT (OF DEGREE N-1) TO THE FUNCTION
C  $Y = F(X)$ . THE (3XN) DATA MATRIX IS A MATRIX OF DATA VECTORS OF HA
C THE FORM (X(I),Y(I),SIGMA(I)).
C CALLING SEQUENCE CALL LSQUAR(DATA,NUMBER,N,A,CHISQ,XM)
C NUMBER= NUMBER OF DATA POINTS
C N= DEGREE OF POLYNOMIAL + 1
C A= ARRAY, DIMENSION N, CONTAINING THE COEFFICIENTS OF THE POLY-
C NOMIAL DEFINED AS  $A(1)+A(2)*X+ \dots +A(N)*X**(N-1)$ 
C CHISQ= REAL VARIABLE, IF CHISQ=0. WHEN ENTERING LSQUARE, ERROR
C MESSAGES, IF ANY, WILL BE PRINTED. UPON NORMAL RETURN TO THE CALLER
C CHISQ CONTAINS SOME POSITIVE NUMBER. IF, DURING INVERSION, AN ERROR
C HAS BEEN ENCOUNTERED, CHISQ IS SET TO A NEGATIVE VALUE,
C -1. IF THE MATRIX WAS SINGULAR,
C -2. IF AN OVERFLOW OR DIVIDE CHECK OCCURED.
COMMON/LSQCOM/TEMP(100)
COMMON/LSQNUM/SING,NORM
LOGICAL RITE
C THE ARRAY XM IS FOR WORKING STORAGE. IT SHOULD BE DIMENSIONED IN THE
C MAIN PROGRAM BY THE FOLLOWING STATEMENT
C WHERE NMAX IS THE MAXIMUM VALUE OF N IN THE CALLING PROGRAM.
C DIMENSION DATA(3,NUMBER),A(N),XM(N,1)
C SAVE SPACE
EQUIVALENCE (M2,KK),(RR,R),(XX,S)
EPS=1.0E-06
RITE=.FALSE.
C IF THE INPUT VALUE OF CHISQ IS 0. ALLOW PRINTING OF ERROR MESSAGES.
IF (CHISQ.EQ.0.) RITE=.TRUE.
ITER=5
IF (RITE) ITER=-ITER
N21=2*N+1
N22=N21+1
N23=N21+2
3 IF (NORM) S,1,4
4 DO 2 I=1,NUMBER
2 TEMP(I)=DATA(1,I)
IF (NORM=1) 1,1,5
5 AVE = 0.0
SIGMA = 0.0
DO 210 I=1,NUMBER
AVE = AVE+DATA(1,I)
SIGMA = SIGMA+DATA(1,I)**2
210 CONTINUE
AVE = AVE/NUMBER
SIGMA = SQRT(SIGMA/NUMBER-AVE*AVE)
DO 220 I=1,NUMBER
DATA(1,I)=(DATA(1,I)-AVE)/SIGMA
220 CONTINUE
SIGMA = 1/SIGMA
AVE = -AVE*SIGMA
1 DO 12 I=1,N
DO 12 J=N21,N23
12 XM(I,J)=0.E0
C COMPUTE THE MOMENTS OF THE DATA HA
M2=2*N
DO 26 I=1,NUMBER
RR=(1.E0/DATA(3,I))**2
XM(2,N21)=XM(2,N21)+RR

```

	XX=DATA(2,I)*RR	63
	XM(1,N23)=XM(1,N23)+XX	64
	IF (N.EQ.1) GO TO 26	65
	DO 21 J=3,M2	66
	RR=RR+DATA(1,I)	67
	IF (J.GT.N) GO TO 22	68
	XM(J,N21)=XM(J,N21)+RR	69
	GO TO 21	70
22	XM(J=N,N22)=XM(J=N,N22)+RR	71
21	CONTINUE	72
	DO 25 J= 2,N	73
	XX=XX+DATA(1,I)	74
25	XM(J,N23)=XM(J,N23)+XX	75
26	CONTINUE	76
C	COMPUTE MATRIX FOR INVERSION	HA 77
	DO 31 I=1,N	78
	DO 31 J = 1, N	79
	K=I+J	80
	IF (K.GT.N) GO TO 32	81
	XM(I,J)=XM(K,N21)	82
	GO TO 31	83
32	XM(I,J)=XM(K=N,N22)	84
31	CONTINUE	85
C	CALL DOUBLE PRECISION MATRIX INVERSION ROUTINE	86
	IF(N.NE.1)GO TO 35	87
	XM(1,1)=(1.0 E 00) / XM(1,1)	
	A(1)=XM(1,1)*XM(1,N23)	89
	GO TO 37	90
35	CALL MLRRAR(N, XM, XM(1,N23), ITER, EPS, A, ITEST, 0, XM(1,N+1))	HA 91
	IF(ITEST.GE.5) GO TO 80	92
C	COMPUTE CHI-SQUARE FOR RESULTING FIT	93
37	CHISQ = 0.0	HA 94
	DO 70 I = 1, NUMBER	95
	S = A(1)	96
	IF(N.EQ.1)GO TO 69	97
	R = 1.	98
	DO 68 J = 2, N	99
	R = R*DATA(1,I)	100
68	S = S+A(J)* R	101
69	CHISQ = CHISQ + ((S -DATA(2,I))/DATA(3,I))**2	102
70	CONTINUE	HA 103
	GO TO 79	104
C	PRINT MESSAGES AFTER INVERSION OF THE MATRIX XM (M IN THE WRITE-UP).	105
80	CONTINUE	106
	SING=5.	107
	IF (RITE) WRITE (6,800) ITEST	108
800	FORMAT(/IX+NO CONVERGENCE? IS,+ITERATIONS?/)	109
	CHISQ = -2.0	110
79	IF ((NORM.EQ.0).OR.(NORM.EQ.1)) RETURN	111
	L=N-1	112
	DO 6 I=1,L	113
	XM(I,1)=AVE**I	114
6	XM(I,2)=0.E0	
	XM(I,2)=1.E0	
	XM(N,2)=0.F0	
	DO 7 I=1,L	118
	K=N-I+1	119
	DO 8 J=2,K	120
8	XM(J,2)=XM(J,2)+XM(J-1,2)	121
	K=I+1	122

	DO 9 J=K,N	123
	9 A(I)=A(I)+A(J)*XM(J-I+1,2)*XM(J-I,1)	124
	A(I)=A(I)*SIGMA**(I-1)	125
	7 CONTINUE	126
	A(N)=A(N)*SIGMA**(N-1)	127
	RETURN	128
	END	129
	RLOCK DATA	130
	COMMON/LSQUUM/SING,NORM	01 131
	DATA NURM/J/	
	END	133
	SUBROUTINE MLSSR(N,RDMTX, V,ITER,EPS,F, IT, INEW,A)	134
C	MLSSR DATE OF OBJECT DECK 06-09-72	135
	LOGICAL RITE	138
C	THE VALUE OF THE SINGULARITY IS AVAILABLE IN THE LABELLED COMMON	139
	COMMON /LSQUUM/ SING	140
C	N = ORDER OF MATRIX	141
C	RDMTX = TWO- DIMENSIONAL ARRAY OF COEFFICIENTS	142
C	V = RIGHT-HAND VECTOR	143
C	ITER = MAXIMUM NUMBER OF ITERATIONS DESIRED	144
C	EPS = TOLERANCE FOR CONVERGENCE (.GE. 1.E-7)	145
C	F = RESULTING VECTOR	146
C	IT = OUTPUT FROM ROUTINE SPECIFYING NUMBER OF ITERATIONS ACTUALLY D	147
C	INEW (FIRST CALL) SET INEW = 1	148
C	(LATER CALLS) IF THE MATRIX IS UNCHANGED AND ONLY THE	149
C	COLUMN VECTOR B IS CHANGED, THEN SET INEW = 1	150
	DIMENSION RDMTX(N,N), V(N), F(N), A(N,N), X(50), IX(50), XT(50)	151
	RITE=.FALSE.	152
	IF (ITER.LT.0) RITE=.TRUE.	153
	ITER=IABS(ITER)	154
	IT = 0	155
	DO 9 I = 1,N	156
	X(I) = V(I)	157
	F(I) = 0.0	158
	9 CONTINUE	159
	NI = N - 1	160
	IF (INEW .EQ. 1) GO TO 181	161
	DO 10 I = 1, NI	162
	DO 10 J = 1, NI	163
	A(I,J) = RDMTX(I,J)	164
	10 CONTINUE	165
	DO 12 I = 1,NI	166
	12 IX(I) = I	167
	SGI = 0.	168
	DO 60 I = 2, NI	169
C	PARTIAL PIVOTING, CHECK FOR MAX ELEMENT IN (I-1)ST COLUMN.	170
	IM1 = I - 1	171
	AMX = ABS(A(IM1,IM1))	
	JMX = IM1	173
	DO 16 J = 1,NI	174
	ABSA = ABS(A(J,IM1))	
	IF (AMX .GE. ABSA) GO TO 16	176
	AMX = ABSA	177
	JMX = J	178
	16 CONTINUE	179
	IF (JMX .EQ. IM1) GO TO 20	180
C	MOVE THE ROW WITH MAX A(J,IM1) TO (IM1)ST ROW.	181
	DO 18 K = 1,NI	182
	T = A(IM1,K)	183

	A(IM1,K) = A(JMX,K)	184
18	A(JMX,K) = T	185
	TI = IDX(IM1)	186
	IDX(IM1) = IDX(JMX)	187
	IDX(JMX) = TI	188
	XI = X(IM1)	189
	X(IM1) = X(JMX)	190
	X(JMX) = XI	191
	SG1 = 1.0	192
20	CONTINUE	193
	TF(A(IM1,IM1).EQ.0.) GO TO 200	194
	NO 55 J = 1, N	195
	CX = A(J,IM1) / A(IM1,IM1)	196
	NO 50 K = 1, N	197
	A(J,K)=A(J,K)-CX*A(IM1,K)	198
50	CONTINUE	199
	A(J,IM1) = CX	200
55	CONTINUE	201
60	CONTINUE	202
C	FORWARD PASS - OPERATE ON RIGHT HAND SIDE AS	203
C	ON MATRIX	204
62	CONTINUE	205
	NO 70 I = 2, N	206
	NO 65 J = 1, N	207
	X(J) = X(J) - X(I-1) * A(J,I-1)	208
65	CONTINUE	209
70	CONTINUE	210
C		211
C	BACKWARD PASS - SOLVE FOR AX = B	212
	X(N) = X(N) / A(N,N)	213
	NO 80 I = 1, N1	214
	SUM = 0.0	215
	I2 = N - I + 1	216
	IM1=I2-1	217
	NO 75 J = I2, N	218
	SUM = SUM + A(IM1,J) * X(J)	219
75	CONTINUE	220
	X(IM1) = (X(IM1)-SUM) / A(IM1,IM1)	221
80	CONTINUE	222
	NO 90 I = 1, N	223
	F(I)=F(I)+ X(I)	
90	CONTINUE	225
	SING=0.	226
	TF(IT.EQ.ITER) RETURN	227
	IT = IT + 1	228
	NO 95 I = 1, N	229
	TF (F(I).EQ.0.) SING=7.23E75	230
	TF (F(I).EQ.0.) GO TO 150	231
	SING= MAX1(SING , ABS(F(I)))	
95	CONTINUE	233
	TF (SING.GT.EPS) GO TO 150	234
C	FINISHED	235
	RETURN	236
C	DOUBLE PRECISION MATRIX MULTIPLICATION	237
150	CONTINUE	238
	NO 170 I = 1, N	239
	R = 0.0E0	
	NO 160 J = 1, N	241
	R = R + RUMTX(I,J) * F(J)	242
160	CONTINUE	243

	X(I) = V(I) - R	244
170	CONTINUE	245
181	IF(SG1 .EQ. 0.0) GO TO 62	246
C	IF SG1 .NE. 0, PERMUTE X BEFORE PERFORMING FORWARD PASS.	247
	DO 182 I=1,N	248
182	XI(I) = X(I)	249
	DO 184 I = 1,N	250
	K = IDX(I)	251
184	X(I) = XI(K)	252
	GO TO 62	253
200	IF (RITE) WRITE (6,510) IM1	254
510	FORMAT(/IX, 'ERROR RETURN FROM MLSTRAR2 DIAGONAL TERM ↑, I2,	255
	I ↑ REDUCED TO ZERO.↑//)	256
	RETURN	257
	END	258

```
FUNCTION FALF(X)
  IF(X.EQ.0.) GO TO 1
  SX=SIN(2.*X)
  X2=X**2
  X3=X2*X
  SX2=SIN(X)**2
  FALF=1./X+SX/(2.*X2)-2.*SX2/X3
  GO TO 2
1 FALF=0.
2 RETURN
END
```

```
FUNCTION FGAM(X)
  IF(X.EQ.0.) GO TO 1
  SX=SIN(X)
  CX=COS(X)
  X2=X**2
  X3=X2*X
  FGAM=4.*(SX/X3-CX/X2)
  GO TO 2
1 FGAM=1.53333333333
2 RETURN
END
```

```
FUNCTION FAFT(X)
  IF(X.EQ.0.) GO TO 1
  CX=COS(X)
  CX2=CX**2
  S2X=SIN(2.*X)
  X2=X**2
  X3=X2*X
  FBET=2.*(1.+CX2)/X2-S2X/X3
  GO TO 2
1  FBET=0.666666666667
2  RETURN
END
```

```

SUBROUTINE SPLINE(X,Y,DY,S2,S3,T,SS,SSI ,S92,LIM,N ,C1)
C
C   SPLINE INTERPOLATION
C
DIMENSION X(1),Y(1),S2(1),S3(1),DY(1),T(1),SS(1),SSI(1),S92(1)
LIM1=LIM-1
DO 10 J=1,LIM1
10  DY(J)=(Y(J+1)-Y(J))/(X(J+1)-X(J))
    DY1=DY(1)
    DO 20 J=2,LIM1
    DX=1./(X(J+1)-X(J-1))
    S3(J)=.5*(X(J)-X(J-1))*DX
    DSQY=(DY(J)-DY1)*DX
    DY1=DY(J)
    S2(J)=2.*DSQY
20  DY(J)=3.*DSQY
    S2(1)=.5*S2(2)
    S2(LIM)=.5*S2(LIM-1)
    OMEGA=1.0717968
    DATA MAXITER/20/
    ITER=0
25  ETA=0.
    ITER=ITER+1
    DO 30 J=2,LIM1
    W=(DY(J)-S3(J)*S2(J-1)-(.5-S3(J))*S2(J+1)-S2(J))*OMEGA
    ETA=AMAX1(ETA,ABS(W))
30  S2(J)=S2(J)+W
    IF(ETA.GT.C1.AND.ITER.LT.MAXITER) GOTO 25
    DO 40 J=1,LIM1
    DX=1./(X(J+1)-X(J))
    DY(J)=(Y(J+1)-Y(J))*DX
40  S3(J)=(S2(J+1)-S2(J))*DX
    ENTRY ABCD
    DO 61 J=1,N
    I=1
    IF(T(J)-X(1)) 58,17,55
55  IF(T(J)-X(LIM)) 57,59,58
56  IF(T(J)-X(1)) 60,17,57
57  I=I+1
    GOTO 56
58  PRINT 44,J
44  FORMAT(1X,I5,* ARGUMENT OUT OF RANGE*)
    GOTO 61
59  I=LIM

```

```
60   I=-1
17   HT1=T(J)-X(I)
      HT2=T(J)-X(I+1)
      PRUD=HT1*HT2
      SS2(J)=S2(I)+HT1*S3(I)
      DSQS=(S2(I)+S2(I+1)+SS2(J))*1.666666667
      SS1(J)=UY(I)+(HT1+HT2)*DSQS+PRUD*S3(I)*1.666666667
      SS(J)=Y(I)+HT1*DY(I)+PRUD*DSQS
61   CONTINUE
      RETURN
      END
```

6 TYPICAL INPUT DATA SET-UP

64							
.0243502926	.0729931218	.1214628193	.1696444204	.2174236437	.2646871622	.3113228720	.3572201583
.4022701579	.4463660173	.4894031457	.5312794640	.5718956462	.6111553552	.6489654713	.6852363131
.7198818502	.7528199073	.7839723589	.8132653151	.8406292963	.8659993982	.8893154460	.9105221371
.9295691721	.946413749	.9610087997	.9733268278	.9833362539	.9910133715	.9963401168	.9993050417
.0486909570	.0485754674	.0483447622	.0479993886	.0475401657	.0469681828	.0462847966	.0454916279
.0445905582	.0435837245	.0424735151	.0412625632	.0399537411	.0385501352	.0370551285	.0354722133
.0338651618	.0320579284	.0302346571	.0283396726	.0263777697	.0243527026	.0222701738	.0201348231
.0179517158	.0157260305	.0134630479	.0111681395	.0088467598	.0065044580	.0041470333	.0017832807
.05							
150	5	20	30	10	1	10	
14	25						
.500	3.	.617	.2	0.0			
.4	.6	.7	.8	.9			
31.23	22.36	19.67	17.60	15.97			
6.07507	5.12506	4.65356	4.55185	4.26112			
.912	.594	.479	.365	.244			
2.81884	4.81005	4.85775	5.53833	6.21720			
.4	5	8	.040				
2.							
.015	.020	.025	.030	.035	.040	.045	.050
.092	.108	.124	.141	.158	.178	.197	.221
.0031	.0037	.0044	.0051	.0058	.0066	.0074	.0083
.03820	.04600	.05440	.06290	.07190	.08120	.09140	.10200
3.							
.020	.025	.030	.035	.040	.045	.050	.055
.086	.102	.120	.137	.155	.172	.190	.209
.0043	.0051	.0060	.0069	.0079	.0090	.0100	.0111
.03760	.04530	.05310	.06120	.06930	.07760	.08590	.09450
4.							
.030	.035	.040	.045	.050	.055	.060	.065
.100	.122	.143	.163	.181	.195	.210	.222
.0071	.0088	.0102	.0115	.0126	.0136	.0145	.0154
.04650	.05450	.06230	.07000	.07720	.08390	.08980	.09510
5.							
.035	.038	.042	.048	.054	.060	.065	.075
.095	.111	.131	.158	.181	.203	.218	.243
.0077	.0093	.0112	.0135	.0154	.0170	.0183	.0206
.04600	.05200	.06110	.07330	.08360	.09270	.09920	.11100
6.							
.042	.045	.050	.055	.060	.065	.070	.075
.094	.113	.144	.171	.195	.215	.231	.245
.0094	.0121	.0156	.0184	.0206	.0225	.0241	.0255
.05220	.06190	.07590	.08720	.09700	.10520	.11200	.11800
.6	5	8	.045				
2.							
.008	.015	.020	.025	.030	.040	.050	.060
.082	.104	.117	.128	.138	.159	.178	.198
.0027	.0035	.0040	.0043	.0046	.0052	.0057	.0063
.02350	.03120	.03430	.03790	.04130	.04730	.05310	.05940
3.							
.013	.020	.025	.030	.035	.045	.055	.065

Preceding page blank

.090	.117	.130	.141	.151	.171	.192	.212
.0043	.0056	.0063	.0069	.0075	.0085	.0095	.0104
.02740	.03510	.03880	.04220	.04540	.05190	.05790	.06380
4.							
.018	.020	.025	.030	.035	.045	.055	.065
.098	.111	.130	.143	.155	.177	.196	.215
.0061	.0070	.0084	.0095	.0103	.0117	.0129	.0141
.02950	.03280	.03880	.04320	.04650	.05320	.05950	.06550
5.							
.023	.026	.029	.035	.040	.045	.055	.065
.102	.124	.137	.154	.167	.178	.199	.218
.0077	.0088	.0098	.0116	.0130	.0141	.0160	.0177
.03350	.03760	.04070	.04630	.05020	.05380	.06110	.06770
6.							
.027	.030	.035	.040	.045	.050	.055	.065
.108	.132	.151	.166	.178	.190	.201	.221
.0104	.0124	.0147	.0165	.0180	.0192	.0203	.0223
.03640	.04000	.04560	.05090	.05520	.05940	.06320	.07020
7	5	8	.025				
2.							
.008	.015	.020	.025	.030	.045	.060	.075
.082	.100	.109	.118	.127	.151	.175	.197
.0025	.0030	.0034	.0037	.0039	.0047	.0055	.0061
.01890	.02310	.02540	.02750	.02960	.03570	.04190	.04780
3.							
.013	.018	.025	.030	.035	.045	.055	.065
.096	.112	.124	.133	.142	.158	.174	.189
.0043	.0052	.0060	.0064	.0068	.0075	.0082	.0088
.02260	.02650	.02970	.03180	.03390	.03790	.04160	.04540
4.							
.017	.020	.025	.030	.035	.045	.055	.065
.101	.115	.130	.140	.149	.165	.181	.196
.0062	.0072	.0083	.0090	.0096	.0107	.0118	.0127
.02530	.02850	.03120	.03340	.03570	.03990	.04390	.04780
5.							
.020	.022	.025	.030	.035	.040	.050	.060
.103	.115	.128	.142	.153	.161	.178	.193
.0072	.0082	.0093	.0108	.0119	.0128	.0145	.0158
.02820	.03050	.03260	.03510	.03770	.03980	.04390	.04770
6.							
.023	.026	.030	.035	.040	.050	.060	.070
.105	.131	.146	.156	.165	.182	.198	.214
.0108	.0130	.0144	.0156	.0166	.0182	.0197	.0208
.03040	.03410	.03680	.03920	.04140	.04580	.04960	.05350
8	5	8	.025				
2.							
.008	.015	.020	.025	.030	.040	.050	.060
.073	.087	.095	.105	.112	.126	.140	.153
.0022	.0026	.0030	.0032	.0035	.0039	.0042	.0047
.01220	.01500	.01680	.01830	.01980	.02240	.02500	.02750
3.							
.012	.015	.020	.025	.030	.040	.050	.060
.084	.092	.103	.114	.122	.137	.150	.162
.0037	.0042	.0048	.0053	.0058	.0064	.0071	.0077
.01520	.01670	.01880	.02050	.02190	.02470	.02710	.02920
4.							
.015	.017	.020	.025	.030	.040	.050	.060
.090	.101	.111	.123	.131	.146	.160	.172
.0054	.0060	.0066	.0075	.0082	.0093	.0102	.0110
.01790	.01920	.02060	.02250	.02390	.02640	.02890	.03110

5.							
.018	.020	.025	.030	.040	.050	.060	.070
.098	.107	.124	.136	.152	.165	.178	.190
.0074	.0080	.0094	.0104	.0120	.0133	.0144	.0154
.02170	.02260	.02430	.02590	.02840	.03090	.03310	.03520
6.							
.020	.023	.028	.033	.040	.050	.060	.070
.100	.123	.137	.148	.158	.171	.184	.196
.0096	.0113	.0131	.0143	.0155	.0169	.0182	.0197
.02380	.02530	.02730	.02860	.03040	.03270	.03490	.03690
.9	5	8	.017				
2.							
.010	.015	.020	.025	.030	.040	.050	.060
.065	.073	.081	.089	.096	.108	.120	.131
.0020	.0022	.0025	.0027	.0029	.0033	.0036	.0040
.00800	.00890	.00990	.01080	.01160	.01290	.01420	.01550
3.							
.013	.019	.025	.030	.035	.040	.050	.060
.077	.090	.100	.108	.145	.121	.132	.142
.0036	.0042	.0047	.0050	.0054	.0057	.0062	.0068
.01010	.01120	.01230	.01320	.01400	.01460	.01590	.01710
4.							
.015	.020	.025	.030	.040	.050	.060	.070
.0865	.099	.110	.118	.133	.145	.156	.166
.0054	.0062	.0069	.0075	.0085	.0092	.0100	.0107
.01330	.01410	.01500	.01590	.01700	.01820	.01910	.02010
5.							
.015	.018	.022	.027	.033	.040	.050	.060
.088	.097	.108	.120	.1305	.141	.154	.165
.0071	.0078	.0088	.0096	.0105	.0113	.0124	.0134
.01500	.01570	.01630	.01720	.01820	.01900	.02000	.02100
6.							
.018	.021	.025	.030	.040	.050	.060	.070
.101	.112	.124	.134	.150	.163	.174	.185
.0097	.0110	.0121	.0131	.0147	.0160	.0173	.0184
.01720	.01820	.01900	.01990	.02090	.02170	.02260	.02340
4	4	3					
2.							
.0091	.0280	.0500					
.1065	.0330	.0160					
3.							
.0179	.0400	.0600					
.1385	.0510	.0390					
4.							
.0261	.0550	.0650					
.1703	.0720	.0690					
6.							
.0412	.0700	.0750					
.2358	.1070	.1000					
6	4	3					
2.							
.0070	.0220	.0600					
.1468	.0560	.0390					
3.							
.0120	.0250	.0600					
.1871	.0870	.0690					
4.							
.0175	.0280	.0600					
.2315	.1170	.1000					
6.							

40259	.0420	.0650
43163	.1750	.1620
37	4	3
2.		
40067	.0200	.0600
41573	.0610	.0430
3.		
40112	.0220	.0400
42049	.0930	.0830
4.		
40157	.0250	.0400
42550	.1240	.1150
6.		
40222	.0400	.0550
43520	.1620	.1740
8	4	3
2.		
40070	.0250	.0400
41584	.0560	.0500
3.		
40109	.0310	.0450
42124	.0850	.0790
4.		
40139	.0350	.0500
42650	.1140	.1050
6.		
40190	.0350	.0500
43760	.1770	.1680
9	4	3
2.		
40074	.0300	.0500
41471	.0440	.0390
3.		
40109	.0330	.0500
42069	.0690	.0640
4.		
40137	.0350	.0500
42669	.0920	.0880
6.		
40169	.0350	.0500
43869	.1390	.1380

UNCLASSIFIED

SECURITY CLASSIFICATION OF THIS PAGE (When Data Entered)

REPORT DOCUMENTATION PAGE		READ INSTRUCTIONS BEFORE COMPLETING FORM
1. REPORT NUMBER Technical Report TC-676	2. GOVT ACCESSION NO.	3. RECIPIENT'S CATALOG NUMBER
4. TITLE (and Subtitle) Development of an Off-Design Predictive Method for Supercavitating Propeller Performance		5. TYPE OF REPORT & PERIOD COVERED Theory Development Report Mar. 1976 - Dec. 1976
		6. PERFORMING ORG. REPORT NUMBER TC-676
7. AUTHOR(s) Okitsugu Furuya		8. CONTRACT OR GRANT NUMBER(s) N00600-76-C-0790
9. PERFORMING ORGANIZATION NAME AND ADDRESS Tetra Tech, Inc. 630 North Rosemead Boulevard Pasadena, California 91107		10. PROGRAM ELEMENT, PROJECT, TASK AREA & WORK UNIT NUMBERS
11. CONTROLLING OFFICE NAME AND ADDRESS		12. REPORT DATE December 1976
		13. NUMBER OF PAGES 146
14. MONITORING AGENCY NAME & ADDRESS (if different from Controlling Office) David W. Taylor Naval Ship R&D Center Code 154 Bethesda, Maryland 20034		15. SECURITY CLASS. (of this report) Unclassified
		15a. DECLASSIFICATION/DOWNGRADING SCHEDULE
16. DISTRIBUTION STATEMENT (of this Report) This document has been approved for public release and sale; its distribution is unlimited.		
17. DISTRIBUTION STATEMENT (of the abstract entered in Block 20, if different from Report)		
18. SUPPLEMENTARY NOTES		
19. KEY WORDS (Continue on reverse side if necessary and identify by block number) Supercavitating propellers Performance prediction method Three-dimensional cascade effect.		
20. ABSTRACT (Continue on reverse side if necessary and identify by block number) The present method incorporates a two-dimensional supercavitating cascade theory into a propeller lifting line theory for downwash induced angle corrections. In addition, cavitation number corrections are made in order to account for choking conditions which occur in flow passages of propeller blades having cascade configuration. The results are compared with experimental data for TMB Model 3770 supercavitating propeller.		

DD FORM 1473
1 JAN 73EDITION OF 1 NOV 65 IS OBSOLETE
S/N 0102-014-6601

UNCLASSIFIED